

https://dspace.org/

Cellular localization of low-molecular-weight penicillin-binding proteins and other cell wall remodeling enzymes in Mycobacterium smegmatis

Maphatsoe, Masethabela Maria

2017
https://hdl.handle.net/10539/24788

Downloaded from a DSpace repository. https://dspace.org/

Cellular localization of low-molecular-weight penicillin-binding proteins and other cell wall remodeling enzymes in *Mycobacterium smegmatis*

Masethabela Maria Maphatsoe

(1316723)



A Dissertation submitted to the Faculty of Health Sciences, University of the Witwatersrand, Johannesburg, in fulfillment of the requirements for the degree of Masters of Science in Medicine.

July 2017

Declaration

I, Masethabela Maria Maphatsoe declare that this Dissertation is my own work, unaided work. It is being submitted for the Degree of Masters in Medicine at the University of the Witwatersrand, Johannesburg. It has not been submitted before for any degree or examination at any other University.



_____

Signature of candidate

12 day of July 2017 in Braamfontein

DEDICATION

THIS WORK IS DEDICATED TO MY FAMILY AND FRIENDS WHO SUPPORTED ME THROUGHOUT MY STUDIES.

Presentations arising from this research project

Conference attended : Molecular Bioscience Research Thrust (MBRT)

Presentation : Oral

Date : 08 December 2016

Place : University of the Witwatersrand, West Campus, Braamfontein

Conference attended : Biennial Research Day and Postgraduate Expo

Presentation : Poster

Date : 01 September 2016

Place : University of the Witwatersrand, Medical School, Parktown

Conference attended : Molecular Bioscience Research Thrust (MBRT)

Presentation : Poster

Date : 03 December 2015

Place : University of the Witwatersrand, West Campus, Braamfontein

Abstract

The majority of bacterial species responsible for the spread of infectious diseases in humans undergo morphological changes enabling them to withstand harsh environmental conditions for survival within host cells. These changes, together with distinct modes of growth, underpin the bacterium's overall ability to maintain its integrity during infection. Amongst the deadliest infectious diseases worldwide, infection with *Mycobacterium tuberculosis*, the causative agent of tuberculosis (TB), ranks the highest in terms of mortality. TB has been a scourge in medical history for decades. The rapid emergence of drug-resistant TB strains has necessitated the development of novel, rapid and effective anti-TB therapy. In this regard, the design of anti-TB drugs which can be co-administered with antiretroviral treatment requires a detailed understanding of the processes associated with bacterial cell assembly and cell division. DD-carboxypeptidases (DD-CPases), classified as low-molecular-weight penicillin-binding-proteins (LMW PBPs) have been implicated in the remodelling of peptidoglycan (PG) in the cell wall and are important for cell growth and division. PG remodelling requires tight spatial and temporal regulation to maintain cell wall integrity and cell size/shape. In this study, we assessed localization patterns of an essential DD-CPase, DacB, and non-essential DD-CPases; MSMEG_1661, MSMEG_2432 and MSMEG_2433 in *Mycobacterium smegmatis*, a non-pathogenic relative of *M. tuberculosis*. For this, we constructed DD-CPase derivatives fused to a C-terminal green fluorescence protein tag to determine their cellular localization patterns. Using a similar approach, we localized other known cell wall remodelling and cell division proteins, namely PonA2, DivIVA and FtsZ to study their localization relative to DacB in wild-type *M. smegmatis* and mutants defective for DD-CPases. We observed unique localization patterns for these proteins that offer new insights in remodelling of the mycobacterial cell surface during division. FtsZ is localized to mid-cell, where cell division is initiated, while DivIVA, a division site selection protein, localized to both poles. Interestingly, DacB localized in a similar manner to the essential high-molecular-weight PBP, PonA2, which localized mainly to both poles. In some cases, PonA2 (9 %) and DacB (10 %), also localized to one pole. Next, we localized these proteins in mutants defective for DD-CPases. For this, a mutant defective in MSMEG_2433 and MSMEG_2432 was constructed by site-specific allelic exchange. Using this strain, in addition to other pre-existing mutants, we demonstrated that loss of DD-CPases results in mis-localization of FtsZ and consequently, the division apparatus. We further assessed the △MSMEG2433 △MSMEG2432 mutant by phenotypic characterization. A growth kinetics analysis showed

that this grew comparably similar to the parental wild-type and had marginal defects in biofilm formation. There were no differences in spatial localization of new PG synthesis. Collectively, this study has contributed to an enhanced understanding of PG remodeling in mycobacteria.

Acknowledgements

"For I know the plans I have for you", declares the LORD, "Plans to prosper you and not harm you, plans to give you hope and a future." ***Jeremiah 29:11***

Firstly, I would like to thank the **Almighty** for guiding me through this challenging, yet rewarding journey. For his blessings and everlasting love which He has bestowed upon me and my family, I will forever cherish.

Secondly, to all funding bodies, the National Research Foundation (NRF), the Department of Military Veterans (DMV) and the Howard Hughes Medical Institute, thank you for your educational support and contribution towards my graduate career. I would also like to thank the sequencing team from the University of Stellenbosch for providing me with useful data.

Thirdly, **Professor Bavesh Kana**, words cannot explain how grateful I am to have had the chance to work with you. Having a supervisor who is influential, supportive, and patient like you is a blessing in disguise. Thank you for grooming me and helping me mature as a scientist. Dr. **Chrisopher Ealand**, thank you for your co-supervision and assistance.

I would also like to thank my parents, **Nkotseng** and **Peter Maphatsoe**, for their prayers and support and their encouragement to always do my best, I have gone this far in life and academically because of you. Thank you for believing in me. To my siblings **Joalane** and **Lebohang Maphatsoe**, who promised to enroll as well so that we all travel this journey together, you have not only taught me power of sacrifice, but you have taught me that there are people out here who are willing go an extra mile to ensure that the journey you travel is a much lighter one and is prosperous. To all my family at large, thank you being there when I need you most, for sharing my joys and sorrows and for always believing in me.

To all the **CBTBR family**, colleagues and senior staff, thank you for helping me in my research and with the administrative work. Thank you for all your support and advices. Your motivation and laughter which we shared during lunch breaks made my experience at the CBTBR a pleasant and an unforgettable one. Thank you for contributing towards the person I am today and thank you for listening to my preparation presentations. Finally, I would like to thank all my friends for their emotional support, motivation and their positive influence.

TABLE OF CONTENTS

Title Page I
Declaration II
Dedication III
Presentations arising from this research project IV
Abstract V
Acknowledgements VII
List of abbreviations/nomenclature and symbols XII
List of figures XIV
List of tables XVII
List of calculations used in this study XVIII
CHAPTER 1: LITERATURE REVIEW 1
1. INTRODUCTION 1
1.1. The impact of molecular biology techniques in the study of mycobacterial infections 1
1.2. Tuberculosis 2
1.2.1. Tuberculosis incidences in South Africa 2
1.2.2. Infection with tuberculosis 3
1.2.3. Tuberculosis pathogenesis 5
1.2.4. Tuberculosis treatment 6
1.2.5. Drug-drug interactions 7
1.2.6. Tuberculosis interventions and drug resistance 8
1.3. The mycobacterial cell wall 9
1.3.1. Peptidoglycan 11
1.3.2. Peptidoglycan biosynthesis 12
1.3.3. Peptidoglycan crosslinking 13
1.3.4. Peptidoglycan remodeling by peptidoglycan hydrolases 13
1.4. Penicillin-binding proteins 14
1.4.1. High-molecular-weight penicillin-binding proteins 15
1.4.2. Low-molecular-weight penicillin-binding proteins 16
1.4.3. Domains / conserved motifs of penicillin-binding proteins in all bacterial organisms 16
1.5. Cell growth and division in mycobacteria 17
1.5.1 Modes of growth in rod-shape bacteria 18
1.5.2. Enzymes involved in bacterial cell division and cell elongation 19

1.5.3. Cell division and growth in mycobacteria 20
1.5.4. Review of selected penicillin-binding proteins and cell wall machinery 22
1.6. Project overview 22
1.6.1. Problem statement 22
1.6.2.Hypothesis 23
1.6.3. Rationale of the study (Aim) 24
1.6.4. Research objectives 24
1.2.5 Expected outcomes 25
CHAPTER 2: MATERIALS AND METHODS 26
Section A: Materials 26
2.1 Chemicals and reagents used in the study 26
Section B: Methods 34
2.2 Media, bacterial strains and culture condition 34
2.3 Transformation of bacterial species 34
2.3.1 Transformation of *E. coli* cells 34
2.3.2 Transformation of *M. smegmatis* by electroporation 35
2.4 DNA extraction methods 36
2.4.1 Plasmid DNA extraction from *E. coli* 36
2.4.2 Chromosomal DNA extraction from *M. smegmatis* 38
2.5 DNA quantitation and visualization 39
2.5.1 DNA quantitation 39
2.5.2 DNA visualization and purification using agarose gel electrophoresis 39
2.6 DNA manipulation 40
2.6.1 Primer design 40
2.6.2 DNA amplification using polymerase chain reaction 40
2.7 Restriction digestion 41
2.8 Modification of DNA overhangs 42
2.9 DNA dephosphorylation 43
2.10 DNA ligation 43
2.11 DNA sequencing 43
2.12 Molecular cloning and construction of recombinants 44
2.12.1 Generation of reporter genes using three-way cloning 45
2.12.2 Generation of controls used for fluorescence analysis using two-way cloning 47
2.13 Microscopic analysis 47

2.13.1 Fluorescence microscopy 47
2.14 Mutant generation 48
2.14.1 Construction of the suicide vector to simultaneously delete MSMEG_2432 and MSMEG_2433 48
2.14.2 Generation of ΔMSMEG_2433 ΔMSMEG_2432 deletion mutant using two-step allelic exchange 50
2.15 Genotypic analysis of mutants 51
2.15.1 Screening of mutants using PCR 51
2.15.2 Screening of mutants using southern blot analysis 52
2.16 Phenotypic analysis of mutant (s) 55
2.16.1 Growth curves and optical density measurements 55
2.16.2 Biofilm formation 56
2.16.3 Crystal violet assay 56
2.17 Click chemistry - copper click reaction with D-alanine analogue 57
2.18 Data representation, statistical analysis and software programs used in this study 58
2.18.1 Data representation and statistical analysis 58
2.18.2 Software used in this study 58
2.3 Ethical considerations 59
CHAPTER 3: RESULTS 60
Section A: Bioinformatics of the DD-CPases investigated in the study 60
3.1. Phylogenetic and structural analysis of DD-CPases investigated in this study 60
3.1.1. Sequence alignment of the DD-CPases in various rod-shape bacteria 60
3.1.2. Divergence of peptidase_S13 of DD-CPase-PBP4 in various rod-shape bacteria 64
Section B: Cellular localization of DD-CPases and cell wall remodelling enzymes in wild-type *M. smegmatis* cells 65
3.2 Identification of gene location and transcription units for the DD-CPases in *M. smegmatis* prior cloning 66
3.2.1 Subcellular localization of the DacB in wild-type *M. smegmatis* cells 67
3.2.2. Subcellular localization MSMEG_1661 in wild-type *M. smegmatis* cells 72
3.2.3. Subcellular localization of the MSMEG_2432 in wild-type *M. smegmatis* cells 74
3.2.4. Subcellular localization of the MSMEG_2433 in wild-type *M. smegmatis* cells 76
3.2.5. Subcellular localization of PonA2 in wild-type *M. smegmatis* 79
3.2.6. Cellular localization of cell wall machinery (FtsZ and DivIVA/Wag31) in wild-type *M. smegmatis* 81
3.3. Localization of cell wall remodelling and cell division enzymes in mutants defective for DD-CPases 82

3.3.1. Cellular localization dynamics of FtsZ and DivIVA in wild-type and mutants defective for DD-CPases. 82

3.3.2. Cellular localization of DacB in the DD-CPases double mutants (Δ1661 Δ2432, Δ2433 Δ1661 and Δ2433 Δ2432) 85

Section C: Gene knockout studies. 88

3.4 Knockout MSMEG_2433 and MSMEG_2432 in combination 88

3.4.1 Confirmation of the DD-CPases double gene knockout mutant (ΔMSMEG_2433 ΔMSMEG_2432) using PCR 89

3.4.2. Confirmation of the DD-CPases double gene knockout mutant (Δ2433 Δ2432) using southern blot. 90

3.4.3. Growth kinetics of the Δ2433 Δ2432 mutant. 91

3.4.4 Biofilm formation in the △2433 △2432 mutant. 92

3.4.5 Click chemistry analysis of the Δ2433 Δ2432 mutant 95

CHAPTER 4: DISCUSSION 97

CHAPTER 5: CONCLUSION 106

CHAPTER 6: REFERENCES 107

CHAPTER 7: APPENDICES 113

List of abbreviations/nomenclature and symbols

Abbreviation and full name

aph: Hygromycin phosphotransferase

ATP: Adenosine triphosphate

bla: Ampicillin-resistant gene encoding β-lactamase

bp: Base-pair

BSA: Bovine serum albumin

CFU: colony-forming units

CNS: central nervous system

CSPD: Disodium 3-(4-methoxyspiro {1, 2-dioxetane-3, 2′-(5′-chloro) tricyclo [3.3.1.13, 7] decan}-4-yl) phenyl phosphate

CTAB: Cetyltrimethylammonium bromide

CuSO4: Copper sulphate

CV: Crystal violet

DCO: Double cross-over

DD-CPase: DD-Carboxypeptidase

DIG: Digoxygenin

DMSO: Dimethylsulphoxide

DNA: Deoxyribonucleic acid

dNTPs: Deoxyribonucleotide triphosphates

DOTS: Directly-observed therapy, short course

DS: Downstream

E. coli: *Escherichia coli*

EDTA: Ethyldiaminetetraacetic acid

EtOH: Ethanol

FDA: Food and Drug Administration

gDNA: genomic DNA

GFP: green fluorescent proteins

HBC: High burden countries

HIV: Human immunodeficiency virus

HMW: High-molecular-weight

Hyg^{R}: Hygromycin resistance

int: intergrase

kan: Kanamycin adenyltransferase encoding gene

Kan^{R}: Kanamycin resistance

kb: Kilobase-pairs

LA: Luria-Bertani agar

lacZ:β-galactosidase gene

LB: Luria-Bertani

Ldt: L,D- transpeptidase

LMW: Low-molecular-weight

LTBI: Latent TB infection

M. smegmatis: *Mycobacterium smegmatis*

M. tuberculosis*: Mycobacterium tuberculosis*

MAP: mycolic acids- arabinogalactan-peptidoglycan

mCherry: monomeric Cherry fluorescence protein

***m*DAP**: *meso*-diaminopimelic acid

MDR: Multidrug-resistant

mRFP: monomeric Red Fluorescence Protein

mTurq: monomeric Turquoise fluorescence protein

NaCl : Sodium chloride

NAG: *N*-acetylglucosamine

NAM: *N*-acetylmuramic acid

NaOAc: Sodium acetate

NaOH: Sodium hydroxide

NEB: New England Biolabs

NTC: No template control

OD: Optical density

Ori: Origin of replication

PASTA: Penicillin-binding protein and Serine/Threonine Kinase-Associated

PBP: Penicillin-binding protein

PBS: Phosphate buffered saline

PBSTB: PBS with 0.05 % BSA and 0.01 % Tween 20

PCR: Polymerase chain reaction

PEG: Polyethylene glycol

PG: Peptidoglycan

pMV: pMV306H

PNK: Polynucleotide kinase

pTw: pTweety

RE: restriction enzyme

RNA: ribonucleic acid

RNaseA: Ribonuclease A

sacB: levansucrase encoding gene

SCO: Single cross-over

sdH_2O: Sterile distilled water

SDS: Sodium dodecylsulphate

SIB: Swiss institute of bioinformatics

SPTK: serine/threonine protein kinases

SSC: Saline sodium citrate

TAE: Tris-acetate-EDTA

TB: Tuberculosis

TBE: Tris-Borate-EDTA

TBTA: Tris[(1-benzyl-1H-1,2,3-triazol-4-yl)methyl]amine

TDR: Totally drug-resistant

TE: Tris-EDTA

Tfb: Rubidium chloride compentent cell solution

Tm: Melting temperature

tRNA: transfer RNA

Tween: Polyoxyethylene sorbitan monooleate

TY: Tryptone, Yeast Extract

US: Upstream

UV: Ultraviolet

WHO: World Health Organization

XDR: Extensively drug -resistant

× g: relative centrifugal force or × g -force

X-gal: 5-bromo-4-chloro-3-indolyl-β-D-galactopyranoside

Abbreviation/Symbol and full name

△: Delta or "knockout"

d: day

m: milli (10^{-3})

mL: milliliter

mM: milliMolar (mmol/L)

ng: nanogram

α: alpha

β: beta

µ: micro (10^{-6})

µl: microliter

Abbreviation/Symbol and full name

Hr.(s): hour(s)

kg: kilogram

mg: milligram

Min (m): min

n: nano (10^{-9})

nm: nanometer

Sec (s): second(s)

V: Volts

µm: micrometer

µM: microMolar(µmol/L)

Ω: Ohm

List of figures

Figure 1.1: Three lists of the high burden countries with tuberculosis incidences……..2

Figure 1.2: Different disease states and stages during tuberculosis infection…….....4

Figure 1.3: Components of the mycobacterial cell wall…….……..……..10

Figure 1.4: Structure of PG in mycobacterial species…….11

Figure 1.5: Biosynthesis and crosslinking of peptidoglycan……..……12

Figure 1.6: Enzymes involved in peptidoglycan synthesis and remodelling……..…....14

Figure 1.7: Illustration of the catalytic center of penicilloyl serine transferases……....17

Figure 1.8: Bacterial replication modalities……19

Figure 1.9: Illustration of anticipated localization patterns of the DD-CPases and other cell division enzymes in *M. smegmatis* that are involved in peptidoglycan remodeling……25

Figure 2.1: Schematic representation of a three-way cloning procedure to create using mRFP fluorescently tagged DacB construct……45

Figure 2.2: Schematic representation of integration of pMV306H into *M. smegmatis* chromosome……46

Figure 2.3: Schematic representing the generation of an unmarked suicide vector……...50

Figure 2.4: Generation of a gene knockout using two-step allelic exchange by homologous recombination……..……..52

Figure 2.5: Diagram showing different steps of conducting a southern blot……..53

Figure 3.1: Illustration showing conserved motifs in PBPs……....61

Figure 3.2: Illustration of structures, domain diagrams and conserved arrangement of catalytic residues of the five PBPs assessed this study……....63

Figure 3.3: Phylogenetic tree showing divergence of PBP4 across rod-shape bacteria…..**....**65

Figure 3.4: Illustration showing gene loci that encode DD-CPases in mycobacteria…….…67

Figure 3.5: Restriction enzyme profiling of the pMV306H_dacB_GFP construct……69

Figure 3.6: Subcellular localization patterns of DacB-GFP in wild-type *M. smegmatis* cells……...71

Figure 3.7: Restriction enzyme profiling of the pMV306H_MSMEG_1661_GFP construct……...72

Figure 3.8: Subcellular localization patterns of MSMEG_1661_GFP in wild-type *M. smegmatis* cells……..……...73

Figure 3.9: Restriction profiling of the pMV306H_MSMEG_2432_GFP construct…….74

Figure 3.10: Subcellular localization patterns of MSMEG_2432_GFP in wild-type *M. smegmatis* cells…….……**...**….76

Figure 3.11: Restriction enzyme profiling of the pMV306H_MSMEG_2433_GFP construct……...…77

Figure 3.12: Subcellular localization patterns of MSMEG_2433 in wild-type *M. smegmatis*……78

Figure 3.13: Subcellular localization patterns of PonA2 in wild-type *M. smegmatis*……....80

Figure 3.14: Subcellular localization patterns of FtsZ and DivIVA in wild-type *M. smegmatis* cells……..…82

Figure 3.15: Subcellular localization of a cell division protein, FtsZ, in wild-type *M. smegmatis* and DD-CPases deficient mutants……**..**…….....84

Figure 3.16: Illustration showing subcellular localization of a cell elongation protein, DivIVA (wag31), in wild-type *M. smegmatis* single cells and the double gene knockout mutants……84

Figure 3.17: DacB localization in wild-type and DD-CPase knockouts……..86

Figure 3.18: Restriction analysis of the suicide plasmid, p2NIL_2433_2432::pG19…….89

Figure 3.19: PCR confirmation of the Δ2433 Δ2432…….……90

Figure 3.20: Southern blot confirmation of the Δ2433 Δ2432 double mutant……...91

Figure 3.21: Growth rate comparison between wild-type (mc2155), mutant (Δ 2432 Δ2433) and complementation strains……..…….92

Figure 3.22: Biofilm formation in the Δ 2433 Δ2432 mutant……94

Figure 3.23: Quantification of biofilm formation of *M. smegmatis* using crystal violet assay…….93

Figure 3.24: Localization of new peptidoglycan synthesis in wild-type and the DD-CPases mutant strains using click chemistry……96

Figure 4.1: Model representing the role of DacB in mycobacterial cell elongation…….104

Figure C1: Molecular weight markers used in this study…….…117

Figure D1: Gel electrophoresis of PCR products……..118

Figure E1: Failed localization with mRFP proteins…….....118

Figure F1: Restriction enzyme profiling of the p2NIL_2433_2432 and pGOAL_19 constructs to create a suicide vector (p2NIL_2433_2432::pG19)…….…….....119

Figure F2: Illustration representing the sucrose sensitivity test to for suicide vector (p2NIL_2433_2432::pG19) used to create a DD-CPases double mutants (Δ2433 Δ2432)……...120

Figure G1.1: Restriction enzyme profiling of the pMV306H integrating plasmid used to create reporter fusion proteins…….....121

Figure G1.2: Restriction enzyme profiling of the pTweety integrating plasmid used to create reporter fusion proteins……..…122

Figure G2.1: Illustration representing restriction enzyme profiling of the pMV306H_dacB_mRFP construct……123

Figure G2.2: Illustration above represents restriction enzyme profiling of the pMV306H_dacB_mTurq construct……....124

Figure G2.3: Restriction profiling of the pTweety_FtsZ_GFP and pTweety_DivIVA_GFP constructs…….……..125

Figure G2.4: Restriction enzyme profiling of the pTweety_PonA2_GFP control construct……126

Figure G3.1: Restriction enzyme profiling of the pMV306H_mRFP control construct….127

Figure G3.2: Restriction enzyme profiling of the pMV306H_mTurq control construct….128

Figure G3.3: Restriction enzyme profiling of the pMV306H_mCherry control construct……129

Figure G4: Illustration representing fluorescence intensity of the fluorescent tagging proteins that were used in this study in *M. smegmatis* cells…….130

List of tables

Table 1.1: Current available first and second line drugs ……...…...…....7

Table 1.2: Different modes of growth in rod-shape bacteria and regions of active peptidoglycan synthesis……...18

Table 1.3: Selected genes used in this study and their mycobacterial homologs……23

Table 2.1: Plasmids used in this study……....26

Table 2.2: Strains used in this study…….…..….28

Table 2.3: Primers used in this study for cloning……....30

Table 2.4: Confirmation primers for mutants and reporter genes generated in this study…..32

Table 2.5: Levels of effective separation of nucleic acids on an agarose gel…….39

Table 2.6: Selection criteria for oligonucleotides……...…40

Table 2.7: Amount of DNA required for efficient restriction enzyme digestion……...42

Table 4.1: Spatial and temporal organization of the DD-CPases during cell division and cell growth based on the localization patterns……103

Table A1: Representation of table of codons or the genetic code……113

Table A2: Representation of table of amino acids and their abbreviations……...113

Table B1: Media used for bacterial growth……..114

Table B2: Media supplementation……...…114

Table B3: Solutions for transformation and preparation of chemically competent cells…115

Table B4: Solutions for genomic DNA extraction……..115

Table B5: Solutions for plasmid DNA extraction……...……115

Table B6: Solutions for DNA precipitation……..116

Table B7: Solutions for DNA electrophoresis…….....116

Table B8: Solutions for DNA precipitation……..116

Table B9: Reagents for click chemistry……117

Table B10: Reagents for crystal violet assay……117

List of calculations used in this study

Colony-forming units (CFU / ml) $=$ Number of colonies counted $*$ $\frac{\text{dilution factor}}{\text{volume of culture plated}}$

Amount of insert DNA (ng) $=$ $\frac{\text{50 ng x size of insert (bp)}}{\text{size of vector (bp)}}$

Melting temperature (T_m) $= 49.82 + 0.41(\%\ \text{GC}) - \frac{600}{\text{L}}$

L= length of the probe sequence

Optimum hybridization temperature (T_{opt}) = T_m - 20 to 25

Determination of inoculum size C1V1= C2V2

C1= Initial concentration (the one you have)

V1= Initial volume (the want you want)

C2= Final concentration (concentration needed)

V2= Final volume (volume needed)

CHAPTER 1: LITERATURE REVIEW

1. INTRODUCTION

1.1. The impact of molecular biology techniques in the study of mycobacterial infections

For years, scientists, healthcare workers, and government/non-governmental organizations have been working together to combat mycobacterial infections (Butcher *et al*., 1996). Tuberculosis (TB) and leprosy are chief among mycobacterial infections that represent a notable public health concern (Scollard *et al*., 2015). Moreover, the problem is exacerbated due to the lack of control, case detection and inaccurate tracing sources of infections (Butcher *et al*., 1996). In combination with other opportunistic infections such as human immunodeficiency virus (HIV), diabetes, and obesity, TB treatment is made more difficult because of drug–drug interactions and toxicity effects (Manosuthi *et al*., 2016). It is thus important to implement and utilize tools that accurately detect, diagnose and treat TB while simultaneously combating the emergence of drug resistance. Conventional laboratory tools such as microscopy and culture-based techniques to detect mycobacterial organisms are already available (Butcher *et al*., 1996). What is lacking in this regard however, is a thorough understanding of the molecular mechanisms of mycobacterial growth.

In this study, we investigate the localization dynamics of proteins involved in the remodeling of peptidoglycan (PG), a critical component of the bacterial cell wall, in *Mycobacterium smegmatis (M. smegmatis)* which serves as a model organism to study *Mycobacterium tuberculosis (M. tuberculosis).* Cellular localization studies will provide insight on how certain proteins are maintained in a specific location (presumably at sites of cell wall synthesis) to carry out their function (Henriques *et al*., 2013, Smith, 2003). For the development of new TB drugs, it is important to target proteins that are central for survival of bacteria inside the host during infection (Henriques *et al*., 2013). Collectively, answers derived from this study will contribute to the overall understanding of proteins involved cell wall remodeling and possibly contribute to the identification of novel drug targets for TB.

1.2. Tuberculosis

The causative agent of TB is *Mycobacterium tuberculosis* (Gengenbacher and Kaufmann, 2012). Approximately 9 million people are annually infected with this bacterium every year, a sub-proportion of which develop clinical disease, with approximately 2 million deaths, making TB the number one killer infection in the world (WHO, 2016).

1.2.1. Tuberculosis incidences in South Africa

TB ranks number one in the top five leading causes of deaths in South Africa (SA), a country that appears on all three World Health Organization (WHO) lists of high burden countries, Figure 1.1(WHO, 2016). This ranking has not changed since 2012 and individuals mostly affected are usually those from low income households, overcrowded living or working conditions and poor health care systems (Baltussen *et al*, 2005, WHO, 2016). A relatively high burden of infectious diseases exists with an equally high rate of immunocompromised patients and drug resistance (Laxminarayan *et al*., 2006). Lastly, of the five population or ethnic groups in SA; African, White, Mixed Race, Indian/Asian and other, the African or black ethnical group is disproportionately affected by TB (Statistics South Africa, 2014).

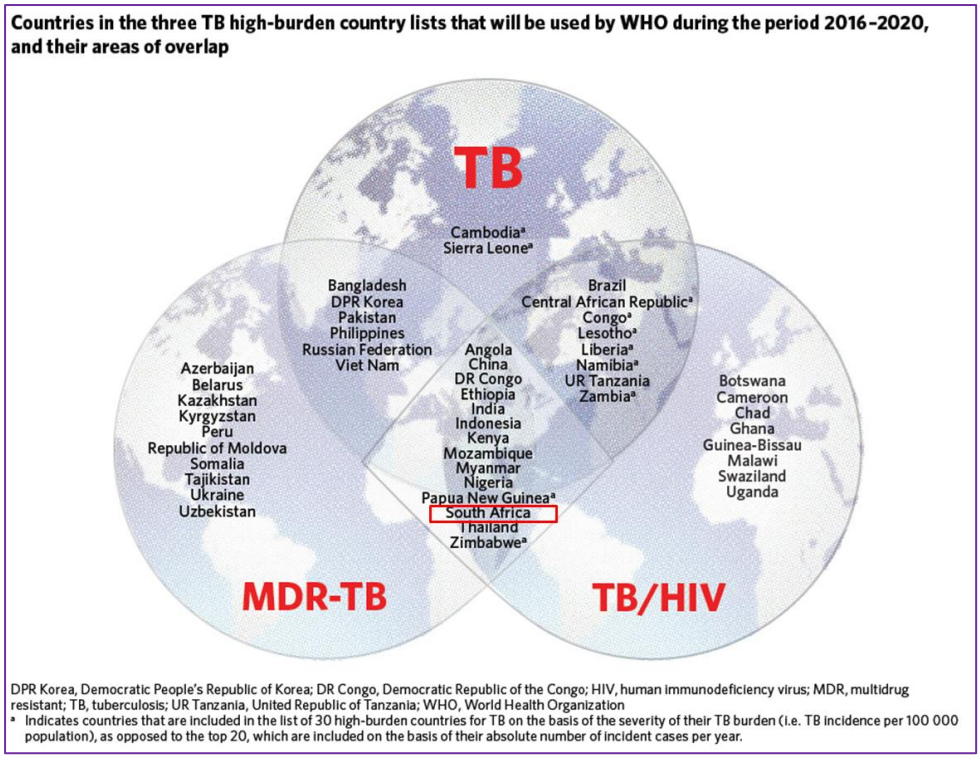


Figure1.1: Three lists of the high burden countries (HBC) with tuberculosis incidences. Each circle represents a list of high burden countries based on TB, MDR-TB and HIV or co-infection with TB/HIV incidence rates.

These are defined based on absolute number of incidence cases and severity of the TB burden globally. Countries in each circle/list are placed in alphabetical order and based on the estimated absolute number per year. Each incidence is measured by a threshold of >10 000, >1000 and >1000 by estimated incidence of TB, TB/HIV and MDR-TB cases per year respectively. The overlap between the circles represents the presence of two or more incidence cases per country. For example, South Africa occurs in all three lists of high burden countries (red box) with highest estimated numbers of incident cases which means it has high incidences rates of TB, HIV and HIV/TB and MDR-TB (WHO, 2016).

1.2.2. Infection with tuberculosis

TB primarily infects the lungs (pulmonary), but can spread to other parts of the body such as the central nervous systems, lymph nodes and bones (extra-pulmonary) in humans (Smith, 2003, Loddenkemper *et al*., 2016). In the case of pulmonary TB (PTB), clinical symptoms include chronic cough, sputum production, loss of appetite, weight loss, fever and night sweats (Loddenkemper *et al*., 2016,). However, these symptoms are only observable in individuals with active TB disease. A different clinical manifestation of TB infection is latent TB infection (LTBI) (Bourai *et al*., 2012). Extra-pulmonary TB (EPTB) on the other hand, is difficult to diagnose, treat and manage due to its clinical features which overlaps with that of the PTB and it having symptoms which are either site/organ related or affecting multiple organs (Loddenkemper *et al*., 2016, Zumla *et al* 2013). However, other than non-specific features such as anorexia and weight loss, the common symptoms in EPTB include fever, pain and enlarged lymph nodes and usually require surgical interventions (Yang *et al*., 2013, Houston and Macallan, 2014).

Active TB disease is symptomatic and transmissible due to the excessive bacterial load that has subverted the host's immune system to contain and eradicate the disease (Gengenbacher and Kaufmann, 2012). LTBI on the other hand, is asymptomatic and non-transmissible and is caused by the non-clearance of bacteria in the lung, bacteria that are in a quiescent state (Gengenbacher and Kaufmann, 2012). Different disease states and stages during pulmonary TB infection are shown in Figure 1.2.

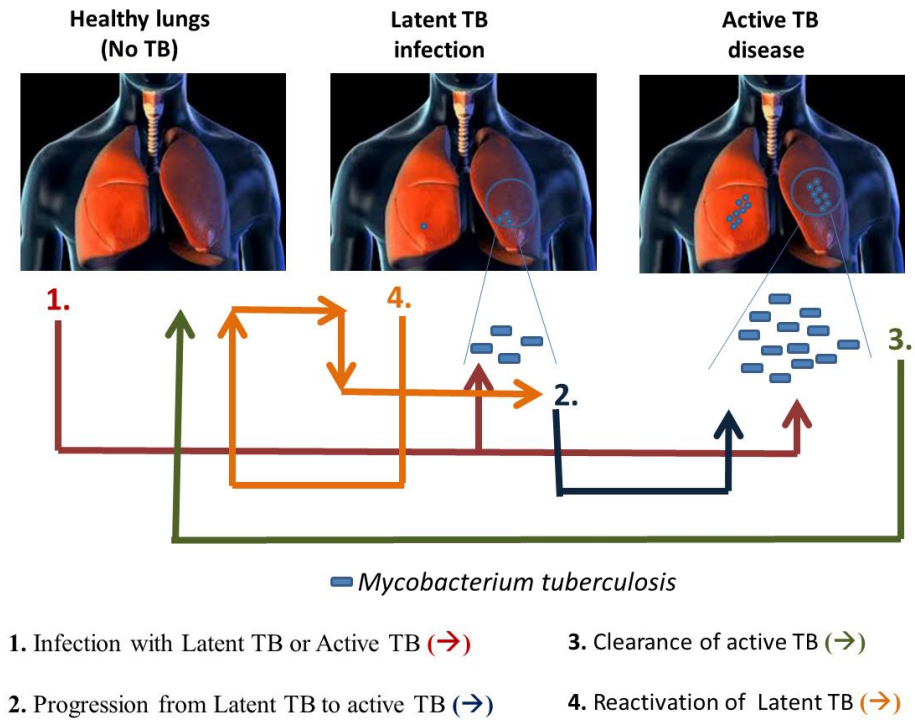


Figure 1.2: Different disease states and stages during tuberculosis infection. Individuals with healthy lungs can get infected with *M. tuberculosis* which can either progress to active infection or become latent. (red arrows, represented by 1) Individuals with latent TB infection are also able to progress from latent TB infection to active TB disease (blue arrow, represented by 2).

About five to ten percent of individuals with LTBI develop active TB disease over their lifetime, but with HIV co-infection, this risk is elevated to 10 % per year (WHO, 2014, Kumar, 2016). Active disease can be cured with a combination of first and second line drugs. Therapy, drug dosage and treatment duration administered to individuals infected with TB is measured based on the severity of infection (i.e. mild, moderate, or severe) as well as the pathological features (Hoppe *et al*., 2016, Cadena *et al*., 2016). For example, individuals with consistent clinical features based on TB diagnosis are usually advised to start treatment as soon as possible without waiting for culture results. These groups are also encouraged to continue with the regimen even after the results are returned as negative to avoid worsening of infection and development of antibiotic resistance TB (Hoppe *et al*., 2016).

1.2.3. Tuberculosis pathogenesis

Following inhalation of droplets containing *M. tuberculosis*, several factors dictate the outcome of disease (Kaplan *et al*., 2003, van Crevel *et al*., 2002). For example, bacillary burden, closeness of contact with the infectious case, host immune status and how virulent the strain is (Ahmad, 2010, Loddenkemper *et al.*, 2016). Due to the relatively small size of the droplet nuclei (1-5 μm or less than 2 μm in diameter), these bacilli are then engulfed by the alveolar macrophages at the site of infection (usually in the lung) in attempt to destroy the bacteria (Ahmad, 2010, Clark-Curtiss and Haydel, 2003). Depending on the activation or inactivation of these macrophages, the bacteria are then killed or they survive. Activation of the macrophages results in bacteria killing by while inactivation aids survival of the bacilli (Clark-Curtiss and Haydel, 2003). Once inside these macrophages, the bacilli replicate in the phagosomes and the soluble effector molecules which regulate host cellular immune responses are produced. These effector molecules include the chemokines, interleukin 12 (IL-12/ dendritic cells), and the cytokines tumor necrosis factor alpha (TNF-α/ CD4+ T cells) and are involved in the granuloma formation (Kaplan *et al*., 2003, Silva Miranda *et al*., 2012).

M. tuberculosis specifically decreases acidification of the phagosome and modifies its phagosome activity as well as preventing it from fusing with the lysozymes when inside the phagocyte (Torrelles and Schlesinger, 2017, Russell *et al*., 2009). In so doing, *M. tuberculosis* avoids the acidic and cytolytic environment within the phagolysosome and remains viable (Corrales *et al*., 2012). At this stage, exponential growth of *M. tuberculosis* takes place until the acquired immune response emerges and this happens simultaneously with granuloma (macrophage-rich cell mass) development (Russell *et al*., 2009). In TB, granulomas are either primarily progressed or established through reactivation. Primary granuloma occurs during the early stages of TB infection although rare and the established granuloma is more present in LTBI infected individuals during the reactivation of TB (Guirado and Schlesinger, 2013). The granulomas are responsible for the containment of the infection in an immune microenvironment and facilitate eradication. The different types of granulomas include the typical one in TB "the caseous granuloma" and others which are non-necrotising, necrotic and fibrotic granulomas (Silva Miranda *et al*., 2012, van Crevel *et al*., 2002). Localized granuloma caseation and necrosis or mature granulomas process ends when the infectious bacteria are released in the airways (Russell *et al*., 2009).

Despite the mounting of an immune attack, *M. tuberculosis* manages to escape, survive and persist in host cells, and allow for the establishment of either active disease or LTBI (Gengenbacher and Kaufmann, 2012). The outcomes of exposure with *M. tuberculosis*, based on innate host defense mechanisms efficiency and can result in either; (1) clearance of *M. tuberculosis* due to high innate immunity and results in no infection, (2) defective adaptive immunity in individuals whose innate immune response fails to protect them from the infection but protected get protected by alternative immunity such adaptive immunity which then results in successful granuloma formation. In some instances however during defective adaptive immunity, the disease progresses but this happens in less than 10 % of infected individuals as explained in paragraphs above and, (3) adaptive immunity or acquired cellular immune response which occurs as a result of TB reactivation (Bhatt and Salgame, 2007, Cooper, 2009). Reactivation of TB is defined as the transition from latent infection to the full blown active diseased state as a result of failed containment of the bacteria by the unfunctional granuloma or by other factors (Gengenbacher and Kaufmann, 2012, Andrea, 2009). Persistence is defined as the ability to persist or survive under harsh conditions such as exposure to antibiotics or the host's immune response (Dutta and Karakousis, 2014).

1.2.4. Tuberculosis treatment

The current treatment options for TB, approved by the US Food and Drug Administration (FDA) includes two classes: first line and second line drugs (Table 1.1), which can be either taken orally or through injection (Laurenzi *et al*., 2007). First line drugs are generally used to treat drug sensitive TB whereas second line drugs are used to treat drug-resistant TB. A typical first line drug regimen consists of a combination of three or more drugs, for example, Rifampicin (RIF) and Isoniazid (INH), Pyrazinamide (PZA) and/or Ethambutol (EMB) (Zumla *et al*., 2013). This will comprise a 2 month intensive phase, whereby the patient takes a cocktail of all four drugs, followed by an extended or continuation phase (~4 months) where two of the first line drugs, namely RIF and INH, must be taken (Pham *et al*., 2015). The extended phase is administered to ensure that all remaining bacteria in the body, especially persisters that increase the risk of reactivation, are killed (Hoagland *et al*., 2016, Laurenzi *et al*., 2007). The length and complexity of this regimen (~6 months of numerous antibiotics) contributes to poor patient compliance, a factor contributing to development of drug-resistant TB (Hoagland *et al*., 2016, Laurenzi *et al*., 2007).

Drug-resistant TB cannot be treated and cured by standard first line drugs and require a more intense regimen using second line drugs (Table 1.1) (Laurenzi *et al*., 2007). The problem with these drugs is that in some patients, they tend to be less effective which necessitates higher dosages / multiple drugs with toxic side effects (Ahuja *et al*., 2012). Under these circumstances, patients are usually forced to prematurely stop treatment or try other regimen leaving them more vulnerable to acquiring additional drug resistance (Schnippel *et al*., 2016). Furthermore, the majority of these drugs are expensive and are inaccessible, especially in developing countries with high incidences of drug-resistant TB and poor healthcare systems (Ahuja *et al*., 2012).

1.2.5. Drug-drug interactions

Another factor which contributes to the emergence of drug resistance is the high prevalence of HIV co-infection (Ramkissoon *et al*., 2012). Interactions between the currently administered anti-TB drugs and anti-retrovirals (ART) results in negative side-effects especially in immunocompromised patients (Ramkissoon *et al*., 2012, Manosuthi *et al*., 2016). These patients are at a greater risk of adverse reactions and stop following their treatment regimen (Manosuthi *et al*., 2016). The most common drug-drug interactions between ART and the first line drugs include ART-Isoniazid interaction and ART-rifampin interaction (Laurenzi *et al*., 2007).

Table 1.1: Current available first and second line drugs (Laurenzi *et al*., 2007, Sulis *et al.*, 2016).

First Line Drugs **(*4 drugs taken for 6-9 months)**	**Second Line Drugs** **(*up-to 6 drugs taken for 2 years)**	
Isoniazid (INH)	Streptomycin	
Rifampicin (RIF)	Capreomycin "	
Pyrazinamide (PZA)	Kanamycin	Aminoglycoside drugs
Ethambutol (EMB)	Amikacin	
	Ethionamide	

	p-Aminosalicylic acid (PAS) “	
	Cycloserine “	
	Ciprofloxacin	
	Ofloxacin	
	Levofloxacin “	Fluoroquinolones
	Moxifloxacin “	
	Gatifloxacin “	
	Clofazimine	
“ : Reserved for special situations (e.g. drug resistance or intolerance) ***** : Number of drugs taken and duration of treatment		

Co-treatment with ART and Isoniazid increases toxicity as they both cause peripheral neuropathy, while ART-rifampin treatment has been shown to interact with liver cytochrome P450 enzymes, which are responsible for the biotransformation of drugs via oxidation (Laurenzi *et al*., 2007, Ogu and Maxa, 2000). Such cases emphasize the need to re-evaluate current treatments and further underscore the importance of developing new antibiotics.

1.2.6. Tuberculosis interventions and drug resistance

The principal intervention currently aimed at treating and diagnosing TB is the Directly-observed therapy (DOTS) short course strategy (WHO, 2016, Baltussen *et al*., 2005). This global TB strategy recommended by WHO is implemented to ensure that patients adhere to their prescribed treatment (WHO, 2016, McLaren *et al*., 2016). Despite the execution of this strategy, emergence of drug resistance, together with HIV/TB co-infection, renders the program ineffective (Whalen, 2006). Therefore, a shorter regimen with specialized and/or personalized therapy should be developed and implemented to combat TB.

Currently, the only available TB vaccine is the bacillus Calmette-Guerin (BCG) (Baltussen *et al*., 2005, Evans *et al*., 2016). BCG is administered to children to protect them from pulmonary and disseminated TB. Unfortunately, this vaccine cannot be used to protect against adult pulmonary TB (Sharma *et al*., 2016). Nonetheless, approximately 16 other TB

vaccines candidates have been tested in the clinical setting over the last ten years (Evans *et al.*, 2016). Among them are those that are derived from whole cells components from *M. smegmatis* and *M. tuberculosis* (Evans *et al*., 2016). None have proven effective and the continued delay in developing an effective TB vaccine further exacerbates the global pandemic.

The most alarming aspect of the TB epidemic is the increasing prevalence of drug resistance, as seen in the outbreaks of multidrug-resistant (MDR), extensively-drug-resistant (XDR) and the totally–drug-resistant (TDR) TB (Smith *et al*., 2012). MDR-TB, the most prevalent form of drug-resistant TB, is classified as resistance to RIF and INH. XDR-TB is classified as MDR-TB that is additionally resistant to one of the injectable first-line drugs and a fluoroquinolone (Zhang *et al*., 2016). TDR –TB is resistant to all current anti-TB therapy (Laddomada *et al*., 2016). This evolution of resistance has highlighted an urgent need for new TB drugs. In mycobacteria, the cell envelope has been shown to confer an inherent tolerance to antibiotics (Flores *et al*., 2005). Designing novel anti-TB drugs would therefore require, amongst other factors, an enhanced understanding of key biological processes such as cell wall assembly and/or division. As these are central to this MSc study, they will be discussed further in the sections below, beginning with the mycobacterial cell wall.

1.3. The mycobacterial cell wall

Mycobacteria are classified as gram variable bacteria because they have characteristics of both Gram-negative and Gram-positive bacteria (Hett and Rubin, 2008). The common Gram-positive characteristics include the lack of a true outer membrane and the presence of a thick PG layer, while common Gram -negative characteristics include the presence of porins in the outer lipid layer and a potential periplasmic space (Hett and Rubin, 2008). The most crucial element of all bacteria is the cell wall. Its complexity and architectural feature allows bacterial cell survival and determination and maintenance of it shape. It is also responsible for the containment of cytoplasmic turgor (Scheffers and Pinho, 2005). A key role of the cell wall is the mediation of intrinsic drug tolerance and adaptation to environmental changes. The mycobacterial cell wall is composed of three components; the plasma membrane, the cell wall core or the mycolic acids- arabinogalactan-peptidoglycan (MAP) complex and the outer

most layer or the capsule-like layer (Grzegorzewicz *et al*., 2016). The central core/inner compartment consists of the covalently linked mycolic acids (M), arabinogalactan (A) and peptidoglycan (PG) layers, which make up the MAP complex (Figure 1.3) (Hett and Rubin, 2008). The complexity in the structure of these layers and the multitude of enzymes required to synthesize and remodel them creates unique opportunities to identify novel drug targets (Hett and Rubin, 2008, Morandi *et al*., 2013). In this study, we focus on enzymes that remodel PG, hence this component of the cell wall is discussed further.

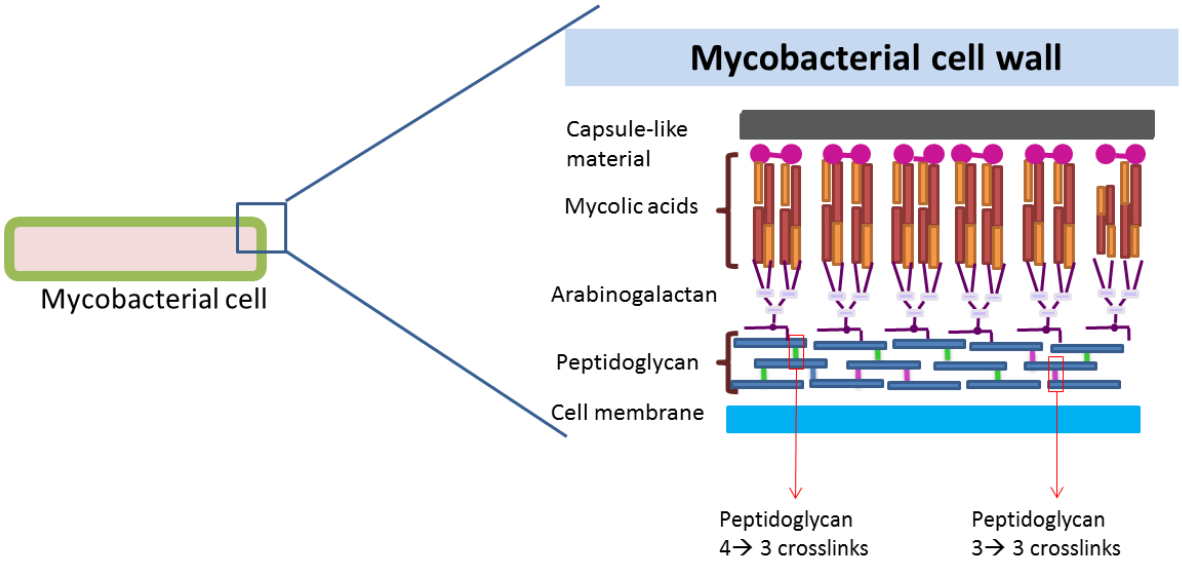


Figure 1.3: Components of the mycobacterial cell wall and the two types of cross-links (4→3 and 3→3 crosslinks) in the peptidoglycan (PG) layer. The structure of the mycobacterial cell wall is composed of the outer layer which consists of the capsule-like material and the plasma membrane. The inner compartments, on the other hand consist of the covalently linked mycolic acids- arabinogalactan- peptidoglycan making up the MAP complex. These layers are attached to the plasmid membrane in an outward manner starting with the peptidoglycan, followed by arabinogalactan and ending with the mycolic acid. In the PG, the 4-3 crosslinks are formed by the linkage of the terminal D-ala and the *meso*-diaminopimelic acid (*m*DAP) residues of alternating stem peptide while the 3-3 crosslinks are formed by the linkage between the alternating L- and D-centers of DAP residues of the PG stem peptide. Adapted from (Hett and Rubin, 2008, Kieser and Rubin, 2014).

1.3.1. Peptidoglycan

PG or murein is the innermost layer of the mycobacterial cell wall (Varma and Young, 2004). Although PG material is rigid, certain flexibility in this layer is required to allow for cell elongation during growth or the insertion of secretion apparatus (Hett and Rubin, 2008, Bertsche *et al*., 2015). PG contains two essential components, namely, the disaccharide unit/backbone (made up of *N*- aceytlmuramic acid [NAM] and *N*-acetylglucosamine [NAG]) and the pentapeptide moiety consisting of five alternating amino acid residues (L-alanyl-D-isoglutaminyl-*meso*-diaminopimelyl-D-alanyl-D-alanine), Figure 1.4 (Scheffers and Pinho, 2005). NAM and NAG are linked via β 1-4 glycosidic bonds and the pentapeptide moiety is attached to the NAM (Lederer *et al*., 1975). The pentapeptide is processed and cross-linked to adjacent peptide chains to form the crosslinked PG polymer. In mycobacteria, some of the NAM residues are *N*-glycosylated muramyl residues, which have been proposed to confer lysozyme resistance (Patru and Pavelka, 2010). For optimal bacterial growth, PG remodelling requires several synthases and hydrolases for processing and incorporation of new units into the existing cell wall (Cava *et al*., 2013).

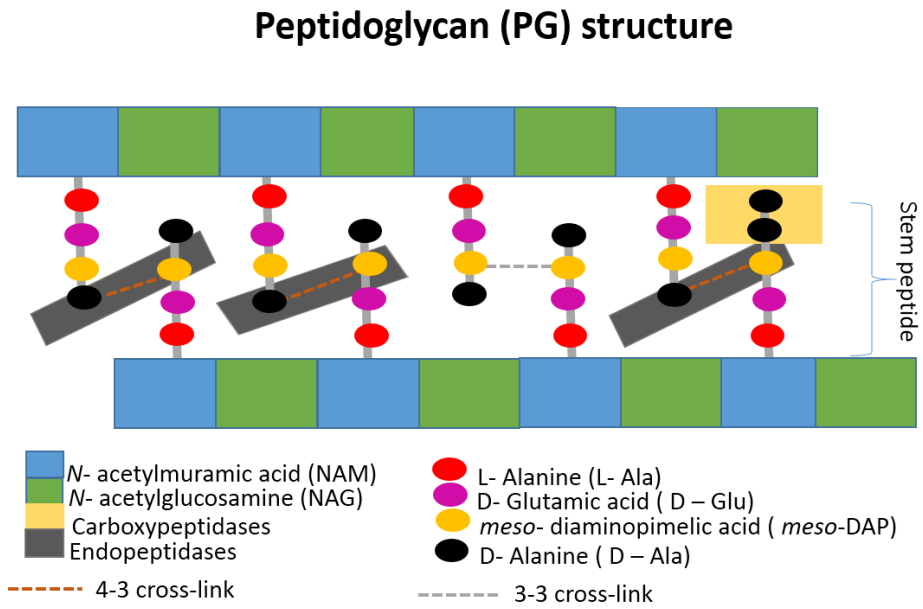


Figure 1.4: Structure of PG in mycobacterial species. Shown above are the NAM and NAG glycan components of the PG, along with the stem peptide residues. Stem peptides can be cross-linked in 4-3 or 3-3 conformations. Adapted from (Kieser and Rubin, 2014) .

1.3.2. Peptidoglycan biosynthesis

PG biosynthesis is divided into distinct steps that occur in the cytoplasm and periplasm (Figure 1.5) (Kong *et al*., 2010). During the first step of PG synthesis, in the cytoplasm, Lipid II or precursor disaccharide pentapeptides (*N*- acetylmuramyl pentapeptides) are generated (Moll *et al*., 2015). In the second, membrane-associated stage, a polysaccharide chain is formed through polymerization of *N*-acetylmuramyl pentapeptide and *N*-acetylglucosamine (Mathews *et al*., 2002). These precursors (Lipid II) are then flipped out of the cytoplasmic membrane into the periplasm, where they are assembled into the existing PG polymer by a group of enzymes termed penicillin-binding proteins (PBPs) (Moll *et al*., 2015).

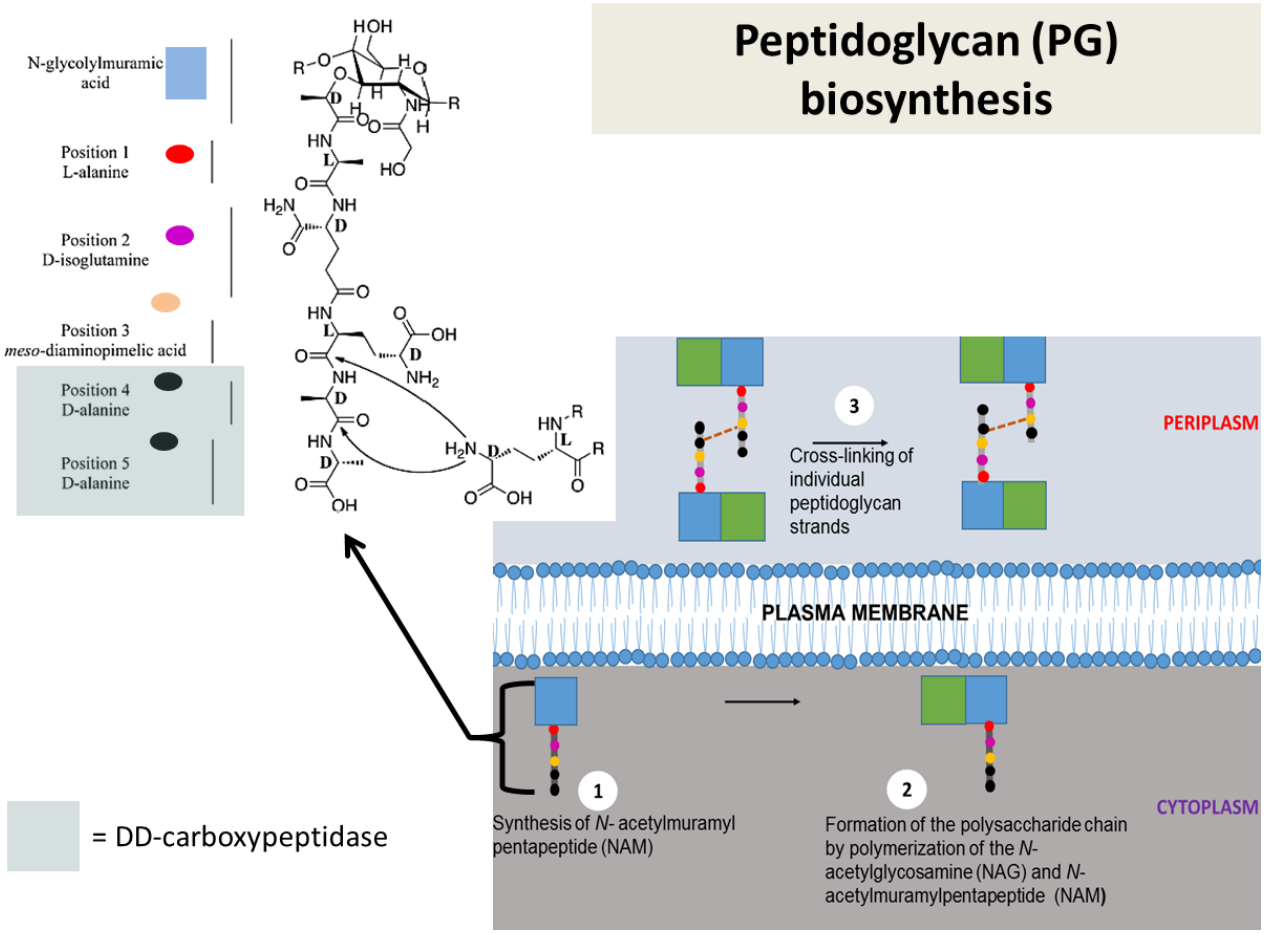


Figure 1.5: Biosynthesis and crosslinking of peptidoglycan. Three events required for the synthesis of PG. Note: *N*-glycolymuramic acid is replaced by *N*-acetylmuramic acid in mycobacteria. PG subunits are synthesized in the cytoplasm and then flipped into the periplasm where they are incorporated into the existing PG polymer. The structure of the individual residues in the PG subunit is shown, together the moieties that are used for catalysing incorporation into the PG by PBP. The position in the stem peptide where DD-Carboxypeptidases, of interest to the work done in this MSc, act is also shown. Adapted from (Wivagg *et al*., 2014, Mathews *et al*., 2002).

1.3.3. Peptidoglycan crosslinking

Approximately 80 % of the PG in *M. tuberculosis* is crosslinked (Patru and Pavelka, 2010). The majority of these links occur between the terminal D-ala residue (carboxyl-group) of the peptide moiety and the *m*DAP residue (amino group) from adjacent peptide, forming the 4→3 crosslink, but 1/3 of the links occur between alternating L- and D-centers of DAP residues forming the 3→3 crosslinks, both crosslinks are shown in Figure 1.3 and Figure 1.4 (Hett and Rubin, 2008, Kieser and Rubin, 2014). The former is thought to be the standard linkage and is catalysed by penicillin-sensitive DD-transpeptidases, while the latter, which is novel, has been hypothesised to be catalysed by LD-transpeptidases (Patru and Pavelka, 2010, Goffin and Ghuysen, 2002). The 3-3 crosslinks are thought to be essential for cell wall reinforcement during environmental stress or during stationary phase or non-replicating states. These two types of crosslinks that occur in PG and the degree of peptide cross-linking are important for bacterial growth and survival . These cross-links are regarded as the products of glycan-synthetic machinery and the enzymes involved in these processes are targets of β-lactam antibiotics (Patru and Pavelka, 2010, Wivagg *et al*., 2014).

1.3.4. Peptidoglycan remodeling by peptidoglycan hydrolases

Bacterial enzymes responsible for the cleavage of bonds in the PG sacculus are called PG hydrolases (Szwedziak and Lowe, 2013, Ghosh *et al.*, 2008). They are thus involved in PG turnover, cell division and separation, recycling and remodelling. The essential mycobacterial PG hydrolases are discussed below and their cleavage sites are described (Figure 1.6A). PG hydrolases are categorized into two classes depending on which bond they cleave. The first class, termed glycosidases, cleave the glycan backbone while the second class, termed peptidases, cleave the peptide side-chain of the PG strand. These two groups are further subdivided based on their cleavage site (Frirdich and Gaynor, 2013). Lytic transglycosylases are responsible for the cleavage of the β 1-4 bond between the NAG-NAM/NAG sugar subunits. This cleavage is accompanied by the formation of a 1,6-anhydrous ring on NAM. In mycobacteria this group of enzymes consist of proteins known as resuscitation-promoting factors (RPFs) (Frirdich and Gaynor, 2013). L,D- transpeptidases are responsible for hydrolyzing amide bonds between a D- and a L- amino acid of the peptide moiety (Frirdich and Gaynor, 2013). They also play a role in converting 4→3 crosslinks to 3→3 crosslinks

through cleavage of the D-ala residue from the side-chain donor and creation of a tripeptide chain in PG during stationary phase (Figure 1.4) (Jankute *et al.*, 2015). Amidases (*N*-acteylmuramyl-L-alanine amidases) are responsible for cleavage of the peptide side-chains from glycan strands by hydrolyzing the bond between the NAM and L-ala residue of the stem peptide (Frirdich and Gaynor, 2013). Endopeptidases cleave bonds between cross-linked stem peptide moieties (Rioseras *et al.*, 2016). This MSc focuses particularly in PBPs, which are discussed further below.

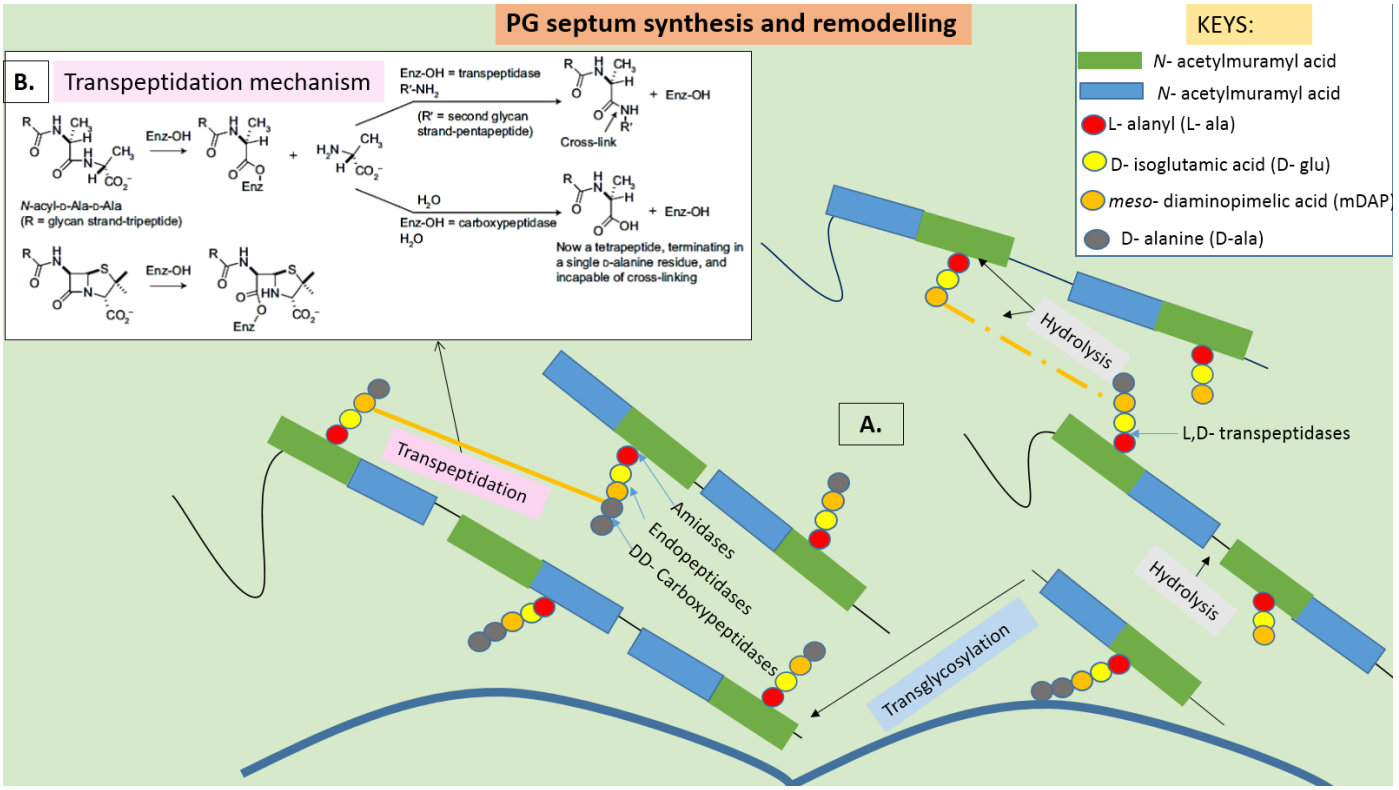


Figure 1.6: Enzymes involved in peptidoglycan synthesis and remodelling. (A.) Illustration showing metabolic reactions contributing to PG synthesis (either at the septum or cell pole) and PG remodelling. Amidases, lytic transglycosylases, and endopeptidases are involved in hydrolysis reaction. Adapted from (Xiao and Goley, 2016). (B.) Illustration of the enzymatic mechanism of transpetidation, which occur similarly between the terminal D-alanyl D-alanine and penicillin. Also shown is the double displacement of the enzymatic transpetidation mechanism for the cross-linking process by β-lactam antibiotics or through carboxypeptidation. Adapted from (Buynak, 2007).

1.4. Penicillin-binding proteins

Penicillin-binding proteins (PBPs) are a group of proteins responsible for the biosynthesis of PG. PBPs are divided into two categories depending on their sizes, i.e. low-molecular-weight (LMW) and high-molecular-weight (HMW) (Sauvage *et al.*, 2008). These are further divided

into three classes and will be discussed below. PBPs and β-lactamases are the molecular targets of β-lactam antibiotics, a class of drugs currently used to treat bacterial infections. The drug irreversibly binds to protein families containing transpeptidase domains (Konaklieva, 2014). These antibiotics account for about 55 % of all currently used antibiotics globally (Bhattacharjee, 2016). They also interfere with machinery responsible for the assembly of bacterial cell wall by inhibiting polymerization of the last step of the PG (Figure 1.5, step 3) (Buynak, 2007). Moreover, considering the function of PBPs in the cell cycle, these proteins are further divided in two categories namely, cell division-associated and peripheral synthesis/elongation associated PBP (Scheffers and Pinho, 2005). It is thought that these proteins exert their functions via association with other proteins and these interactions can occur in one of two ways, namely, 1) interaction of PBPs and other proteins involved in cell wall synthesis and/or 2) interaction of various PBPs in multi-enzyme complexes (Scheffers and Pinho, 2005). As most PBPs depend on each other for targeting their site of activity, this study will investigate the localization of DD-carboxypeptidases (hereafter referred to as DD-CPases), together with other cell wall remodeling enzymes in *M. smegmatis*.

1.4.1. High-molecular-weight penicillin-binding proteins

HMW PBPs mediate polymerization of the PG and are usually bifunctional enzymes possessing both transglycosylase and transpeptidase domains (Hett *et al*., 2010). Moreover, they are classified as essential for growth (Basu *et al*., 1996). The *E. coli* genome encodes three bi-functional PBPs (i.e. PBP1A, PBP1B and PBP1C)(Szwedziak and Lowe, 2013, Kieser et al., 2015). In contrast, the genomes of *M. tuberculosis* and *M. smegmatis* encode two bifunctional PBPs (PonA1 and PonA2) and three (PonA1, PonA2 and PonA3), respectively (Machowski *et al*., 2014, Kieser *et al.*, 2015). In *M. tuberculosis*, PonA1 and PonA2 are targeted to the perisplamic space via a signal peptide. In addition to the domains previously described, they also have additional (PBP and serine/threonine-kinase [STPK] associated) domains and a transmembrane helix (TM) (Jankute *et al*., 2015). Interestingly, both PonA1 and PonA2 from *M. tuberculosis* are hypothesized to interact with Ldt (Kieser *et al*., 2015). The genetic association of these genes means that although they serve a similar function, each one could have distinct cellular roles with varying susceptibility to host-derived stresses or exposure to antibiotics (Kieser *et al*., 2015).

1.4.2. Low-molecular-weight penicillin-binding proteins

LMW PBPs display one of two activities, namely exolytyic DD-CPase activity (targeted at cleavage of the terminal D-alanine from the pentapeptide side-chain or endopeptidase activity, which cleaves previously formed cross-links (Fisher and Mobashery, 2014). LWM PBPs or "the accessory cell division proteins" are involved in cell maturation/recycling of the PG and regulate the amount of PG crosslinking (Ghosh *et al.*, 2008, Egan and Vollmer, 2013). In *E. coli*, there are seven LMW PBPs which are individually non-essential for survival, however combinatorial deletion of these results in defects in cell shape (Sauvage *et al*., 2008). These observations suggest that due to their highly homologous nucleic acids sequences, a multiplicity of homologues is able to compensate for the loss of any given member. Despite being dispensable, a fine balance between the activities of HMW and LMW PBPs needs to be maintained in order to ensure viability (Basu *et al*., 1992).

1.4.3. Domains / conserved motifs of penicillin-binding proteins in all bacterial organisms

The active sites of LMW PBPs contain conserved residues with the sequences S*XX*K (Motif 1) which contains the catalytic serine, the S*X*N/S*X*C (Motif 2) and [K/H][T/S]G (Motif 3) triads (Goffin and Ghuysen, 1998, Laddomada *et al*., 2016, Goffin and Ghuysen, 2002) (Figure 1.7). The orientation of these three sites allows for two crucial processes to occur, namely acetylation and deacetylation (Rossi *et al*., 2016). Additionally, these conserved motifs have been hypothesized to occur in the same order and roughly the same spacing along polypeptide chains (Goffin and Ghuysen, 2002, Scheffers and Pinho, 2005). For example, the three conserved motifs have been identified in PBP4 from *E. coli*, PBP4a from *B. subtilis*, D,D-peptidase from *Actinomadura* R39, DD-transpeptidase from *Streptomyces* K15 (Figure 1.7) and PBP4 (DacB) of *Pseudomonas aeruginosa* (Rossi *et al*., 2016). The molecular structure of PBP4 (DacB) from mycobacterial species has not yet been solved. As mentioned previously, the prevailing evidence suggests that LMW PBPs play accessory roles in cell division. This hypothesis was investigated further in this MSc. For further context, cell division in rod-shape bacteria and mycobacteria are discussed in the next few sections.

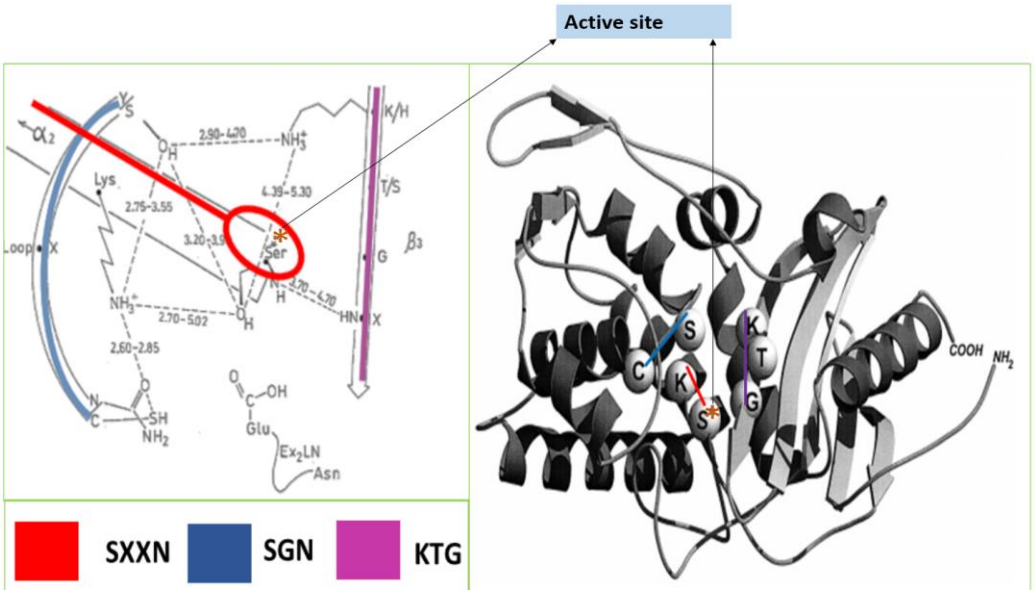


Figure 1.7: Illustration of the catalytic centre of penicilloyl serine transferases. Shown is the location of three conserved motifs of bacterial PBP. Red= motif 1 (SXXK), blue=motif 2 (SXN/SXC) and purple= motif 3 ([K/H][T/S]G). The (*) represents the essential serine residue. The model species used to show the conserved regions is *Streptomyces* strain K15 PBP. Adapted from (Goffin and Ghuysen, 1998, Goffin and Ghuysen, 2002).

1.5. Cell growth and division in mycobacteria

The ability of *M. tuberculosis* to remain dormant for extended periods of time before it can grow and progress into active TB disease is one of the most remarkable features of the non-sporulating mycobacterial species (Hett and Rubin, 2008, Kang *et al*., 2008). Biological mechanisms that enable this are not well defined and/or have only been described in select organisms (Hett *et al*., 2010). Challenges involving understanding these processes include uncertainties of how bacteria retain their normal architecture as cells start to divide and once division has been completed, how bacterial cells carry out the synthesis and breakdown of the cell wall components for separation of daughter cells remains only partially resolved (Hett and Rubin, 2008). Moreover, the mechanisms that enable bacterial cells to regulate cell division in order to contain cytoplasmic turgor pressure or respond to environmental stimuli requires further elucidation (Hett and Rubin, 2008). In this regard, synthesis and regulation of peptidoglycan (PG), a cell wall component, has been proposed to be one of the features that can be used to understand bacterial growth and cell division (Szwedziak and Lowe, 2013).

1.5.1 Modes of growth in rod-shape bacteria

Bacterial cell growth is achieved by directing the synthesis of new cell wall material to specific sites/regions inside the bacterial cell where nascent PG is inserted (Table 1.2 and Figure 1.8) (Joyce *et al*., 2012, Hett and Rubin, 2008). At these specific locations, PG hydrolases (autolysins) and PG synthases incorporate new units into the existing structure, thereby expanding the cell wall (Hett *et al*., 2010). Failure to properly coordinate these processes may lead to cell lysis (Kieser and Rubin, 2014). Inner membrane and periplasmic complexes involved in spatio-temporal organization of the cell wall materials during PG remodeling and those that govern PG synthesis are known as the elongasome and divisome complexes, respectively (Szwedziak and Lowe, 2013). The steps which ultimately leads to the production of two daughter cells follows a sequential process (see Figure 1.3 B), namely, plasma membrane synthesis during cytokinesis (usually at mid-cell), PG synthesis during septation (septum/mid-cell), cell wall constriction (at mid-cell), septum hydrolysis and physical separation of daughter cells by binary fission (Kieser and Rubin, 2014).

Table 1.2: Different modes of growth in rod-shape bacteria and regions of active peptidoglycan synthesis (Randich and Brun, 2015). The modes of growth applicable to mycobacteria are highlighted in yellow.

Growth Modes	**Region of active PG synthesis**	**Rod-shape bacteria**
Lateral elongation	Dispersed or along sidewalls	*E. coli, B. subtilis, C. crescentus*
Polar elongation	One or both cell poles	*Actinobacteria (including mycobacteria) and Rhizobiales*
Septation/Cytokinesis	Septum/mid-cell	
Pre-septal or Medial elongation	Near division plate/ mid-cell	*C. crescentus, E. coli, A. tumefaciens*
Budding	End of stalks and/or off cell body	*Hyphomicrobiacae, Bradyrhizobiaceae*
Stalk elongation	Cell stalk junction	*Caulobacter, Asticcacaulis*

Key words: *Agrobacterium tumefaciens* (*A. tumefaciens); Bacillus subtilis (B. subtilis); Caulobacter crescentus (C. crescentus); Escherichia coli* (*E. coli);* Peptidoglycan (PG)

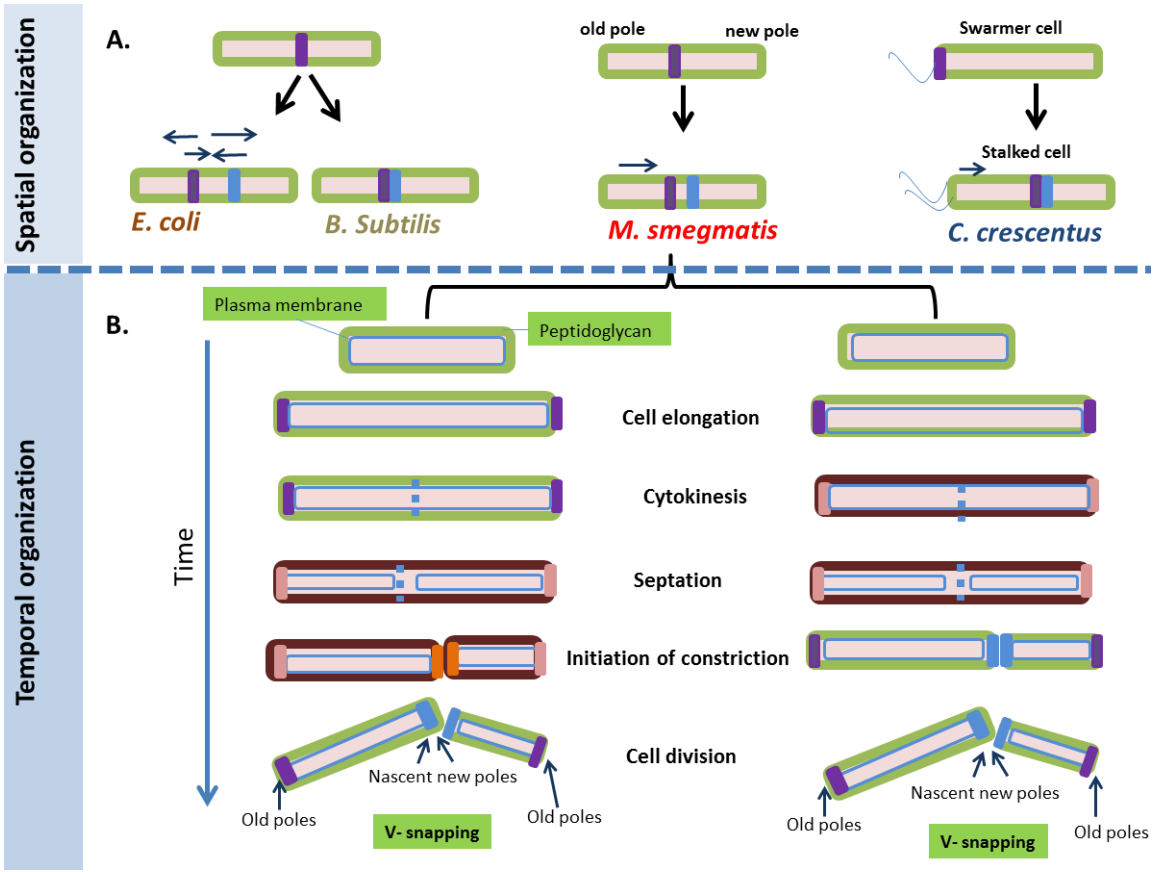


Figure 1.8: Bacterial replication modalities. (A) Spatial and temporal organization of rod-shape bacteria of various organisms through cell division. (B) Asymmetrical cell growth. Arrows in (A) represent the direction of the replisome (shown in purple and blue) movement and arrows in (B) show PG synthesis at the cell pole (Trojanowski *et al*., 2015, Kieser and Rubin, 2014).

1.5.2. Enzymes involved in bacterial cell division and cell elongation

The Tubulin-like protein, FtsZ. Before bacterial cell division can occur, a Z-ring must form followed by constriction which also requires the recruitment of other cell division proteins to the division site in *E. coli* (Varma and Young, 2004). This Z-ring comprises of FtsZ polymers and determines the septation sites in addition to acting as a scaffold for downstream PG remodelling enzymes (Kieser and Rubin, 2014). The FtsZ protein usually initiates cell division and together with other cell division protein, generally localizes at the middle/septum of the bacterial cell (Scheffers, 2005, Scheffers and Pinho, 2005)

The Tropomyosin-like protein, DivIVA (Wag31). DivIVA (or Wag31 in mycobacteria) is essential for growth and is required for spatial regulation of peptidoglycan synthesis (Joyce *et al*., 2012). Unsurprisingly, it is also determines sites of cell growth and morphology in mycobacteria (Joyce *et al*., 2012, Meniche *et al*., 2014). Its association with cell wall

biosynthesis enables it to act as an adapter for various enzymes including penicillin-binding proteins (PBPs) (Joyce *et al*., 2012, Plocinski *et al*, 2012). Its localization at cell poles, post cell division, and at sub-poles during cell elongation corresponds to nascent cell wall deposition sites (Cameron *et al*., 2015, Meniche *et al*., 2014). Differential concentrations of DivIVA at the cell poles has been shown to play a role in the determination of growth site and in its absence, cell division is blocked, thereby resulting in a filamentous phenotype with anucleate cells (Meniche *et al*., 2014, Cameron *et al*., 2015).

PonA2. PonA2 is a PBP that contains a Penicillin-binding protein and Serine/Threonine Kinase-Associated (PASTA) domain, which is thought to interact with the terminal D-ala D-ala of PG pentapeptides that are not cross-linked (Fleurie *et al*., 2012). This domain allows PonA2 to interact with PG pentapeptide precursors and acts as a mechanism for sensing whether cells are dividing or not (Patru and Pavelka, 2010). PonA2 is also classified as bifunctional High-molecular-weight (HMW) PBP and forms part of the elongasome (Strobel *et al*., 2014).

1.5.3. Cell division and growth in mycobacteria

In actinobacteria, including mycobacteria, *B. subtilis* and *E. coli*, the anchor protein DivIVA guides cell wall synthesis. In *B. subtilis* and *M. tuberculosis*, DivIVA (Wag31) identifies the curvature in the membrane and ensures that cell extension occurs at the poles whilst simultaneously recruiting other components of complex (Dworkin, 2009, Lybarger and Maddock, 2001). DivIVA has also been suggested to interact with lipid II, the PG precursor that flipped into the periplasm for crosslinking and PG extension. The localization of DivIVA to the sub-polar regions of the cell pole is followed by recruitment of biosynthetic enzymes required for synthesis of mycolic acids and arabinogalactan, the additional layers of the mycobacterial cell envelope. The resulting enzyme complex allow for elongation of the cell pole, through insertion of new cell wall material at the sub-polar region (Meniche *et al*., 2014). Post cell elongation, mycobacteria then divide to form two daughter cells. This division occurs asymmetrically through the coordination of the divisome complexes (Kieser and Rubin, 2014, Laddomada *et al*., 2016). This co-ordination of PG synthesis, splitting and division of cells is driven by numerous proteins including the PG synthases and hydrolases (PBP1b and possibly PBP1a), cytoskeletal-like proteins and the structural proteins. All

bacterial division complexes involve the FtsZ proteins, while the elongation apparatus may or may not involve the murein region ´e´ (Mre) complex (Szwedziak and Lowe, 2013).

Cytoskeletal *mre* genes were first identified in *E.coli,* but have now been discovered in a variety of eubacteria and archaea including the commonly studied rod-shape bacteria *B. subtilis* and *C. crescentus* (Steward, 2005, Wang *et al*., 2012). Proteins belonging to the Mre family (MreB or Mbl, MreC and MreD) have been shown to play a role in helical and actin-like cables formation in the bacterial cell wall (Daniel and Errington, 2003). MreB cytoskeleton has been also shown to play a role in the directional helical insertion of the PG which then orders the bacterial cell wall to either twist to the left or right during elongational growth (Wang *et al*., 2012). The left- or right-handed chirality of filaments in elongating bacteria plays a role in coordinating the insertion, rod-shape formation and cross-linking of the cell wall during PG synthesis by twisting the cell wall as the cell grows (Huang *et al*., 2012). *E. coli* twists in a left-handedness direction while *B. subtilis* twists in a right-handedness direction during elongational growth. Such physical principles links cell growth to the mechanisms of cell wall synthesis (Wang *et al*., 2012). Additionally, during cell elongation or lateral PG synthesis, MreB and/or Mbl helicases either acts as a permanent scaffolding protein, transient scaffold protein and/or secondary protein (Osborn and Rothfield, 2007). In the first mechanism, they are hypothesized to play a role in the recruitment and maintenance of multiprotein assembly during cell elongation/ lateral cell wall synthesis. In the second mechanism, they are hypothesized to be involved in the biosynthesis apparatus maintenance and in the third mechanism MreB acts as a secondary-recruited protein associated with the assemblage of murein (PG) biosynthetic complex scaffolding the pre-existing helicases in the cell wall (Osborn and Rothfield, 2007). Mutational analysis of the *mre* genes (for example, mutated *mreB* and/or *mreBCD* gene deletion) in *E. coli* have been shown to play a role in the rod-to-spherical shape conversion and negative regulation of PBP3 also known as FstI protein during septal synthesis (Stewart, 2005, Osborn and Rothfield, 2007).

Mycobacteria do not contain homologs of the Min or Mre systems, which are required for nucleoid occlusion and lateral cell wall growth respectively (Joyce *et al*., 2012). As a result, alternative systems that regulate cell shape and division are used. These include the serine/threonine protein kinases (STPK) such as the *pknB,* the gene for which is located at cell division clusters near the origin of replication (*ori*) and *pknA* which regulates the action of FtsZ via phosphorylation (Thanky *et al*., 2007, Kieser and Rubin, 2014).

1.5.4. Review of selected penicillin-binding proteins and cell wall machinery

Recent work done in our laboratory suggests that the *dacB*-encoded DD-CPase in the genome of *M. smegmatis* is an essential gene due to the inability to produce a knockout mutant strain. To further study its function, a knockdown strain was created (Ealand *et al*., unpublished). An interesting phenotype observed in this case was the loss of PG precursor staining on one cell pole. It has been demonstrated that mycobacterial cell elongation occurs via extension from both cell poles, which implicates DacB in regulation of PG synthesis (Ealand *et al*., unpublished). Additionally, DacB repression caused cells to be shorter than the wild-type strain. To further study the function of DacB, this project will focus on protein localization together with other cell division proteins in *M. smegmatis.* The selected genes used and corresponding counterparts in *M. tuberculosis*, together with their essentiality in mycobacteria are listed in Table 1.3.

1.6. Project overview

1.6.1. Problem statement

The cause and spread of drug-resistant TB is influenced by numerous factors ranging from the basic (health care) to the most complex (molecular interplay and metabolic flexibility of *M. tuberculosis* during treatment). These factors include socio-demographics (impoverished households, ethnicity etc.), epidemiology (high incidence countries), pathogenesis, genetics (development of drug-resistant TB strain) and the actual drug mechanism (biological and mechanistic processes). The first two factors pose a major threat and have huge impact in the accelerated transmission of drug-resistant TB strain. As a result and especially in countries where the TB endemic is high, these factors influence the economy, politics and social dynamics. The last three factors dictate the success or failure rate of drugs administered to TB patients, which then contribute to the development of drug-resistant TB strains. Design of improved, shorter treatment regimens, which can be used in combination with antiretroviral therapy (ART), requires a detailed understanding of key biological processes that modulate different disease states, such as cell division processes. Currently, our understanding of the cell division machinery in mycobacteria is incomplete. We will attempt to address this problem, to some extent, in this MSc by localizing LMW PBPs in mycobacteria.

Table 1.3: Selected genes used in this study and their mycobacterial homologs.

Gene	Gene Homolog in *Mycobacterium smegmatis*	Gene Homolog in *Mycobacterium tuberculosis*	LMW / HMW PBP	Activity \ Product	Essentiality in bacteria	
					Non-essential	Essential
dacB	MSMEG_6113	Rv3627c	LMW PBP	DD-endopeptidase DD-carboxypeptidases		✓
dacB1	MSMEG_1661	Rv3330	LMW PBP	DD- carboxypeptidase	✓	
N/A	MSMEG_2432 (duplicate of MSMEG_2433)	N/A	LMW PBP	DD- carboxypeptidase	✓	
dacB2	MSMEG_2433	Rv2911	LMW PBP	DD- carboxypeptidase	✓	
ponA2	MSMEG_6201	Rv3682	HMW PBP	Transglycosylase/ Transpeptidase		✓
divIVA	MSMEG_4217	Rv2145c	-	DIVIVA protein		✓
ftsZ	MSMEG_4222	Rv2150c	-	Cell division protein FtsZ		✓

LMW = Low molecular weight **HMW**= High molecular weight **PBP**= Penicillin binding protein

1.6.2. Hypothesis

We hypothesize that DacB, a bifunctional DD-Cpase localizes at sites of cell wall synthesis and that it is involved in the coordination of cell division and cell growth in *M. smegmatis.* We also presume that the mislocalization can be used to monitor disruption of PG crosslinking. We also hypothesize that DacB interacts and co-localizes with other known cell division-associated enzymes, including PonA2, FtsZ and DivIVA in the wild-type strain and that this pattern may be disrupted in mutant strains lacking two or three DD-CPase homologues.

1.6.3. Rationale of the study

Ideal TB drugs are those that can completely kill the bacteria, including persister cells, in a relatively short space of time. Current TB drug regimens fall short of this requirement and in combination with the emergence of drug-resistance, necessitate the identification of novel drug targets. In general, bacterial proteins must localize at specific regions in or around the cell membrane to perform their specific function. During cell division, accurate protein localization depends on multiple factors which influences cellular processes (e.g. cell elongation and division; cell signaling; secretion and sorting). Mycobacteria have very complex cell walls with several layers. This study focuses specifically on the PG to elucidate the localization pattern of certain proteins required for its biosynthesis. Ultimately, we hope to identify potential novel drug targets for TB.

1.6.3.1 Aim of the study

The aim of the study is to elucidate the localization patterns of proteins required for peptidoglycan biosynthesis in *M. smegmatis.*

1.6.4. Research objectives

The objectives for this study are:

1. Create localization plasmids that allow for expression of fusion proteins to localize DD-CPases in *M. smegmatis* using three-way cloning strategy.
2. Create plasmids that allow for localization of key cell division proteins such as FtsZ, PonA2 and DivIVA using three-way cloning strategy.
3. Create a mutant of *M. smegmatis* that lacks two DD-CPases (MSMEG_2433 and MSMEG_2432) using two-step allelic exchange by homologous recombination.
4. Examine the localization of DacB in DD-carboxypeptidase double gene knockout mutants Δ1661 Δ2432, Δ1661 Δ2433, and Δ2433 Δ2432 using microscopy and study their localization relative to DacB in wild-type *M. smegmatis* and mutants defective for DD-CPases using Click chemistry.

5. To investigate the localization PonA2, FtsZ and DivIVA in mycobacteria to study their localization relative to DacB in wild-type *M. smegmatis* and mutants defective for DD-CPases

6. To evaluate the role of DD-CPases in *M. smegmatis* wild-type, mutant (Δ2433 Δ2432) and the complemented (△2433 △2432:: 2433/2432) strains during *in vitro* growth and biofilm growth. This was done by measuring pellicle formation of the biofilms using microscopy and quantifying biomass of the biofilms using crystal violet assay.

1.2.5 Expected outcomes

The anticipated localization patterns for the proteins targeted in this MSc are shown in Figure 1.9. At the end of this project, we should be able to:

1. Identify the cellular localization pattern of DacB, whether at the septum (mid-cell), uni/bi-polar, or sub-polar in relation to other HMW PBPs and cell division proteins

2. Determine if the localization patterns of DacB and PonA2, FtsZ and DivIVA overlap, suggesting possible interactions.

3. Determine if DD-CPase localization in mycobacteria requires a full complement of these LMW PBPs.

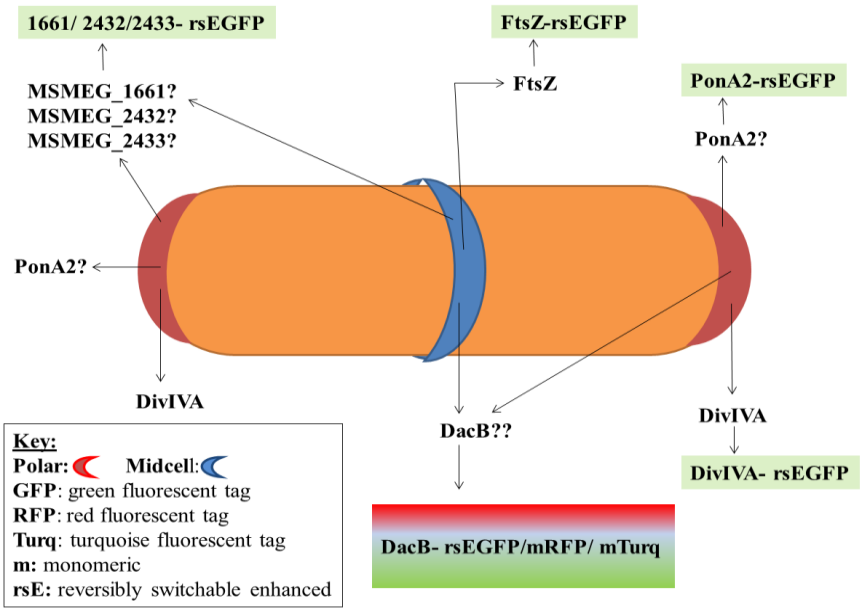


Figure 1.9: Illustration of anticipated localization patterns of the DD-CPases and other cell division enzymes in *M. smegmatis* that are involved in PG remodelling. We expect that the DD-CPases MSMEG_1661, MSMEG_2433, MSMEG_2432 will assume polar localization patterns. Given its essentiality for growth, we expect that DacB will assume a septal or possibility a polar and septal localization pattern.

CHAPTER 2: MATERIALS AND METHODS

Section A: Materials

2.1 Chemicals and reagents used in the study

Restriction enzymes, DNA amplification reagents, and other enzymes used for molecular DNA modification purposes were either supplied by Roche (Roche, Johannesburg, RSA), New Lab Biolabs (NEB) from Inqaba Biotech™, Sigma (Sigma-Aldrich®, Johannesburg, RSA) or Thermo Scientific™ (ThermoFisher Scientific, Johannesburg, RSA) companies. All primers used in this study were purchased from Inqaba Biotech™ (Inqaba, Pretoria, RSA), unless otherwise stated.

2.1.1 Plasmids, strains and primers used in this study

Table 2.1: Plasmids used in this study

Name	Description	Source
Cloning vectors		
pMV306H (pMV)	L5 integrating proficient *E. coli–Mycobacterium* shuttle vector integrating at $tRNA^{Gly}$; Hyg^r	Stover *et al*. (1991)
pTweety (pTw)	L5 integrating proficient *E. coli–Mycobacterium* shuttle vector integrating at $tRNA^{Lys}$: Kan^r	Pham *et al*. (2007)
p2NIL_2433_2432	Gene knockout vector for creating an in-frame (or out-of-frame) deletion in MSMEG_2433 and MSMEG_2432	Ismail *et al*. (unpublished)
pGOAL_19	Plasmid carrying *lacZ-sacB-Hyg*^{r} markers as a *PacI* cassette; Hyg^r	(Parish and Stoker, 2000)
Plasmids		
p2NIL_pac_1661	Gene knockout vector for creating MSMEG_1661 mutant	Ealand *et al*. (unpublished)
p2NIL_pac_2432	Gene knockout vector for creating MSMEG_2432 mutant	Ealand *et al*. (unpublished)
p2NIL_2433_2432::pG19	Derivative of mc^2155 carrying an unmarked deletion in *M. smegmatis MSMEG_2433*	This study
pMV306H_1661	Derivative of MSMEG_1661 (plus native	Ealand *et al*.

	promoter /150 bp upstream of start codon); Hyg^r	(unpublished)
pMV306H_2432	Derivative of MSMEG_2432 (plus native promoter /150 bp upstream of start codon); Hyg^r	Ealand *et al*. (unpublished)
pMV306H_2433	Derivative of MSMEG_2433 (plus native promoter /150 bp upstream of start codon); Hyg^r	Ealand *et al*. (unpublished)
pMV_dacB_GFP	Derivative of DacB (plus native promoter /150 bp upstream of start codon), carrying an in-frame C-terminal rseGFP tag; Hyg^r	This study
pMV_dacB_mRFP	Derivative of DacB (plus native promoter /150 bp upstream of start codon), carrying an in-frame C-terminal mRFP tag; Hyg^r	This study
pMV_ DacB_mTurq_	Derivative DacB (plus native promoter /150 bp upstream of start codon), carrying an in-frame C-terminal mTurquiose tag; Hyg^r	This study
pMV_ DacB_mCherry_	Derivative of DacB (plus native promoter /150 bp upstream of start codon), carrying an in-frame C-terminal mCherry tag; Hyg^r	This study
pMV_MSMEG_1661_GFP	Derivative of MSMEG_1661(plus native promoter /150 bp upstream of start codon), carrying an in-frame C-terminal rseGFP tag; Hyg^r	This study
pMV_MSMEG_2432_GFP	Derivative of MSMEG_2432 (plus native promoter /150 bp upstream of start codon),carrying an in-frame C-terminal rseGFP tag; Hyg^r	This study
pMV_MSMEG_2433_GFP	Derivative of MSMEG_2433 (plus native promoter /150 bp upstream of start codon),carrying an in-frame C-terminal rseGFP tag; Hyg^r	This study
pTw_ PonA2_GFP	Derivative of PonA2 (plus native promoter /150 bp upstream of start codon), carrying an in-frame C-terminal rseGFP tag; Hyg^r	This study
pTw_ FtsZ_GFP	Derivative of FtsZ (plus native promoter /150 bp upstream of start codon),carrying an in-frame C-terminal rseGFP tag; Kan^r	This study
pTw_ DivIVA_GFP	Derivative of DivIVA (plus native promoter /150 bp upstream of start codon), carrying an in-frame C-terminal rseGFP tag; Kan^r	This study
pMV_GFP	Derivative of a green fluorescence protein retaining the native start and added stop codons; Hyg^r	This study
pMV_ mRFP	Derivative of a monomeric red fluorescence protein retaining the native start and added stop codons; Hyg^r	This study
pMV_ mTurq	Derivative of a monomeric turquoise fluorescence protein retaining the native start and added stop codons; Hyg^r	This study
pMV_ mCherry	Derivative of a monomeric cherry fluorescence	This study

	protein retaining the native start and added stop codons; Hyg^r	

Table 2.2: Strains used in this study

Name	Description	Source
Strains		
mc^2 155	*M. smegmatis* electrocompetent strain ept-1 derived from *mc^{2}6*	Lab stock
E. coli (DH 5 α)	*Escherichia coli* SupE44 ΔlacU169 hsdR17 recA1 endA1 gyrA96 thi-1 relA1	Promega
mc2 155::pMV_DacB_GFP	Derivative of mc^2 155 carrying in-frame DacB_GFP in pMV306H with plasmid integrating at the L5 *attB* site; Hyg^r	This study
mc2 155::pMV_DacB_Mrfp	Derivative of mc^2 155 carrying in-frame dacB_mRFP in pMV306H with plasmid integrating at theL5 *attB* site; Hyg^r ;	This study
mc^2 155::pMV_DacB_mTurq	Derivative of mc^2 155 carrying in-frame DacB_mTurquoise with plasmid integrating at the L5 *attB* site; Hyg^r	This study
mc^2 155::pMV_MSMEG_1661_GFP	Derivative of mc^2 155 carrying in-frame MSMEG_1661_GFP in pMV306H with plasmid integrating at the L5 *attB* site; Hyg^r	This study
mc^2 155::pMV_MSMEG_2432_GFP	Derivative of mc^2 155 carrying in-frame MSMEG_2432_GFP in pMV306H with plasmid integrating at the L5 *attB* site; Hyg^r	This study
mc^2 155::pMV_MSMEG_2433_GFP	Derivative of mc^2 155 carrying in-frame MSMEG_2433_GFP in pMV306H with plasmid integrating at the L5 *attB* site; Hyg^r	This study
Δ2433 Δ2432	Derivative of ΔMSMEG_2433 carrying an unmarked , in-frame deletion in ΔMSMEG_2432	This study
Δ2433 Δ2432 :: pMV_DacB_GFP	Derivative of ΔMSMEG_2433 and ΔMSMEG_2432 carrying in-frame DacB _GFP in pMV306H with plasmid integrating at the L5 *attB* site; Hyg^r	This study
Δ2433 Δ2432::pTw_FtsZ_GFP	Derivative of ΔMSMEG_2433 and ΔMSMEG_2432 carrying in-frame FtsZ_GFP in pTweety, with plasmid integrating at the *attP* site; Kan^r	This study
Δ2433 Δ2432::pTw_DivIVA_GFP	Derivative of ΔMSMEG_2433 and ΔMSMEG_2432 carrying in-frame	This study

	DivIVA_GFP in pTweety, with plasmid integrating at the *attP* site; Kan^r	
Δ2433 Δ2432::pTw_PonA2_GFP	Derivative of ΔMSMEG_2433 and ΔMSMEG_2432 carrying in-frame PonA2_GFP in pTweety, with plasmid integrating at the *attP* site; Kan^r	This study
Δ1661Δ2432	Derivative of ΔMSMEG_2432 carrying an unmarked , in-frame deletion in mc2155 MSMEG_1661	Ismail *et al*. (unpublished)
Δ1661 Δ2432::pMV_DacB_GFP	Derivative of ΔMSMEG_1661 and ΔMSMEG_2432 carrying in-frame *dacB*_GFP in pMV306H with plasmid integrating at the L5 *attB* site; Hyg^r	This study
Δ1661 Δ2432::pTw_FtsZ_GFP	Derivative of ΔMSMEG_1661 and ΔMSMEG_2432 carrying in-frame *ftsZ*_GFP in pTweety with plasmid integrating at the *attP* site; Kan^r	This study
Δ1661 Δ2432::pTw_DivIVA_GFP	Derivative of ΔMSMEG_1661 and ΔMSMEG_2432 carrying in-frame *divIVA*_GFP in pTweety with plasmid integrating at the *attP* site; Kan^r	This study
Δ2433 Δ2432::2432	Derivative of ΔMSMEG_2433 and ΔMSMEG_2432 complemented with pMV306H_2432 vector	This study
Δ2433 Δ2432::2433	Derivative of ΔMSMEG_2433 and ΔMSMEG_2432 complemented with pMV306H_2433 vector	This study
Δ1661 Δ2432::pTw_PonA2_GFP	Derivative of ΔMSMEG_1661 and ΔMSMEG_2432 carrying in-frame *ponA2*_GFP in pTweety with plasmid integrating at the *attP* site; Kan^r;	This study
Δ2433 Δ1661	Derivative of ΔMSMEG_2433 carrying an unmarked , in-frame deletion in *mc^2155* MSMEG_1661	Ismail *et al*. (unpublished)
Δ2433 Δ1661::pMV_DacB_GFP	Derivative of ΔMSMEG_2433 and ΔMSMEG_1661 carrying in-frame *dacB*_GFP in pMV306H with plasmid integrating at the L5 *attB* site; Hyg^r	This study
Δ2433 Δ1661::pTw_FtsZ_GFP	Derivative of ΔMSMEG_2433 and ΔMSMEG_1661 carrying in-frame *ftsZ*_GFP in pTweety with plasmid integrating at the *attP* site; Kan^r	This study
Δ2433 Δ1661::pTw_DivIVA_GFP	Derivative of ΔMSMEG_2433 and ΔMSMEG_1661 carrying in-frame *divIVA*_GFP in pTweety with plasmid integrating at the *attP* site; Kan^r	This study
mc^2 155::pTw_PonA2_GFP	Derivative of mc^2 155 carrying in-frame	This study

	PonA2_GFP in pTweety with plasmid integrating at the *attP* site; Kan^r	
mc^2 155::pTw_FtsZ_GFP	Derivative of mc^2 155 carrying in-frame FtsZ_GFP in pTweety with plasmid integrating at the *attP* site; Kan^r	This study
mc^2 155::pTw_DivIVA_GFP	Derivative of mc^2 155 carrying in-frame DivIVA_GFP in pTweety with plasmid integrating at the *attP* site; Kan^r	This study
ΔMSMEG_1661	Derivative of mc2155 carrying an unmarked, in-frame deletion in *M. smegmatis* MSMEG_1661	Ismail *et al.* (unpublished)

Table 2.3: Primers used in this study for cloning

Gene product	**Primer used**	**Primer Sequence (5'-3')**	**Fragment size in base pairs (bp)**
pMV_ DacB_GFP	DacB_F	GCG C **AAG CTT** *HindIII* TCT CGT GAT CCA CCT CGT ACT	1590 bp
	DacB_R	GCG C **CT GCA G** *PstI* TCT CGT GAT CCA CCT CGT ACT	
	GFP_F	GCG C **CT GCA G** *PstI* AT GGT GAG CAA GGG CGA G	748 bp
	GFP_R	GCG C **TC TAG A** *XbaI* TT ACT TGT ACA GCT CGT C	
pMV_ DacB_mCherry	DacB_F	GCG C **AAG CTT** *HindIII* TCT CGT GAT CCA CCT CGT ACT	1590 bp
	DacB_R	GCG C **GAA TTC** *EcoRI* TGC GCC GCA TCC GCA GCT GCG	
	mCherry_F	GCG C **GA ATT C** *EcoRI* GT GAG CAA GGG CGA GGA G	705 bp
	mCherry_R	GCG C **TCT AGA** *XbaI* CTT GTA CAG CTC GTC CAT	
pMV_ DacB_mRFP	DacB_F	GCG C **AAG CTT** *HindIII* TCT CGT GAT CCA CCT CGT ACT	1590 bp
	DacB_R	GCG C **GAA TTC** *EcoRI* TCT CGT GAT CCA CCT CGT ACT	
	mRFP_F	GCG C **GAA TTC** *EcoRI* GTG AGC AAG GGC GAG GAG	705 bp
	mRFP_R	GCG C **TCT AGA** *XbaI* CTT GTA CAG CTC GTC CAT	
pMV_ DacB_mTurq	DacB_F	GCG C **AAG CTT** *HindIII* TCT CGT GAT CCA CCT CGT ACT	1590 bp
	DacB_R	GCG C **GAA TTC** *EcoRI* TGC	

		GCC GCA TCC GCA GCT GCG	
	mTurq_F	GCG C **GA ATT C** *EcoRI* GT GAG CAA GGG CGA GGA G	751 bp
	mTurq_R	GCG C **TC TAG A** *XbaI* CT TGT ACA GCT CGT CCA T	
pMV_ MSMEG_1661_GFP	1661_F	GCG C **AA GCT T** *HindIII* GA GAA GTT CGA GTA ACG C	1341 bp
	1661_R	GCG C **CC ATG G** *NcoI* GT GCT GCG GGC GCT GAT T	
	GFP_F	GCG C **CC ATG G** *NcoI* GT TGT TGC CGC GGT TGA A	748 bp
	GFP_R	GCG C **TC TAG A** *XbaI* TT ACT TGT ACA GCT CGT C	
pMV_ MSMEG_2432_GFP	2432_F	GCG C **AA GCT T** *HindIII* CC GAC GTA CTG GGA TCA G	975 bp
	2432_R	GCG C **CT GCA G** *PstI* CT GGC TGA AGC CGT AGT C	
	GFP_F	GCG C **CC ATG G** *PstI* GT TGT TGC CGC GGT TGA A	748 bp
	GFP_R	GCG C **TC TAG A** *XbaI* TT ACT TGT ACA GCT CGT C	
pMV_ MSMEG_2433_GFP	2433_F	GCG C **AA GCT T** *HindIII* C GTCC GGG GTG AAC ACC G	1038 bp
	2433_R	GCG C **CT GCA G** *PstI* GA GCG CCC CGA TGC TCG C	
	GFP_F	GCG C **CC ATG G** *PstI* GT TGT TGC CGC GGT TGA A	748 bp
	GFP_R	GCG C **TC TAG A** *XbaI* TT ACT TGT ACA GCT CGT C	
pTw_ FtsZ_GFP	FtsZ_F	GCG C **GA ATT C** *EcoRI* GT CGG CGC GCC TGC CAC G	1308 bp
	FtsZ_R	GCG C **CC ATG G** *NcoI* GT GCC GCA TGA AGG GCG G	
	GFP_F	GCG C **CC ATG G** *NcoI* AT GGT GAG CAA GGG CGA G	748 bp
	GFP_R	GCG C **TC TAG A** *XbaI* TT ACT TGT ACA GCT CGT C	
pTw _ DivIVA_GFP	DivIVA_F	GCG C **GA ATT C** *EcoRI* CG GAG CCG TAA GAA GAT T	966 bp
	DivIVA_R	GCG C **CC ATG G** *NcoI* GT TGT TGC CGC GGT TGA A	
	GFP_F	GCG C **CC ATG G** *NcoI* AT GGT GAG CAA GGG CGA G	748 bp
	GFP_R	GCG C **TC TAG A** *XbaI* TT ACT TGT ACA GCT CGT C	
pTw _ PonA2_GFP	PonA2_F	GCG C **GA ATT C** *EcoRI* GG GGA TGC GCC CGT CGG G	2571 bp

	PonA2_R	GCG C **CT GCA G** *PstI* CG GCG GTG GCG GCG GCG G	
	GFP_F	GCG C **CT GCA G** *PstI* AT GGT GAG CAA GGG CGA G	748 bp
	GFP_R	GCG C **TC TAG A** *XbaI* TT ACT TGT ACA GCT CGT C	
pMV_ GFP	GFP_cont_F	GCG C **CC ATG G** *NcoI* AT GGT GAG CAA GGG CGA G	751 bp
	GFP_cont_R	GCG C **TC TAG A** *XbaI* TC AAG GAG TCC AAG CTC A	
pMV_ mCherry	mCherry _cont_F	GCG C **AA GCT T** *HindIII* ATGGT GAG CAA GGG CGA G	711 bp
	mCherry _cont_R	GCG C **TC TAG A** *XbaI* TC AAG GAG TCC AAG CTC A	
pMV_ mRFP	mRFP _cont_F	GCG C **AA GCT T** *HindIII* AT GGT GAG CAA GGG CGA G	711 bp
	mRFP _cont_R	GCG C **TC TAG A** *XbaI* TC AAG GAG TCC AAG CTC A	
pMV_ mTurq	mTurq _cont_F	GCG C **CC ATG G** *NcoI* AT GGT GAG CAA GGG CGA G	751 bp
	mTurq _cont_R	GCG C **TC TAG A** *XbaI* TC ACT TGT ACA GCT CGT C	

Table 2.4: Confirmation primers for mutants and reporter genes generated in this study

Gene product	Primer name	Primer sequence (5' -3')	Gene product	Primer name	Primer sequence (5' – 3')
MSMEG_1661 (DNA sequencing)	1661_F1	ATG ACG CGA CGC GCG GTG A	**FtsZ** (DNA sequencing)	FtsZ_F1	CGC CAG CTG GCG AAA GGG
	1661_F2	CCC CGC GAG CAT CAT CAA		FtsZ_F2	CTG ATG AGC GAC GCC GAC
	1661_F3	TCC CCG GGC GCG ACG GCG		FtsZ_F3	CTC ATG GAC GCG TTC CGC
	1661_F4	TCG TGT TCA TGC TGA TTC		FtsZ_F4	TGA CCG TCA TCG CGG CCG
MSMEG_2432 (DNA sequencing)	2432_F1	GTG CGA AGA CTG TTC GCG		FtsZ_F5	CAT CTG CAC CAC CGG CAA
	2432_F2	TGC TGG ACG CGC TGC TGA		FtsZ_F6	CAG AAC ACC CCC ATC GGC
	2432_F3	CGC CGG TTG GTG GTG GTG	**DivIVA** (DNA	DivIVA_F1	ATT ACG CCA GCT GGC GAA
MSMEG_2433	2433_F1	ATG TGG AGG		DivIVA_F2	TGC GTC AGC

(DNA sequencing)		TAC GCC TTC	sequencing)		GGG TCG CCG
	2433_F2	CAC CGC ACG CCA ACT GCT		DivIVA_F3	CAG TTG CGG CAG GCC CAG
	2433_F3	GCG CAG CGC GAC GGG CGC		DivIVA_F4	CGG CAA GCT GAC CCT GAA
DacB (DNA sequencing)	DacB_mRFP_ F1	ACG ACG TCG AAC TCC ACC		DivIVA_F5	CGG CAG CGT GCA GCT CGC
	DacB_mRFP_ F2	ATC ACA GGC CGC ATC ACC	**PonA2** (DNA sequencing)	PonA2_F1	ATT ACG CCA GCT GGC GAA
	DacB_ mRFP _F3	CAT GGA ATC GGT GAT GCT		PonA2_F2	ACA CCA TCG CGT GGC TGT
	DacB_ mRFP _F4	GGT CAA CGC CGC TGC CGG		PonA2_F3	CAG GAC GCC GCC CAG ACG
	DacB_ mRFP _F5	CGA GGG CCG CCC GTA CGA		PonA2_F4	GGC CAT CGA CAG CAT CGC
	DacB_ mRFP _F6	TAC GAC GCG GAG GTC AAG		PonA2_F5	AGC TCA TCT CGC AGA TCG
DacB (DNA sequencing)	DacB_ mCherry_F1	ATG GCC ATC ATC AAG GAG		PonA2_F6	GTG GGC TGG AAC CTG CCG
	DacB_ mCherry_F2	GAC GGC CCC GTA ATG CAG		PonA2_F7	GCG GTC GGG CAC CGT CGT
	DacB_ mChe_F3	CTC AGT TCA TGT ACG GCT		PonA2_F8	TGC CCT GGC CCA CCC TCG
	DacB_ mCherry_F4	CTG AAG GAC GGC GGC CAC		PonA2_F9	GGC GAC GGC CCC GTG CTG
Att primers (PCR confirmation)	AttL2 (Forward)	CTT GCA TCC TCC CGC TGC GC	**Δ2433Δ2432** (DNA sequencing)	Suicide vector_F1	TGC CTG ACT GCG TTA GCA
	Att BS1 (Reverse)	ACG TGG CGG TCC CTA CGC		Suicide vector _F2	TGC GCA CGC TCG CTG TCG
	AttBS2 (Forward)	ACA GGA TTT GAA CCT GCG GC		Suicide vector _F3	CGC CAG CCC TCG GGC GTG
	Att L4 (Reverse)	AAT TCT TGC AGA CCC CTG GA		Suicide vector _F4	ACA CGA CTA GGC TGG CCG
Δ2433Δ2432 (PCR confirmation)	K.O_conf_24 32_R1†	CGG ATC TGG TGA TCC TGC		Suicide vector _F5	CGC GGC CGC GAC ACG CTC
	K.O_conf_24 33_F1‴	GCA GTC GAA TAG TCC ACC		Suicide vector _F6	CTC GAT GTC GAT CGG CAC
	K.O_conf_24 33_R2‡	AGT GCC GTG CTG AGG GCG		Suicide vector_F7	ACT TCA GCT TCG ACA GGT
F: Forward **R**: Reverse	†: Primer set in middle of the gene that has been knocked out ‡: Primer set 100 bp after the stop codon of the gene that has been knocked out			‴: Primer set 100 bp before the start of the gene that has been knocked out	

Section B: Methods

2.2 Media, bacterial strains and culture condition

Culturing in liquid media: *Escherichia coli* DH5α strains were grown on Luria-Bertani (LB) broth, while *M. smegmatis* mc^2155 wild-type strains and derivative strains were grown in Middlebrook 7H9 broth (Difco) supplemented with 1× Glucose salts (0.20 g glucose, 0.085 g NaCl), glycerol and 25 % Tween 80. Plasmids propagated in *E. coli* that were less than 8 kb were grown at 37 °C, whereas those greater than 8 kb were grown at 30 °C. This was carried out to avoid any plasmid re-arrangement. All cultures were grown in a shaking incubator, shaking at 100 rpm. For the transformation of electro-competent *E. coli* cells and recombinant vectors, cells were grown in 2× TY (20 g tryptone, 10 g NaCl, 10 g yeast extract). Sautons (4 g asparagine, 0.5 g MgSO4, 2 g citric acid, 0.5 g KH2PO4, 0.05 g ammonium ferric citrate, 60 ml glycerol) media at pH 7.2 was used to wash off the tween supplemented in the 7H9 media during the biofilm formation assay procedure. Medium and reagents used in this are listed in Appendix B, Table B1-B2.

Culturing on solid media: *E. coli* strains were streaked on Luria-Bertani agar (LA) plates supplemented with the appropriate antibiotics (AppendixB, Table B2) and grown at the appropriate temperatures (30 °C or 37 °C) depending on the size of plasmid propagated . *M. smegmatis* strains were streaked on Middlebrook 7H10 media containing appropriate antibiotics and were incubated at 37 °C. Antibiotics used in this study were; Kanamycin (50μg/ml in *E. coli* and 25μg/ml in *M. smegmatis*) and Hygromycin (200μg/ml in *E. coli* and 50μg/ml in *M. smegmatis*).

2.3 Transformation of bacterial species

2.3.1 Transformation of *E. coli* cells

Chemically competent cells used in this study were prepared using rubidium chloride (Appendix B, Table B3). This method was adapted from the Promega *Protocols and Applications Guide* (Promega). Briefly, a single colony of DH5α was inoculated into 2.5 ml of LB broth (without antibiotic). The culture was grown at 37 °C in a shaking ($6 \times g$)

incubator overnight. This culture was then re-inoculated into 250 ml LB and cells were grown till they reached OD_{600} between 0.4 – 0.6. Upon obtaining the required OD_{600nm}, cells were then transferred into 50 ml centrifuge tubes and were centrifuged at 1494 × *g* for 5 minutes (min) at 4 °C to harvest the cells. Cell pellets obtained were then re-suspended in ice cold TBFI buffer (30 mM potassium acetate, 100 mM rubidium chloride, 10 mM calcium chloride, 50 mM manganese chloride, 15 % v/v Glycerol), centrifuged for 5 min, and re-suspended in ice cold TBFII buffer (10 mM MOPS, 75 mM calcium chloride, 10 mM rubidium chloride, 15 % v/v Glycerol). Competent cells were then stored on ice for 15-30 min. Thereafter, 500 µl aliquots were distributed in tubes. Cells were then used immediately or quick-frozen in 100 % ethanol and stored at -80 °C.

For transformation of plasmids into *E. coli* strains, plasmid DNA (between 100 and 1000 ng) was added to 100 µl of the competent cells, followed by incubation for 15 min on ice. Cell suspensions were then incubated at 42 °C for 90 seconds to serve as a heat shock. Following heat shock, cells were immediately incubated on ice for 3 min and 800 µl 2×TY media was added to the cells, followed by incubation for an hour at 37 °C. After incubation, transformants were streaked on LA agar plates containing appropriate antibiotics and incubated overnight at 30 °C or 37 °C (depending on size of plasmid). Colonies arising from these plates were considered potential clones.

2.3.2 Transformation of *M. smegmatis* by electroporation

For the introduction of plasmid DNA into *M. smegmatis* cells, electro-competent *M. smegmatis* cells were prepared as previously described (Larsen, 2000). Briefly, cells were prepared by inoculating 100 – 200 µl of culture from a freezer stock into 5 ml 7H9 broth and grown overnight at 37 °C. This pre-culture was inoculated into 50 – 100 ml 7H9 broth and was grown at 37 °C in a shaking incubator until mid-log phase (OD_{600nm} = 0.5 - 0.8). Cells were then centrifuged at 2360 × *g* for 10 min at 4°C and 30 ml of ice cold 10 % glycerol was added to the bacterial cell pellet for re-suspension. The re-suspended pellet was harvested at 2360 × *g* for 10 min at 4 °C. This washing step was repeated twice before final re-suspension in X × 400 µl 10 % glycerol (X = number of samples to be electroporated). The cell suspension was then split into 400 µl aliquots in eppendorf tubes, kept on iced and used the same day for electroporation purposes.

Electroporation of *M. smegmatis* was conducted by adding 1 – 5 µg of plasmid DNA into the 400 µl aliquots of ice-cold electro-competent *M. smegmatis* cells followed by a gentle mix using a pipette. Cells were then transferred into a 0.2 cm electroporation cuvette to perform electroporations using the BIO-RAD Gene Purser XCell^{TM} system. Parameters were as follows: Voltage = 2500 V, Time constant = 25 µF, Resistance = 1000 Ω and Distance = 0.2 cm. Cells were pulsed and immediately rescued with 800 µl 2× TY media. To allow for phenotypic expression of selectable markers, transformed cells were grown for 3 – 16 hours in a 37 °C shaking incubator. Transformations were plated on 7H10 plates with appropriate antibiotics and/or selective supplements and incubated for 3-7 days. Colonies arising from these plates were considered as potential clones.

2.4 DNA extraction methods

2.4.1 Plasmid DNA extraction from *E. coli*

2.4.1.1 Mini-prep DNA extraction

Extraction of plasmid DNA from *E. coli* clones was initiated by inoculating single colonies into 2 ml of LB broth and grown overnight at 37 °C using reagents listed in Appendix B Table B5. About 1 ml of the overnight culture was aliquoted into a sterile 2 ml Eppendorf tube and the cells were harvested at 12 470 × *g* for a minute by centrifugation. The pellet was re-suspended with 100 µl of Solution I (50 mM glucose, 25 mM Tris-HCl (pH 8.5), 10 mM EDTA) followed by addition of 200 µl Solution II (1 % SDS, 0.2 M NaOH), which was then mixed by a gentle inversion (6 - 8 times) and incubated for 5 min at room temperature. Lastly, 150 µl of Solution III (3 M potassium acetate, 11.5 % acetic acid) was added to the sample, followed by incubation on ice for 5 min. The sample was then centrifuged for 5 min at 12 470 × *g* and the supernatant was transferred into a clean 1.5 ml eppendorf tube. About 1 µl of RNaseA (10 mg/ml) was added to the supernatant and incubated for 15 min at 42 °C. Plasmid DNA was precipitated by adding a 600 µl aliquot of isopropanol and the mixture was centrifuged for 20 min at room temperature (20 °C - 25 °C). Alternatively, the mixture was stored at -20 °C for ~2 hours prior centrifugation step. The supernatant was then removed gently and the pellet was washed with 1 ml of 70 % ethanol and centrifuged at 12 470 × *g* for

one minute. The ethanol supernatant was discarded and the pellet was dried and re-suspended in 100 µl of sdH_2O.

2.4.1.2 Sodium acetate/ ethanol (NaOAc/ EtOH) precipitation for DNA purification

A one tenth volume of 3 M sodium acetate (pH 5.2) was added to suspension containing DNA. Sodium acetate was prepared as shown in Appendix B, Table B6. Three volumes of 100 % ice cold ethanol were subsequently added to the suspension followed by centrifugation for 20 min at 12 470 × *g*. The supernatant was discarded and the pellet was vacuum-dried (Speedvac) for ~20 min or ~10 min at 45 °C or 60 °C, respectively. This pellet was then re-suspended in 30-50 µl sdH2O followed by DNA quantitation using NanoDrop and visual analysis on an agarose gel electrophoresis.

2.4.1.3 Maxi-prep DNA extraction

For bulk DNA extraction from *E. coli*, volumes in section 2.4.1.1 were scaled up. In brief, a single colony or liquid culture (i.e. from a freezer stock) was grown in 5 ml of LB media at 37 °C overnight. On the following day, 1 ml of the pre-culture was inoculated into 30-50 ml of LB media. Cells were collected by centrifuging at 4 °C for 15 min at 3901 × *g* . Approximately 600 µl – 1 ml of Solution I (50 mM glucose, 25 mM Tris-HCl (pH 8.5), 10 mM EDTA) was added to the pellet and the re-suspended sample was aliquoted into 3-5 separate Eppendorf tubes. These cells were harvested again at 12 470 × *g* for one minute followed by re-suspension with 200 µl of Solution I with 5 µl RNaseA (10 mg/ml). 400 µl of Solution II was added, followed by gentle mixing and incubation at room temperature for 5 min. Finally, 300 µl of Solution III was added, followed by gentle mixing and incubation on ice for 5 min. The suspension was centrifuged for 5 min at 12 470 × *g*. From here onwards, the protocol for mini-prep was followed. However, 3 µl of RNaseA (10 mg/ml) was added instead of 1 µl and 800 µl instead of 600 µl of isopropanol due to increased or scaled up culture volume. Following EtOH wash and drying of the pellet, 50 – 100 µl of sdH_2O was used for re-suspension followed by sodium acetate/ethanol purification. Solution I, II, III and RNase was prepared using the recipes shown in Appendix B, Table B5.

2.4.2 Chromosomal DNA extraction from *M. smegmatis*

2.4.2.1 Small scale genomic DNA extraction - colony boil method

A portion of a single colony was re-suspended in 40 µl of nuclease-free distilled water in Eppendorf tubes with a safety locks. The sample was incubated at 95 °C for 5 min. Following incubation, cells were mixed by vortexing. An equal volume (40 µl) of chloroform: isoamyl alcohol (24:1) was added followed by a gentle agitation (Appendix B, Table B6). The sample was then incubated at 95 °C for 5 min and was centrifuged at 12 470 × *g* for 5 min. The supernatant (~50 µl) served as a DNA template for subsequent PCR reactions.

2.4.2.2 Large scale genomic DNA extraction- *Cetyltrimethylammonium bromide* method

M. smegmatis cells were grown to confluence on 7H10 plates. Approximately five loopfuls were scraped from this plate and re-suspended in 500 µl of 1X TE buffer. Alternatively, strains were grown in 5 ml 7H9 broth, of which 3 ml were harvested at 12 470 × *g* for a minute and re-suspended in 500 µl of 1X TE buffer. In both cases, *M. smegmatis* cells were heat killed at 65 °C for 20 min, followed by the addition of 50 µl of lysozyme (10 mg/ml) and incubation at 37 °C for 1 hour. A mixture of 10 % SDS (70 µl) and proteinase K (6 µl) was added to the suspension followed by incubation at 65 °C for 30 min to 2 hours. Five-hundred microliters (µl) of NaCl and 80 µl of the pre-warmed CTAB/NaCl were added into the suspension and mixed well and the mixture was incubated 65 °C for 10 min. An equal volume (~750 µl) of $CHCl_3$/isoamyl alcohol (24:1 v/v) was added, mixed vigorously and centrifuged at 12 470 × *g* for 5 min. The top aqueous layer was removed and placed into a sterile Eppendorf and 0.6 volume (~450 µl) of isopropanol was added. The suspension was then incubated on ice for 10 min prior precipitation by centrifugation for 12 470 × *g* for 15 min at 4 °C. The pellet was washed with 70 % EtOH, centrifuged for a minute and dried prior to re-suspension in 50 µl of TE buffer or nuclease free distilled water. DNA was quantified using NanoDrop (ND-100, Thermofiosher) and visualized by agarose gel electrophoresis (Vacutec G:Box SYNGENE system). Reagents used for DNA extraction using CTAB method are listed in Appendix B, Table B4 and Table B6.

2.5 DNA quantitation and visualization

2.5.1 DNA quantitation

Nucleic acids samples were evaluated for purity and concentration. DNA samples with absorbance ratios (A260nm/A280nm) of ~ 1.8 -2.2 were considered pure and were used for downstream application (e.g. DNA manipulation, bacterial transformation and electroporation). Alternatively, agarose gel electrophoresis was used to quantitate DNA by estimating DNA concentration relative to DNA molecular weight markers.

2.5.2 DNA visualization and purification using agarose gel electrophoresis

2.5.2.1 DNA visualization

Agarose gels were prepared using appropriate agarose concentrations (0.8 % - 2 %) dependant on expected fragment sizes (see Table 2.5 below). Agarose was dissolved in 1X TAE buffer and a final concentration of 0.5 μg/ml ethidium bromide (EtBr) was added to the solution. DNA samples and a molecular weight marker was mixed with loading dye before loading into the gel. Electrophoresis was conducted at 80 – 100 V and DNA fragments were viewed using UV-light (Vacutec G:Box SYNGENE; GeneSnap acquisition software). The percentage of agarose used was determined by effective separation values shown in Table 2.5.

Table 2.5: Levels of effective separation of nucleic acids on an agarose gel (Adapted from CBTBR Methods 2015 booklet, unpublished)

Levels of effective separation of nucleic acids on an agarose gel		
Concentration (%, w/v)	**Effective separation (Fragment range)**	**Agarose for 50 ml gel (g)**
0.8	500 bp – 12 kb	0.4
1	400 bp – 10 kb	0.5
1.5	200 bp – 4 kb	0.75
2	100 bp – 2 kb	1
4	10 bp – 400 bp	2

2.5.2.2 DNA purification using agarose gel electrophoresis

DNA fragments corresponding to the expected sizes were excised from agarose gels (0.8 %) and purified using the NucleoSpin® Gel and PCR Clean-up Kit according to the manufacturer's instructions. DNA integrity and concentration was assessed using agarose gel electrophoresis (as described above).

2.6 DNA manipulation

2.6.1 Primer design

Primers used in this study were designed using the Clone Manager 9 software or an online program called Primer 3 (http://frodo.wi.mit.edu/). For the latter program, primer sequences were selected based on the selection criteria listed in the Table 2.6.

Table 2.6: Selection criteria for oligonucleotides (Adapted from CBTBR Methods 2015 booklet, unpublished)

Oligonucleotide sequences selection			
	Size	**Tm**	**% GC**
Minimum	18	55	55
Maximum	25	63	65
Optimum	23	60	62

2.6.2 DNA amplification using polymerase chain reaction

2.6.2.1 PCRs using FastStart Taq

All PCR reactions for screening and mutant confirmation were conducted using a non-proofreading DNA polymerase, FastStart Taq (Roche, Johannesburg, RSA) according to the manufacturer's instructions. Primers (forward and reverse) were added to a final of concentration of 1 µM and dNTPs, to a final concentration of 200 µM. Approximately 10 – 100 ng/µl of DNA was used as template. DNA amplification was carried out using the following cycling conditions: one cycle of initial denaturation at 94 °C for 4 min followed by

30-40 cycles of denaturation at 94 °C for 30 sec, annealing at 55- 65 °C for 30 sec and elongation at 72 °C for 30 – 90 sec which was then followed by a final extension step at 72 °C for 5-7 min.

2.6.2.2 High Fidelity PCR, Phusion and Q5

M. smegmatis genes and fluorescent tags used for cloning were amplified using a high-fidelity proof-reading enzyme, Phusion DNA polymerase (Finnzymes/ ThermoFisher Scientific, Johannesburg, RSA), as per the manufacturer's instructions in a final volume of 25 µl. Approximately 10 – 100 ng/µl of DNA was used as template. The following cycling parameters were used: Denaturation temperature of 98 °C for 5 min; thirty-five cycles of 98 °C for 30s, 59 °C for 15s and 72 °C for 50s; and a final extension step at 72 °C for 7 min. An alternative DNA polymerase was also utilised in this study, i.e. Q5® High-Fidelity Polymerase. Although the two enzymes required very similar PCR cycling conditions, different enhancers or additives were used for the latter (5X Q5 High GC enhancer) as well as varying amounts of DNA template per reaction (i.e. < 250 ng for Phusion and <1000 ng for Q5).

2.7 Restriction digestion

Restriction enzymes were used to routinely screen plasmids and for cloning of DNA fragments into plasmids. These enzymes were purchased from Roche (Roche, Johannesburg, RSA), Thermo Scientific™ (ThermoFisher Scientific, Johannesburg, RSA) or New England Biolab (NEB) at Inqaba Biotech™ (Inqaba, Pretoria, RSA). The restriction digest pattern of a plasmid of interest or gene to be cloned into the plasmid was first determined using Clone manager 9. This program allows identification of enzyme sites with their cleavage location on a plasmid and also aids with cloning simulations. After identification and selection of restriction enzymes for the actual restriction digestion, restriction digests were carried out as per manufacturer's instruction with recommended buffers. Bovine serum album (BSA) was also added were necessary. Double digests were either carried out simultaneously or sequentially, depending on the buffer used and compatibility between enzymes. In the case of a sequential digestion, enzymes were washed out using sodium acetate/ ethanol precipitation

method (NaOAc/ EtOH) described in 2.4.1.2, and the DNA re-digested with the second enzyme. In both digests, simultaneous and sequential digests, samples were heat inactivated at 65 °C for 20 min after digestion with last enzyme(s). The amount of DNA required per digestion reaction depending on the restriction digests performed and periods of incubation are listed in Table 2.7

Table 2.7: Amount of DNA required for efficient restriction enzyme digestion (Adapted from CBTBR Methods 2015 booklet, unpublished)

DNA Digestion purpose	**Amount of DNA required (µg)**	**Reaction volume (µl)**	**Incubation period (hr.)**
Plasmid screening	0.5-1	10-20	1*■
Bulk digest for cloning (plasmid DNA/ PCR products)	1-3	15-30	1■
Bulk digest of chromosomal DNA for southern blot analysis	2-5	20-50	< 16■

*unless otherwise recommended ■ recommended temperature

2.8 Modification of DNA overhangs

Post restriction enzyme digestion, the 3' and/or 5' overhangs are sometimes formed and are sometimes necessary for cloning purposes. When needed for cloning, the formed overhangs create blunt-ends to fill in the gaps or remove them by fragment blunting, a process needed to improve the compatibility of DNA to other fragments with blunt-ends and vectors. In order to catalyse DNA synthesis from primed single stranded DNA, T4 DNA Polymerase (NEB) was used as it keeps the 3'→5' exonuclease activity. The T4 DNA Polymerase is used for the blunting of fragments which have both 3' and 5' overhangs. However, when the 5' overhang is the only one present in the digested DNA fragment, the Klenow Fragment (NEB) was used to retain polymerase activity. Both methods used for were conducted according to the manufacturer's instructions. These reactions were carried out at 37 °C for 10 min, in the presence of 1× buffer (10× reaction buffer), DNA, dNTPs, enzyme and sdH_20 in the reaction. Following the incubation step, samples were then heat inactivated at 65 °C for 20 min.

2.9 DNA dephosphorylation

Phosphate groups in the termini of a linearized DNA fragment vector were removed to prevent plasmids from self-ligation during cloning. Removal of the 5' phosphate from the DNA fragment was accomplished through the addition of Antartic Phosphatase (NEB) to the DNA. Depending on the amount of DNA used, an appropriate amount of Antartic Phosphatase (AnP) was added accordingly (for instance, in a 20 µl reaction with 1 µg DNA, 1 µl of 5U AnP was added). The supplied buffer and enzyme used were always made up to 1/10 final volume and sdH_20 added was also added to make up to the final reaction volume. As in all cases of enzyme digestions, samples were heat inactivated at 65 °C for 20 min.

2.10 DNA ligation

DNA fragments and vectors were joined using T4 DNA ligase (Thermo Scientific™) or T4 DNA ligase using Epicentre Biotechnologies Fast-Link DNA Ligation Kits (Sigma-Aldrich®, Johannesburg, RSA). A total amount 50 ng of vector DNA plus the amount of insert DNA (using calculation below) were used in the ligation reaction for a 1: 1 (vector to insert ratio) reaction.

$$\textit{Amount of insert DNA (ng)} = \frac{\text{50 ng x size of insert (bp)}}{\text{size of vector (bp)}}$$

In order for the ligation reaction to be successful, optimum ratios (inserts DNA: vector DNA) were used. Ratios varied from 1:1, 2:1, 4:1 and 1:2. An additional ligation control (vector only) was included. For a 15 µl final volume reaction, an appropriate volume of DNA, 1 µl of enzyme, 0.75 µl of ATP, 1× volume of supplied buffer (10× T4 DNA ligase buffer) and sdH_2O (to make up the final volume) were added. These reactions were incubated for 20 min at room temperature. Following the incubation period, samples were heat inactivated at 65 °C for 10 min prior transformation.

2.11 DNA sequencing

All plasmids created and/or used in this study were confirmed by DNA sequencing. This was done to check if any mutations were introduced into the genes of interest during PCR amplification. DNA samples were sent to the DNA Sequencing Facility at Stellenbosch

University for sequencing where they were analysed using the Big Dye terminator v3.1Cycle Sequencing Kit and the Bioline Half Dye Mix. For DNA sequence analysis, and alignment, the BioEdit and Clone Manager 9 programs were used.

2.12 Molecular cloning and construction of recombinants

Two cloning strategies that were used to create reporter genes in this study are the two-way (standard) and the three-way cloning strategies. Two-way cloning strategy involves ligating /joining one insert into one vector (insert DNA: vector DNA), while three-way cloning involves ligating two inserts into one vector (insert1 DNA: insert2 DNA: vector DNA).In both these strategies, the DNA of genes of interest and/or fusion proteins (the inserts) are first amplified using PCR as described in section 2.12.1and 2.12.2 with primers listed in Table 2.3. The PCR products/fragment DNA with appropriate restriction sites were then digested with restriction enzymes and ligated into the cloning vector (Table 2.1 and Figure 2.1). Circular vector DNA/plasmid was linearized by digestion with restriction enzymes at the restriction sites occurring within regions of the multiple cloning sites (MCS)/polylinker and was then dephosphorylated with AnP prior ligation. The linearized vector DNA was re-ligated with fragment DNA to produce a recombinant DNA molecule. This recombinant DNA molecule was then introduced into the electro-competent *E. coli* cells (Table 2.2) by transformation as described in section 2.3 to allow multiplication of the recombinant DNA molecule, phenotypic expression and division of the host cell/bacterium. The two plasmids used to create fluorescently-tagged proteins are pMV306H and pTweety (Table 2.1) and selection of these plasmids was based on them having functionally essential regions which are MCS, origin of replication region and the drug-resistant gene (Stover *et al*., 1991, Pham *et al*., 2007). Additionally, these plasmids were selected based on their ability to integrate into a mycobacterial chromosome.

2.12.1 Generation of reporter genes using three-way cloning

The *dacB* gene and three other DD-CPases (MSMEG_1661, MSMEG_2432 and MSMEG_2433) were cloned upstream of GFP or other additional tags for the *dacB* gene specifically (mTurq or mRFP) into pMV306H (pMV) to produce; pMV_dacB_GFP or pMV_dacB_mTurq and/or pMV_dacB_mRFP (Figure 2.1). A high-molecular-weight PBP, PonA2 and other cell wall remodelling enzymes or components of the cell division/elongation machineries, i.e. DivIVA and FtsZ, were also cloned upstream of GFP into the pTweety(pTw) integrating vector to produce pTw_PonA2_GFP, pTw_DivIVA_GFP and pTw_FtsZ_GFP. Primers used for cloning are listed in Table 2.3.

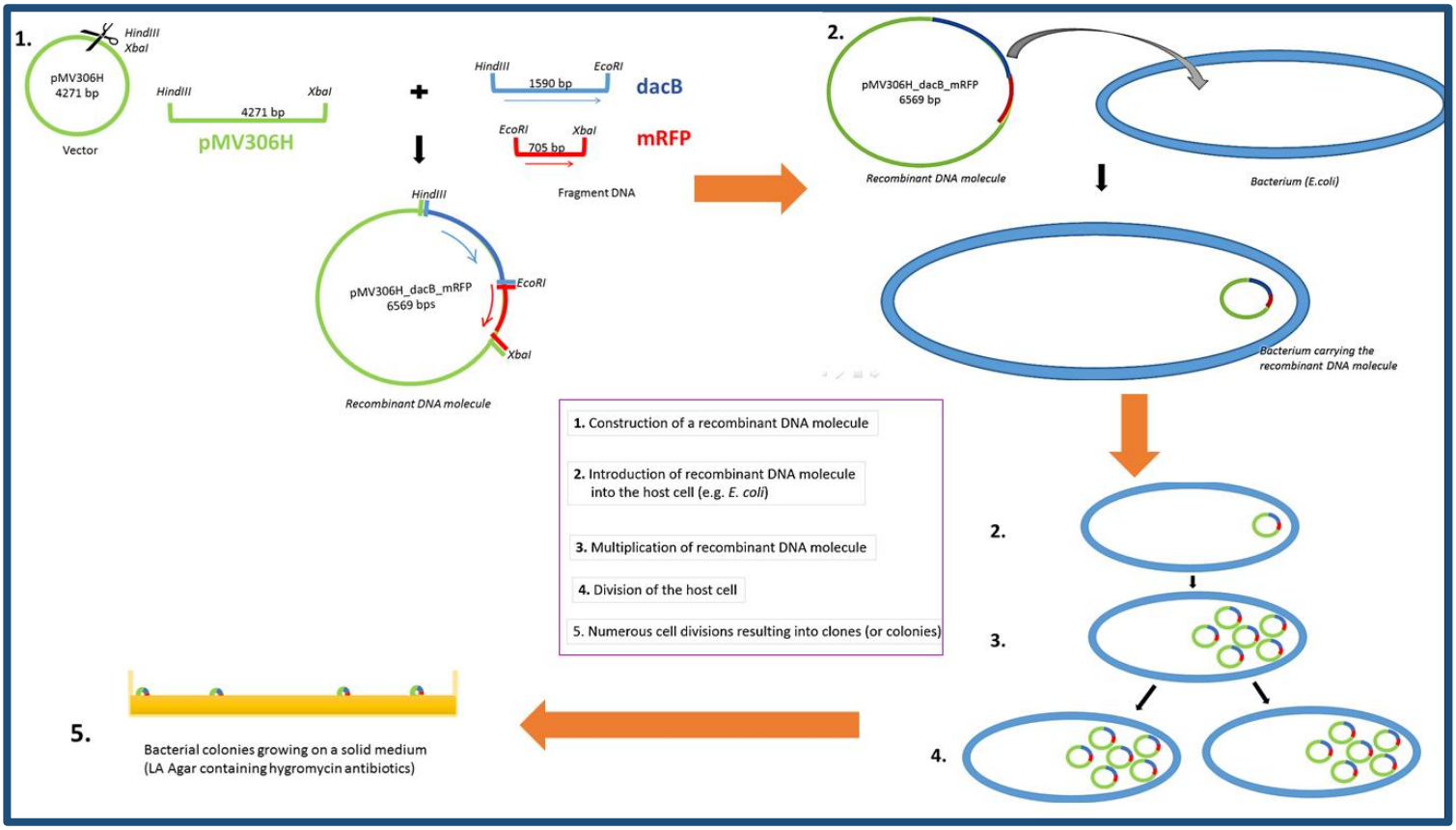


Figure 2.1: Schematic representation of a three-way cloning procedure to create using mRFP fluorescently tagged DacB construct as an example. 1. The pMV306H vector backbone is digested with *HindIII* and *Xba*l restriction enzymes to produce a linearized pMV306H vector. The PCR products of *dacB* and mRFP fragments were digested with restriction enzymes. The *dacB HindIII/ EcoRI* fragments and mRFP *EcoRI/XbaI* fragments were then ligated into the linearized pMV306H vector molecule to produce pMV_dacB_mRFP. 2. The pMV_dacB_mRFP plasmid was then incorporated into the bacterium (*E. coIi*) by transformation. 3. Inside the bacterium, pMV_dacB_mRFP plasmids were replicated. 4. Following DNA replication, *E. coli* cells divided. 5. Bacterial cells were then plated on an antibiotic (hygromycin) selection plate. Bacterial colonies were then selected and isolated and the resulting products were confirmed with a polymerase chain reaction (PCR). Following PCR, recombinants cells were visualized under the fluorescence microscope.

All plasmids were first propagated in *E. coli* and genetic integrity confirmed by extensive restriction profiling. Following confirmation of clones by PCR and DNA sequencing, the plasmid DNA was electroporated into *M. smegmatis*. PCR was conducted to confirm integration of pMV306H into *M. smegmatis* genome (data not shown due to space limitation but may be submitted upon request) using the *att* primers listed in Table 2.4. Plasmid pMV306H is a mycobacteriophage-L5 integrating proficient *E. coli-M. smegmatis* shuttle vector that intergrates at transfer RNA ($tRNA^{GLY}$) . This integrative-proficient vector contains a phage attachment site, *attP*, which is located close to the phage/L5 intergrase, *int*, a gene responsible for site-specific recombination. The *attP* site which is plasmid-borne integrates into a chromosome/bacterial attachment site, *attB* via the integrase (Figure 2.2). Additionally, *attP* and *attB* sites are known to share a conserved 43 bp region overlapping at the at tRNA gene at the 3´-end in *M. smegmatis*.

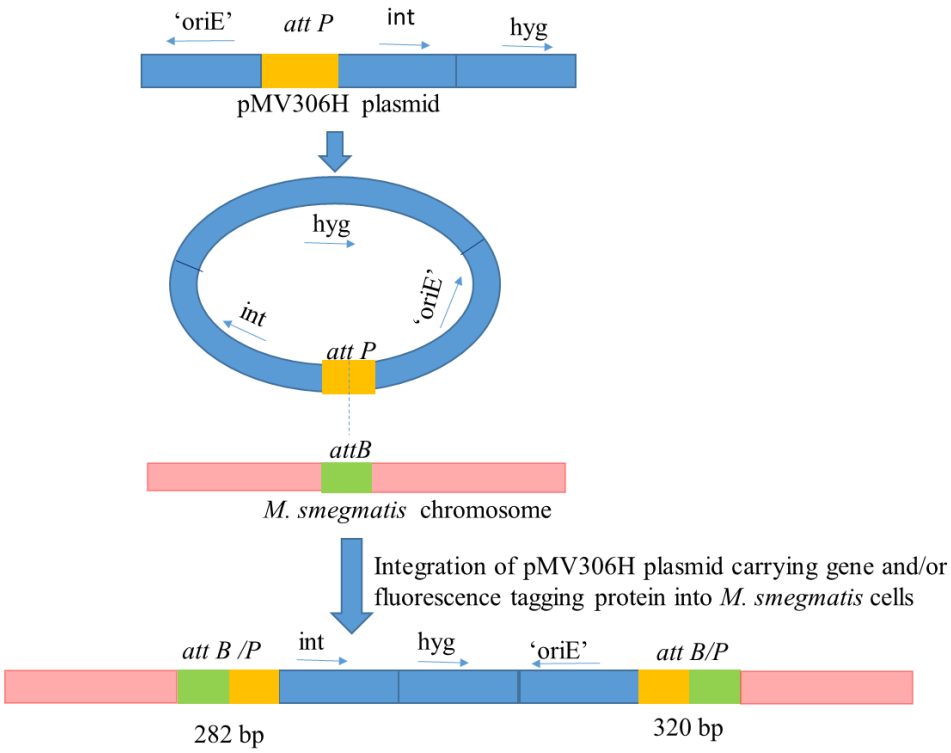


Figure 2.2: Schematic representation of integration of pMV306H into the *M. smegmatis* chromosome. Key: origin of replication in *E. coli (oriE)*, phage attachment site (*attP*), chromosome/bacterial attachment site (*attB*), phage/L5 intergrase (int) and hygromycin drug-resistant gene (*hyg*).

2.12.2 Generation of controls used for fluorescence analysis using two-way cloning

Sequences for the fluorescence tags used in this study were downloaded from the Addgene website (https://www.addgene.org/) and were used to design controls for fluorescence analysis. Controls which were created in this study were pMV_GFP, pMV_mCherry, pMV_mRFP and pMV_mTurq, whereby GFP, mCherry, mRFP and mTurq fluorescent proteins were cloned into the pMV306H vector. Constructions of these controls were done following these steps: Firstly, the start codons were added in the beginning of each fluorescent protein sequence and stop codons were added at the end of each fluorescent protein sequence. Secondly, the DNA of the florescent proteins mentioned was amplified using PCR. After obtaining the amplicons or DNA fragments, these fragments were then digested with respective restriction enzymes and cloned into the pMV306H integrating vector using the T4 DNA ligase. Lastly, all controls were confirmed with restriction enzyme profiling and DNA sequencing followed by electroporation into *M. smegmatis* cell to see if the resulting proteins fluoresce and localize.

2.13 Microscopic analysis

2.13.1 Fluorescence microscopy

Fluorescence microscopy was used to assess cellular localization of proteins and protein interactions, through assessment of co-localization patterns of reporters, in *M. smegmatis*. Localization patterns of DacB, the other *M. smegmatis* DD-CPases and cell wall remodelling enzymes (DivIVA/ FtsZ/ PonA2) were viewed on the Zeiss Axio Observer.Z1 fluorescence microscope (Zeiss) using Immersol™ 518F, an immersion oil for fluorescence microscopy (Zeiss). Strains analysed were grown in 5 ml 7H9 broth, supplemented with appropriate antibiotics until they reached an OD_{600nm} between 0.5 – 0.8 (exponential phase). Agarose (2 %) pads were prepared using 50 ml of 1x TAE and 1g agarose. After boiling and cooling (~ 55 °C) of the agarose, 600 – 700 µl of the molten agarose was the spread onto glass slides and a second glass slide was place on the agarose gel and this solution was left to cast (~15 min). Thereafter, 3-6 µl of cells were spread unto the casted gel and a cover slip was placed on top of the cells. These were then visualized immediately under the Zeiss Axio Observer.Z1 fluorescence microscope using Zen lite blue edition (2012) version 1.1.2.0. Only cells that appeared in both fluorescent image and bright field image were considered for the

classification of patterning. Localization patterns were classified by eye and computationally (i.e. Image J/Fiji programs and/or the graphic feature on the Zeiss microscope software).

2.14 Mutant generation

Mutants created and/or used in this study were generated using two-step allelic exchange by homologous recombination as described by Gordhan and Parish (Gordhan and Parish, 2001). This method involved the creation of a suicide vector (non-replicating vector in mycobacteria) by fusing both up and downstream regions of the gene(s) investigated, leading to the construction of an inactive, truncated version of this gene(s). Post introduction of this truncated gene into the *M. smegmatis* cells via electroporation, two homologous recombination events (single cross-over (SCO) and double cross-over (DCO) events), took place and these occurred sequentially. In the initial SCO event, the suicide vector integrated into *M. smegmatis* cells and blue colonies were formed in the presence X-gal, Kan and Hyg antibiotics as the suicide vector carries the *aph, hyg* and *lacZ* selectable marker genes that encode these phenotypic traits. The presence of the selectable marker genes allows selection for SCO homologous recombinants. Additionally, this suicide vector contained a *sacB* gene, a counter selectable marker. In the presence of this counter-selectable marker, cell death occurs when cells are plated on sucrose. This facilitates a double crossover, removing the vector backbone and depending on the region where the second crossover occurs (either upstream or downstream), a knock-out mutant or the wild-type allele is generated. These are observed as white colonies. Due to the fact that the colony picked can either be a mutant or wild-type genes, genotypic (PCR and Southern blot) analysis is carried out to identify the mutant strain.

2.14.1 Construction of the suicide vector to simultaneously delete MSMEG_2432 and MSMEG_2433

The p2NIL vector (6890 bp) harbouring the upstream and downstream region of MSMEG_2433 and MSMEG_2432 was created by another student. This vector was digested with *PacI* and the marker gene cassette (*PacI* cassette) on vector pGOAL19 (10435 bp) was excised with *PacI* as well to create linearized fragments to be used for cloning purposes. Following digestion with *PacI* in both vectors, p2NIL yielded a 6890 bp fragment while

pGOAL19 yielded two fragments (7939 and 2496 bp). In the latter vector, the 7939 bp fragment was then excised from the 0.8 % agarose gel using gel extraction method (see section 2.5.2.2). Following digestion, dephosphorylation of the vector and heat inactivation of these enzymes, the ligation was carried out, Figure 2.3. Unfortunately, after multiple attempts to create the suicide vector, no clones or colonies were obtained. An alternative method was then used which was a slight modification to the one explained above. Instead of excising the 7939 bp fragment from the pGOAL19 vector, the entire pGOAL19 vector was partially digested with *Pac*I and the linear vector was cloned into p2NIL. The cloning yielded blue colonies with a functional *lacZ* and *sacB* genes (these were tested phenotypically). The suicide vector (p2NIL_2433_2432::pGOAL19) was sequenced and restriction profiled, followed by electroporation into *M. smegmatis* cells

Sucrose sensitivity testing (knockout mutant screening protocol). A single blue colony, from *E. coli* carrying the suicide vector was re-suspended into 100 µl of the LB liquid media containing appropriate supplements (see Appendix B, Table B1) and was grown overnight at 30 ˚C shaking incubator. On the following day 80 µl of the culture was inoculated in 5ml LB media containing appropriate supplements and antibiotics (hygromycin, kanamycin). The remaining 20 µl was stored. The culture was incubated at 30 ˚C overnight in a shaking incubator. On the following day, this pre-culture was then used for sucrose sensitivity testing (Appendix F, Figure F2). The inoculum was diluted into serial dilutions of 10^1 up to 10^6 and these dilutions were spotted on two different LB Agar plates containing Kanamycin, Hygromycin and X-gal antibiotics supplemented with or without sucrose. In the presence of sucrose no growth should be observed and in the absence of sucrose growth should be observed. After passing the sucrose sensitivity test, glycerol stocks of the sucrose-sensitive single cross-overs were prepared and stored and were later used for the generation of the double cross-over mutants.

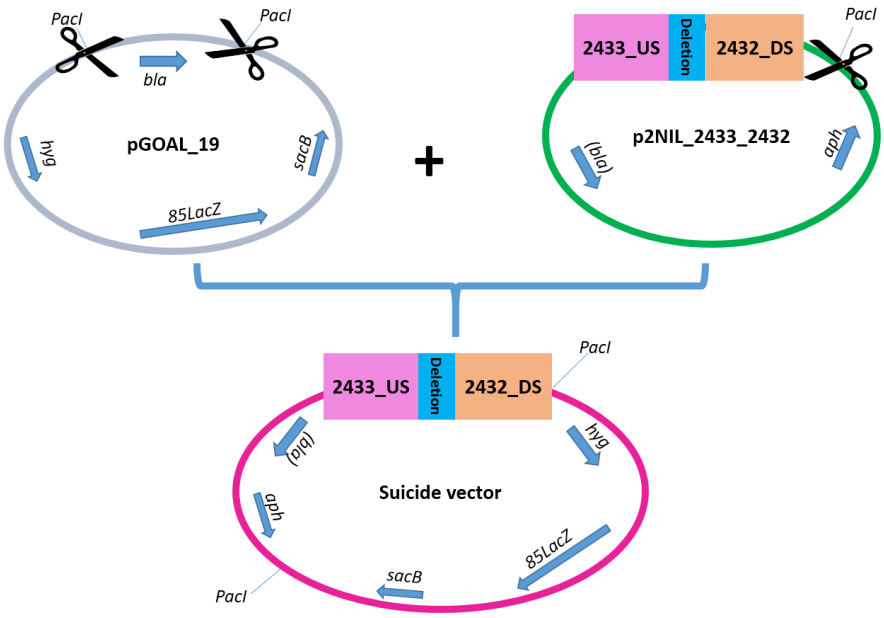


Figure 2.3: Schematic representation of the generation of an unmarked suicide vector. Plasmid p2NIL (6890 bp) carrying the upstream and downstream region of MSMEG_2433 and MSMEG_2432 was digested with *PacI* restriction enzyme and the marker gene cassette (*PacI* cassette - 7939 bp) was then excised from the pGOAL19 plasmid with the same enzyme, *PacI*. The *PacI* cassette was then ligated with the linearized p2NIL to create a suicide vector. This suicide vector carried selectable marker genes which *aph*, *hyg*, *lacZ*.

2.14.2 Generation of ΔMSMEG_2433 ΔMSMEG_2432 deletion mutant using two-step allelic exchange

After conducting the sucrose sensitivity test, the correct suicide vector (p2NIL_2433_2432::pGOAL19) was used to generate double cross-over mutants (△MSMEG_2433 △MSMEG_2332) by electroporation of the suicide vector into *M. smegmatis* cells using purified DNA at concentrations of 1, 3, 5 µg DNA and streaking these on 7H10 plates containing Kan, Hyg, and X-gal (0.004 %). Positive controls such as integrating vectors were also included in the electroporation and the transformation efficiency was calculated for both positive controls and knockout vectors. Post electroporation, plates were incubated at 37 °C for 3 – 7 days or until a blue colonies were observed. One or more blue colonies, representing an SCO, were then inoculated into 100 µl of 7H9 media. From this, 80 µl of the solution was inoculated into 5 ml 7H9 media containing kanamycin and hygromycin antibiotics while the remaining 20 µl was stored for future use. The culture was grown overnight at 37 °C in a 100 rpm shaking incubator. On the following day, 200 µl of the overnight culture was inoculated in 10 ml 7H9 media without antibiotic and incubated at 37 °C overnight. A glycerol freezer stock was then prepared at this stage. The next day, the overnight culture was centrifuged at 1494 × *g* for 10 min (at 4° C) and the pellet was re-

suspended in 400 µl 7H9 broth, from which 100 µl was used to prepare a serial dilution ranging from 10 to 10^7-fold diluted. In addition, 100 µl was plated on 7H10 with and without 2 % sucrose, another 100 µl of culture was plated on 7H10 supplemented with 2 % sucrose plus X-gal and this was done in duplicate, the remaining 100 µl was then plate 7H10 without antibiotics and all these plates were grown at 37 °C for 3 – 5 days until blue and white colonies emerged. White colonies were potential mutants/wild-type while the blue remained were *sacB* mutants. The mutants were confirmed with PCR and Southern blotting. A schematic of the genomic processes that occurred during site-specific allelic changed is given in Figure 2.4.

2.15 Genotypic analysis of mutants

2.15.1 Screening of mutants using PCR

All white colonies selected were screened using PCR to confirm the genotype. The colony boil extraction was conducted and the supernatant obtained was used as the DNA template. Primers used for DNA amplification are listed as Δ2433Δ2432 (PCR confirmation) primers in Table 2.4 and are listed as K.O_conf_2432_R1†, K.O_conf_2433_F1‴, K.O_conf_2433_R2‡ and regions in which they bind to is also listed (last green row in the table). The SCO, wild-type mc^2155 and suicide vector were also analysed using this PCR and were used as controls. FastStart PCR was used for this analysis and the PCR products were run on agarose gels (0.8 % -1 %) depending on fragment size expected. Expected size from the mutant and suicide vector was 263 bp, the SCO was 1.1 kb and 263 or 2 kb and 263 bp and wild-type *M. smegmatis* was 2 kb.

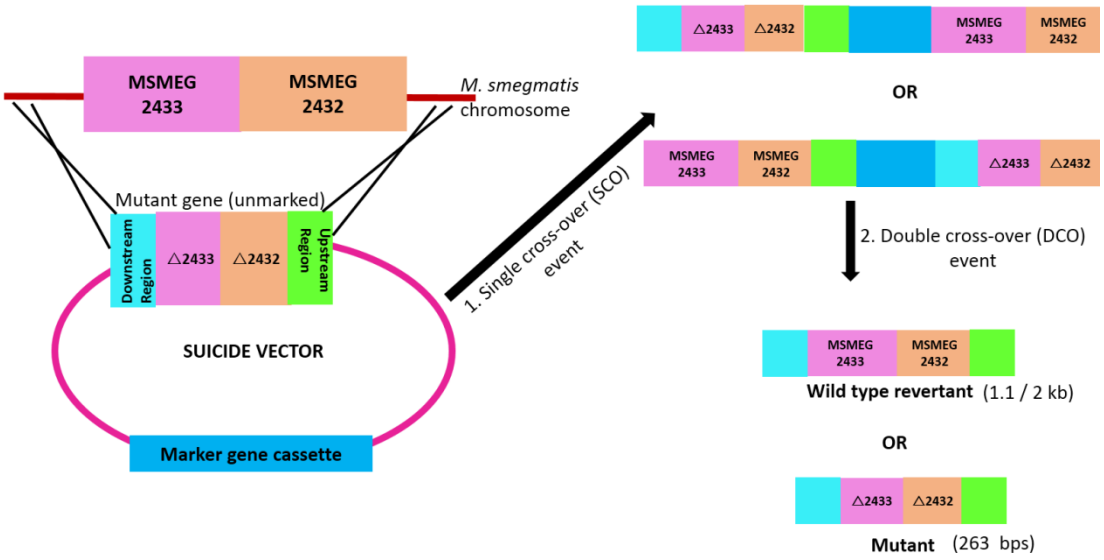


Figure 2.4: Generation of a gene knockout using two-step allelic exchange by homologous recombination. Following confirmation of the suicide vector by restriction enzyme profiling and DNA sequencing, the suicide vector which carried the truncated version of MSMEG_2433 and MSMEG_2432 (△2433 △2432) was then electroporated into *M. smegmatis* cells to allow integration of the gene into the *M. smegmatis* genome. Two cross-over events (single crossover and/or double crossover) then occurred. Integration of a suicide vector into the *M. smegmatis* genomel occurred through the initial event of homologous recombinant event called single crossover (SCO) in the presence of selectable markers. In the presence of a counter-selectable marker gene (*sacB*), cell death occurs, and a double crossover (DCO) is facilitated, removing the vector backbone, and depending on the side on which mutation occur during this event, a knock-out mutant or wild-type allele is generated.

2.15.2 Screening of mutants using southern blot analysis

Following genomic confirmation using PCR, these mutants were further confirmed using Southern hybridization. A diagrammatic representation of the different steps used in Southern Blotting is given below. Solutions used for southern blotting are listed in Appendix B, Table B8.

2.15.2.1 Probe labelling

Probes used in this study for Southern blotting were synthesized with PCR DIG Probe Synthesis Kit using Roche Taq Polymerase (Roche) as per the manufacturer's instructions. Reagents used for amplification included; 10X buffer+ $MgCl_2$, GC-rich buffer, dNTPs (10 mM), forward and reverse primers (10 µM each), distilled water, DIG-mix 2, genomic DNA

and the Taq polymerase (Roche). The probe used for synthesis was 2433-US (Upstream region). The amplified DNA was represented by HOT (actual experiment), COLD (positive control) and NTC (negative control), see Figure 2.5 below.

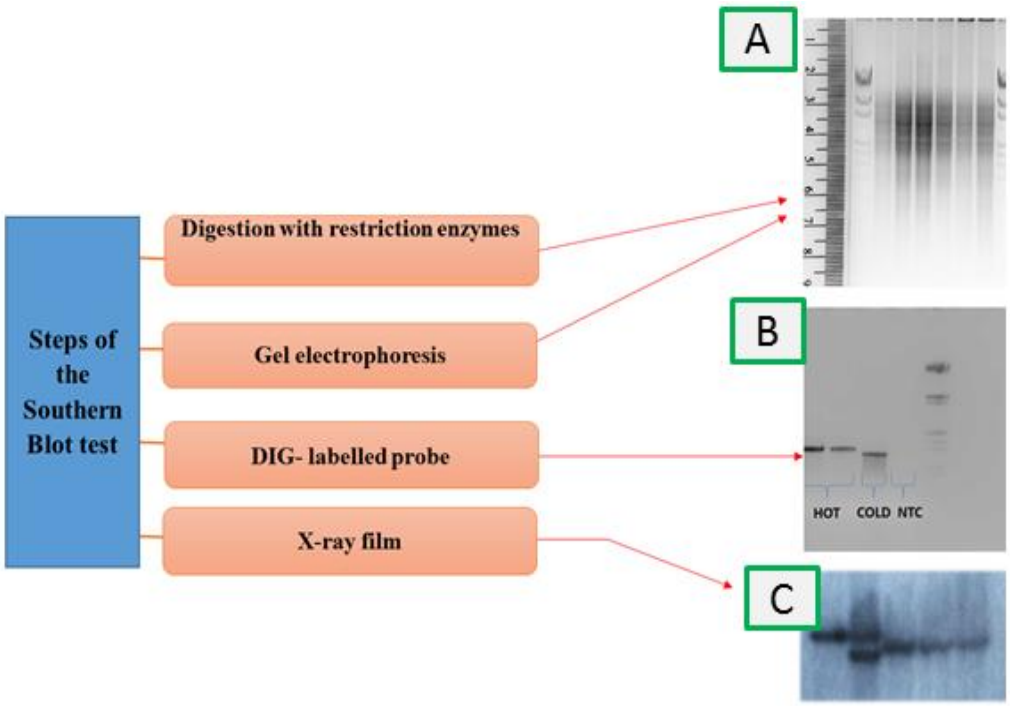


Figure 2.5: Diagram showing different steps in a Southern Blot. (A.) Genomic (g) DNA was digested with the restriction enzyme of choice (i.e. *PstI*). The digested DNA was then run on an agarose gel electrophoresis alongside the marker (Marker IV). The Image of the gel electrophoresis with fragments fractionated by size alongside ultraviolet (UV) ruler was taken using the Geldoc. The smear on the gel represents very large number of fragments. This gel was then washed with appropriate washes (see Appendix B, Table B8.) and was transferred to the nitrocellulose filter. The DIG labelled probe (B.) was synthesized with PCR DIG probe synthesis kit. HOT represents PCR amplification including the DIG mix and gDNA. COLD represents PCR amplification excluding the DIG mix but with gDNA. No template control (NTC) represents PCR amplification excluding both DIG mix and gDNA. For probe to be correct "HOT" has to be higher than "COLD" and "NTC" has to be clear and no band should occur. The nitrocellulose filter with DNA fragments should be positioned exactly the same as those in the gel. The hybridization step with a DIG labelled DNA probed (B.) then followed. Lastly, (C.) the radiograph which showed the hybrid DNA was observed on an X-ray film (Adapted from (Mathews *et al*., 2002)

2.15.2.2 Electro-blotting

Genomic DNA between 2µg to 5µg were digested with a restriction enzyme in reaction volumes of 20 µl to 50 µl and was incubated at 37 °C overnight. The digested DNA was then run on a 0.8 % agarose gel for two hours alongside with Marker IV (Appendix C1) and the image of the gel was captured alongside a ruler on the GelDoc. Post agarose gel

electrophoresis and imaging of the gel, the gel was then depurinated by washing gel using solution I (2X SSC, 0.1 % SDS and dH_2O) for 15 min and denatured by a second wash using solution II (0.5X SSC, 0.1 % SDS and dH_2O) for 30 min, see Appendix B, Table B8. Post washing steps, this agarose gel was then equilibrated with 1X TBE and was transferred onto a hybrid nitrocellulose filter using the sandwiching method. In this method, the gel was "sandwiched" or covered by nitrocellulose filter or nylon membrane, filter papers and sponges. At the bottom was the glass/plastic dish followed by two thin soaked sponges, 2X soaked filter papers, nylon membrane, washed agarose gel, 2X soaked filter papers, sponge and another glass/plastic dish. Two plastics dishes were pressed together and clicked to close or hold contents together. All these sandwiching steps were carried out in 1X TAE buffer. The sandwiched contents were then quickly transferred into Southern Blot tank containing fresh 1X TAE buffer and the DNA was transferred for 2 hours at the voltage (V) of 0.5 and amp (A) of 0.6. Once the DNA was transferred to the nylon membrane, this membrane was then cross-linked at 2000 mJ/cm^2 and was then either used immediately or stored in maleic acid buffer for later usage.

2.15.2.3 Hybridization

DNA High Prime DNA labelling and Detection Starter Kit II (Roche, Johannesburg, RSA) were used to hybridize the probe to the membrane containing DNA and the procedure was conducted as per manufacturers' instructions. The hybridizer was first warmed up according to the hybridization temperature (i.e. 55 ˚C for 2433_US Probe). Since hybridization temperatures are specific for individual probes, the calculation used to identify the precise hybridization temperature for the probes is **Melting temperature (T_m)** $= 49.82 + 0.41(\%\ \mathrm{GC}) - \frac{600}{\mathrm{L}}$ where L represents length of the probe sequence and **Optimum hybridization temperature (T_{opt})** = T_m - 20 to 25. The hybridization process was carried out in roller bottles (Hybaid HB-OV-BM) in a hybridization oven (Hybaid Micro-4) at the specific temperature for the probes. Post cross-linking of the of the DNA-containing nylon membrane, these membrane(s) were inserted into roller bottles containing 10-12 ml of Digoxygenin (DIG) Easy Hyb solution and pre-hybridised at an appropriate temperature for 30-120 min. The probe was then denatured at 95 ˚C for 5 min followed by immediate placement of the denatured probe on ice. The probe was then added to the DIG Easy Hyb solution in the bottle (about ~2 µl/ml of the hybridization solution), followed by hybridization

overnight. On the following day, hybridized membranes were then washed (through stringency washes) with solution I at room temperature for 5 min and by solution II at 68 ˚C for 15 min. This was done to decrease background that may occur on the blots. Recipes for these solutions are listed on Appendix B, Table B8. The decanted Hyb buffer plus probe into a falcon tube was stored in a -20 freezer.

2.15.2.4 Immunological detection

The membrane was then rinsed with washing buffer for 5 min followed by incubation in blocking solution for 30 min. The membrane was then incubated in an antibody solution for 30 min followed by washing of the membrane twice by with the washing solutions for 15 min each. Once the washing steps were completed, the membrane was equilibrated with detection buffer for 5 min. The membrane was then placed into a hybridization bag (with DNA side facing up) and 1 ml of CSPD. The CSPD allows the emission of a luminescent signal that can be detected on X-ray film. The CSPD substrate was spread evenly on the membrane (make sure all bubbles are removed) and was incubated at room temperature for 5 min. The excess substrate was then squeezed out followed by incubation of the membrane at 37 ˚C for 5 min. The membrane together with the cassettes and films were then taken into the dark room and the X-ray film was exposed for 5 min or longer (10-15 min), depending on the required intensity. The X-ray films were then developed by being passed through the Axim automated developer. Recipes for solutions used for southern blotting are listed on Appendix B, Table B8.

2.16 Phenotypic analysis of mutant (s)

2.16.1 Growth curves and optical density measurements

To assess whether the genes deleted were dispensable for growth or not, growth kinetics assays were conducted. For growth kinetics analysis, a single colony was picked and inoculated into 5ml 7H9 media supplemented with glucose salts (100×) and 25 % Tween80 and was grown overnight or until the culture reached an OD_{600nm} of ~1.0 – 1.5 (log-phase). On the following day, the overnight pre-culture was inoculated into fresh media (50 ml 7H9 media supplemented with glucose salts [100X] and 25 % Tween80) and diluted to a starting

value or OD_{600nm} of ~ 0.050 (~10^{-6} CFU/ml). In the case where OD_{600} values were in log or linear phase, an equation (***Determination of inoculum size*** *= C1V1= C2V2)* was used to calculate the starting value. Optical density (OD_{600nm}) between 0.03 – 0.05 was used as the starting value and this was taken as time (T) = 0. Optical density readings were taken every 3 hours for 36 hours. Three biological repeats were done to show consistency of the results.

2.16.2 Biofilm formation

To analyse the biofilm of the wild-type (mc^2 155) *M. smegmatis* cells, mutants defective for DD-CPases(△2433 △2432) and the genetically complemented strains (△2433 △2432::2432 and △2433 △2432:: 2433), cells were grown in 50 ml 7H9 liquid media containing glucose salts (100X) and 25 % Tween80 supplement. (Appendix B, Table B1) Wild-type and mutants strains were grown in 7H9 media without antibiotics while the complements were grown in media containing hygromycin antibiotic. Cells were then harvested and washed in Sauton's Media in order to wash off the Tween supplemented in the 7H9 media. These cells were then harvested re-suspended in 1 ml of Sauton's Media (Appendix B, Table B1). The optical density (OD) of these cells were adjusted to OD_{600nm} = 2 or 1. Multi-well plates were used for biofilms and in each well, about 2 ml of the Sautons media was added, followed by 20 µl of the culture (in serial dilutions of 10^1 to 10^6). To prevent biofilms from drying out, distilled water (< 1ml) was added in some wells. This experiment was done in triplicates. Once the preparations were done, plates were incubated in a non-shaking incubator with temperature of 37 ˚C for 7-10 days prior visualization under the microscope.

2.16.3 Crystal violet assay

In order to measure the biomass of the biofilms and to stain living or dead cells, a crystal violet (CV) assay was conducted using reagents listed in Appendix B, Table B10. This experiment was done 7-10 days post incubation and visualization of the biofilms under the microscope. For measuring the biomass of the biofilms, 1 ml of the filtered 0.1 % crystal violet stain (dark purple dye) was added into each well on the multi-welled plated to allow for staining of the biofilm (adherent bacteria) and the culture-CV mix was incubated at room

temperature for 10 min. The planktonic bacterium (solution under the biofilms) was then pipetted out and the plates were left to dry for 15 min at room temperature. This was then followed by the addition of 1 ml of 99 % filtered ethanol in each well and incubation at room temperature for 10 min. The ethanol-biofilm-CV combination was mixed well before the incubation step. One in hundred (1:100) dilution of biofilm-ethanol solution (10 µl ethanol-biofilm-CV combinations + 990 µl filtered 99 % ethanol) was prepared and the biofilm growth was measured at absorbance (A) of 600 nm. The experiment was done in three biological repeats. Staining with a classical dye such as crystal violet (dye binding to negative charges) helps target molecules of various bacteria and extracellular polymeric substances and therefore allows for quantification and staining of the total biomass and direct optical visualization.

2.17 Click chemistry - copper click reaction with D-alanine analogue

The click chemistry technique was used as a biochemical procedure to investigate *in vivo* PG biosynthesis. Reagents used for click chemistry assay are shown in Appendix B, Table B9. *M. smegmatis* cells (mc^2155) wild-type, mutants and complemented strains) were grown overnight to an OD of 0.5-0.6. On the following day, 2 ml of the culture was harvested by centrifugation and re-suspended in 1 ml 1X PBS. The D-alanine analogue (1 M) was added to the bacteria/re-suspended and the mixture was grown for 3 hours in a shaking 37℃ incubator (NB: tubes were places on the holding rack and the racks were covered in foil). After 3 hours, cells were pelleted and washed three times with PBSTB (PBS + 0.05 % BSA + 0.01 % tween). For copper click reaction (alkyne-D-alanine and azido-probe), 500 µl PTSTB, 500 µl CuSO4 (1M from 50 mM stock) and 500 µl TBTA (128 uM from 6.4 mM stock) were added in the order as listed. Ten microliters (µl) of the freshly prepared sodium ascorbate (1.2 mM from the 60 mM stock) followed by 10 µl Azido-PEG488 or azido probe (20 uM from 1 mM stock). The reaction was incubated for 30-60 min at room temperature. Once this process was done, the growing bacteria were washed three times with PBS and placed on an agarose pad and was visualized under the fluorescent microscope.

2.18 Data representation, statistical analysis and software programs used in this study

2.18.1 Data representation and statistical analysis

Statistical significance (T-Test): The t-test statistics was used to compare the localization of DacB in wild-type (mc^2155) and mutants defective for DD-Carboxypeptidases in *M. smegmatis*. This was conducted for the determination of significant differences (P-value) between strains and was calculated using GraphPad. The P-values are represented in asterisks (*): * for $P \leq 0.05$, ** for $P \leq 0.01$, *** for $P \leq 0.001$ and **** for $P \leq 0.0001$. One asterisk means significant, two asterisks means highly significant, three asterisks means very highly significant and four asterisks means extremely significant. In terms of the cut-off value for level of significance, an alpha of 0.05 ($\alpha = 0.05$) was used.

2.18.2 Software used in this study

*SmegmaList (*http://mycobrowser.epfl.ch/smegmalist.html). SmegmaList was used obtain sequences of the proteins that were used in the study from *M. smegmatis* strain MC2 genome.

ExPASy - Translate tool (http://web.expasy.org). **ExPASy** is a tool used to translate nucleotides into protein sequences. It was also used to identify or confirm if the genes are in-frame or not.

BioCyc Collection of Pathway/Genome Databases (http://www.biocyc.org). **BioCyc** is a program used to integrate genome sequences with the predicted metabolic pathways. This programs allows identification of operons of the genes of interest in various organisms.

Clone Manger Professional Edition 9. **Clone Manager** is a multi-purposed tool used for cloning operations (cloning simulations, graphic map drawing, and sequence analysis), Primer design and analysis, alignment operations and other features including editing integrated sequences, finding open reading frames and options for formatting sequences.

Multiple Alignment using Fast Fourier Transform- MAFFT)
*(*http://mafft.cbrc.jp/alignment/software*).* **MAFFT** is a program used to align multiple and larger DNA sequences at a high speed. It was also used to detect functional residues that infer the evolutionary history of protein family of interest. It can be used to draw trees that show the graphical relationship between different genomic sequences, species or organisms (For example, NJ / UPGMA phylogeny). The abbreviation NJ stands for Neighbor-Joining and UPGMA stands for Unweighted Pair Group Method with Arithmetic Mean.

*I-TASSER (*http://zhanglab.ccmb.med.umich.edu/I-TASSER/about.html). **I-TASSER** is a program used to predict protein structure and function.

2.3 Ethical considerations

The study does not involve any human or animal participants therefore no consent and ethics forms were handed out and returned, but an ethics waver was applied for and granted. A copy of approved ethics weaver is attached herewith in the Appendix.

CHAPTER 3: RESULTS

This MSc addressed key questions regarding localization dynamics of DD-CPases and other cell wall remodelling enzymes in an attempt to describe their roles in cell division and cell growth in *M. smegmatis.* Our answers to these questions are described in the results below, which have been divided into three sections: Section A - C. Section A consists of bioinformatics analysis of the DD-CPases investigated in the study. Section B consists of data obtained from cellular localization studies in wild-type *M. smegmatis* and double gene knockout mutants. Section C consists of results obtained from gene knockout studies (i.e. analysis of a double DD-CPases knockout mutant created in this study).

Section A: Bioinformatics of the DD-CPases investigated in the study

3.1. Phylogenetic and structural analysis of DD-CPases investigated in this study

Conserved catalytic residues across bacterial LMW PBPs (including DD-CPases) that aid acetylation (acylation of the serine at the active site of PBP during catalysis) and deacetylation are categorized into three, previously mentioned amino acid motifs (Goffin and Ghuysen, 1998). These presence and amino acid content of these motifs (S*XXK or Motif 1 which contains catalytic serine, the SXN or Motif 2 and KTG or Motif 3) allow for the separation of evolutionary lines of DD-CPases and other LMW PBPs from different organisms (Rawlings and Barrett, 1993).

3.1.1. Sequence alignment of the DD-CPases in various rod-shape bacteria

To investigate the divergence and/or identify conserved catalytic residues in the four DD-CPases found in *M. smegmatis* (DacB, MSMEG_1661, MSMEG_2432 and MSMEG_2433), we compared sequences of these proteins to other DD-CPases of the commonly studied rod-shape bacteria including *E. coli, B. subtilis, Actinomadura R39, Streptomyces K15* and *P. aeruginosa*, by aligning sequences using the MAFFT program. The results of these analysis confirmed presence of the all three conserved motifs in the mycobacterial homologues, Figure 3.1. However, only the first motif (S*XXK) occurred in the same position across all species, whereas SXN and KTG positioning varied across different species, suggesting these homologues may perform different functions . According to these results MSMEG_1661/2432/2433 all belong to the same family and DacB seems to be functionally

distinct as it varies in the content of the three signature motifs. This suggest that MSMEG_1661/2432/2433 may perform overlapping functions during cell division, that may be different to that of DacB. Additionally, DacB, which seems to be similar PBP4, may have overlaping roles or functions to that of PBP4s in other rod-shape bacteria.

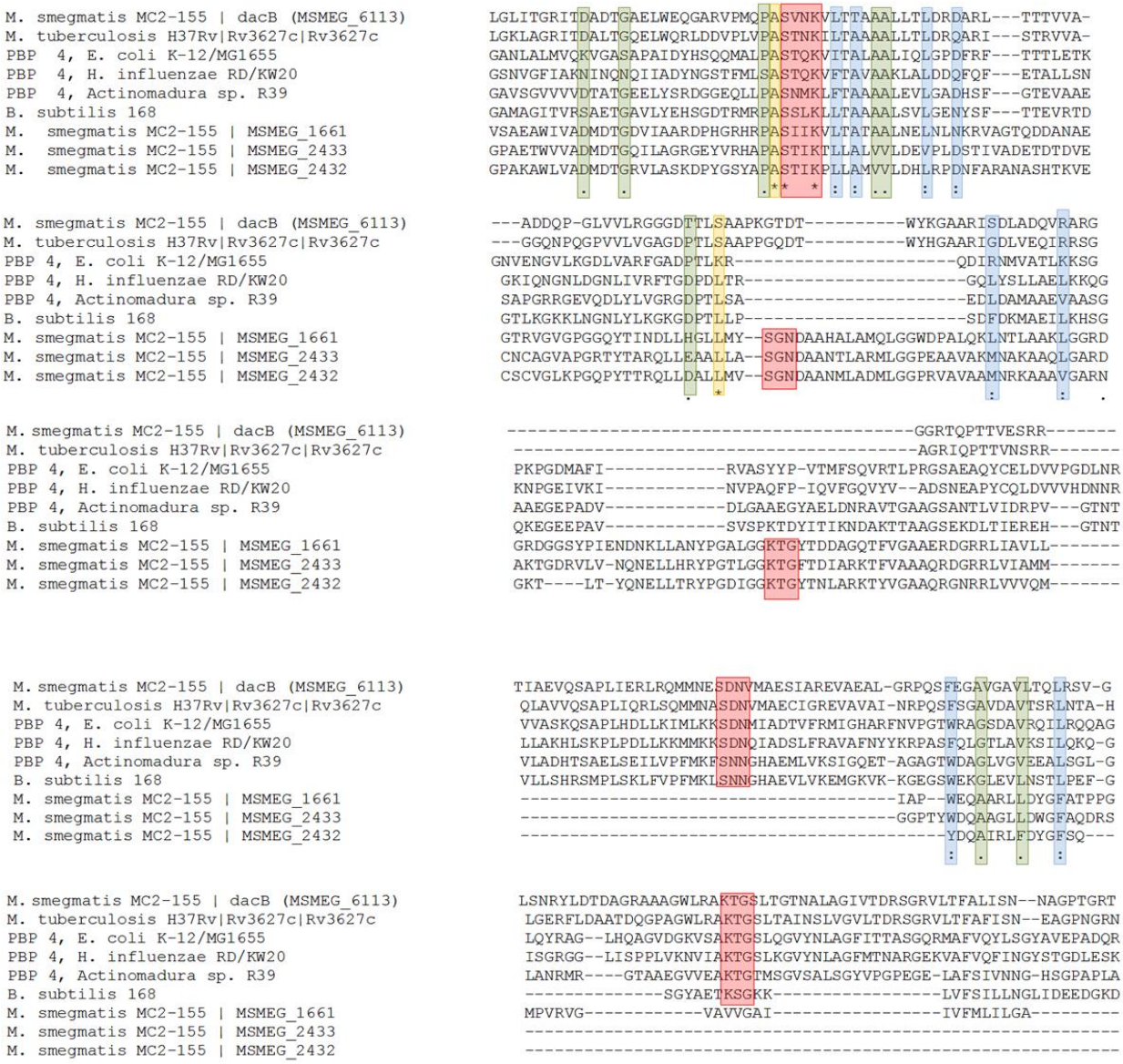


Figure 3.1: Illustration showing conserved motifs in PBPs. Depicted is the sequence alignment of the DD-CPases, the LMW PBPs, in various rod-shape bacteria. Protein sequences highlighted in red represent the three conserved motifs of PBP, S*XXK (Motif 1), the SXN (Motif 2) and [K/H][T/S]G (Motif 3). Protein sequences highlighted in green, yellow and blue represent semi-conservative variations, conserved variations and divergent variations respectively. S* represents essential serine residue. X represents the variable amino acid.

The three motifs have been proposed to occur in the same order and spacing along the polypeptide chain in PBPs. Additionally, the structural similarities and catalytic diversity of PBPs have been hypothesized to be associated with divergence in their function (Goffin and Ghuysen, 1998). To investigate relationship between structure-function and evolution of the selected *M. smegmatis* LMW PBPs, the three dimensional structure of these proteins was predicted with the I-TASSER program, using the PyMOL software to view structures. The structures resulting from this analysis are shown in Figure 3.2, A-E. A list of amino acid residues is shown in appendix A, in Table A1 and Table A2.

Structures of DD-CPases; MSMEG_1661, MSMEG_2432, MSMEG_2433 each containing 397, 275, 296 amino acids residues respectively (Figure 3.2 A-C) revealed a number of structural similarities. Firstly, the triad of motifs was localized at around same regions, spacing and order in the polypeptide chain, as described above for other organisms. In this regard, the S*XXK motif, represented by the red, SXN, represented by blue, and KTG motif, represented by purple, localized in a similar fashion (SXXK → SXN→KTG) as seen on both the crystal structure and the domain architecture diagrams, Figure 3.2 A-C. Secondly, these three LMW PBPs contained a beta-lactamase/transpeptidase-like domain and belong to the Serine Peptidase Family S11. The peptidase_S11 contain only the D-ala-D-ala peptidase with some members being partially inhibited by the thiol-blocking agents (EMBL-EBI, 2016). Lastly, in contrast to the MSMEG_1661 and MSMEG_2433, which retained a transmembrane helix, MSMEG_2432 lacked this domain, suggesting that it is not secreted or anchored to the membrane. DacB consisted of similar features to the other DD-CPases including the beta-lactamase/ transpeptidase like domain and a transmembrane helix, Figure 3.2D. However, the orientation/sequence of placement the three conserved PBP motifs varied from the other DD-CPases. Additionally, according to its domain architecture, DacB did not belong to the Serine Peptidase Family S11, as with other DD-CPases, but rather classified as a peptidase_S13-type PBP. Proteins belonging to this group have D-ala D-ala peptidase, bind to penicillin and have a D-amino peptidase activity (EMBL-EBI, 2016).

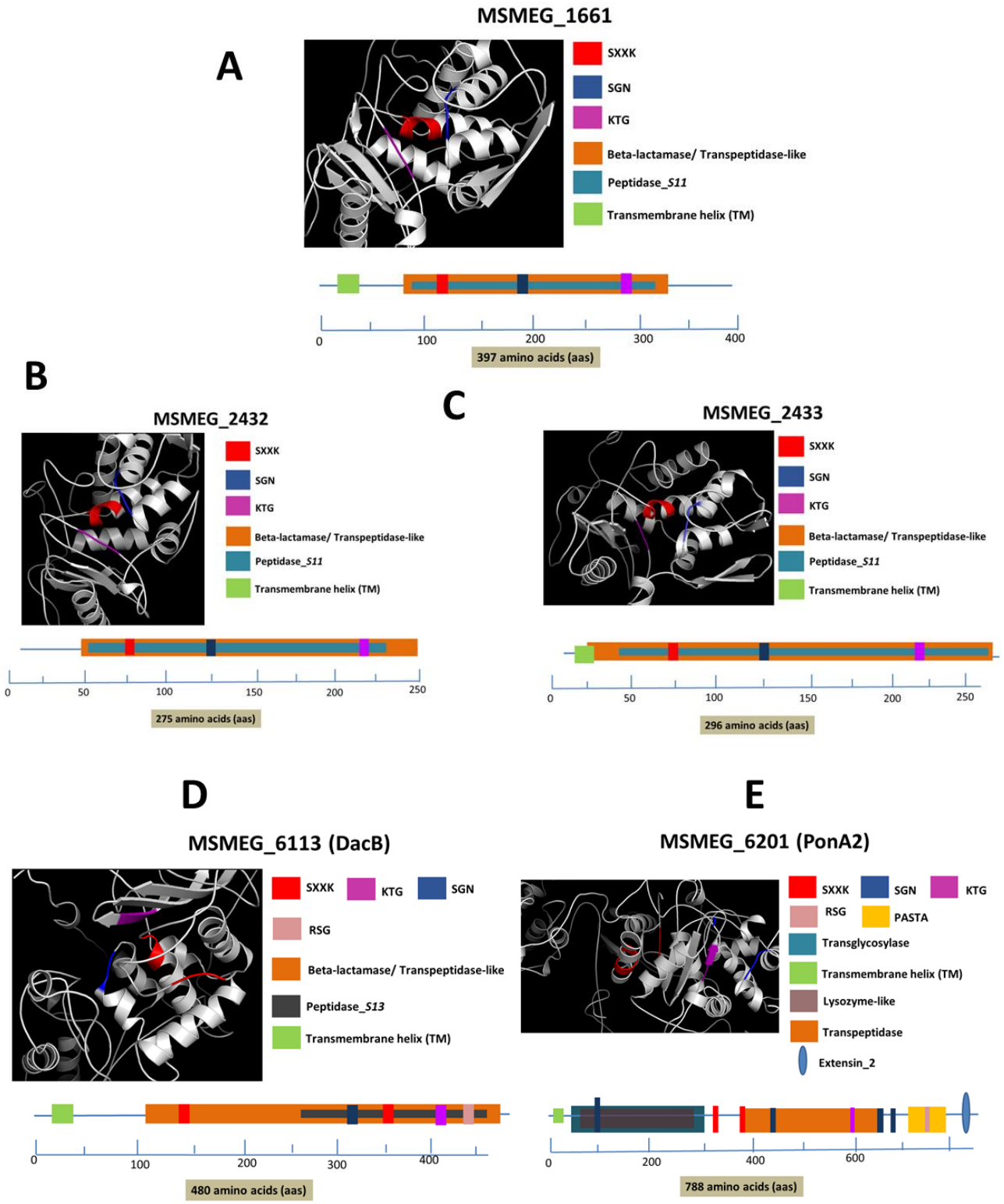


Figure 3.2: Illustration of structures, domain diagrams and conserved arrangement of catalytic residues of the five PBPs assessed this study. **(A)** – **(C)** represents ribbon diagrams of LMW PBPs, MSMEG_1661, MSMEG_2432 and MSMEG_2433, respectively, showing the three conserved motifs (SXXK→red, SXN→ dark blue and KTG→purple), position of transpeptidase-like domain (orange) and Peptidase_S11 Pfam family (light blue). The position of transmembrane helix is represented by green colour in the domain diagram. **(D)** Represents the ribbon diagram of a LMW PBP MSMEG_6113 (DacB), three conserved motifs (SXXK→red, SXN→dark blue and KTG→purple), an additional motif (RSG→dark pink), position of transpeptidase-like domain (orange) and Peptidase_S13 Pfam family (grey). Position of transmembrane helix is represented by

green colour in the domain diagram. **(E)** Represents a ribbon diagram of a HMW PBP PonA2, (SXXK→red, SXN→dark blue and KTG→purple) and an additional motif (RSG→light pink), position of PASTA domain is shown in addition to the position of two bifunctional domains found in HMW PBP (transglycosylase → light blue and transpeptidase →orange). Also shown is theposition of lysozyme-like domain (brown) and a novel Extensin_2 like-region. Note: Domain diagrams of the PBP are shown in diagrams below the crystal structure.

Lastly, we compared the structures of all DD-CPases to PonA2, a bi-functional HMW PBP with both transglycosylase and transpeptidase activities, which play a role in cell elongation during bacterial cell growth and division (Kieser *et al.*, 2015). The results of this analysis showed that PonA2 had a similar structure to that of DacB, which included similar features such as multiple S*XXK motifs and the presence of RSG motif, found in Class A and Class C beta-lactamases, Figure 3.2 A and D. In the case of PonA2, the predicted structure revealed transglycosylase, lysozyme-like, and transpeptidase regions, in addition to a PASTA domain (Figure 3.2E). Moreover at the end of the amino acid sequence, there is an Extensin_2 region, which belongs to hydroxyproline-rich glycoproteins usually found in cell walls of plants (Stafstrom and Staehelin, 1986)

3.1.2. Divergence of peptidase_S13 of DD-CPase-PBP4 in various rod-shape bacteria

Comparing similarities and difference in organisms with a common shape has been suggested to have an impact in determining key roles or general principles that determines shape as well as evolutionary origin (Chang and Huang, 2014). For this, we compared PBP4s of rod-shape bacteria belonging to peptidase_S13 family namely, *Actinomadura sp*., *H. influenza*, *E. coli*, *B. subtilis*, *M. tuberculosis*, *P. aerugonosa*, and *M. smegmatis.* Sequences obtained were aligned using a multiple sequence alignment program called MAFFT. Using the same program a phylogenetic tree was drawn and the tree was viewed on Phylo.io. A representation of results obtained is shown in, Figure 3.3. As expected, PBP4s of *M. tuberculosis* and *M. smegmatis* were highly related compared to all other organisms. Secondly, considering two most commonly studied organisms, *B. subtilis* and *E. coli*, PBP4 of *M. smegmatis* (DacB) displayed closer relatedness to PBP4 of *B. subtilis* than *E. coli*, while *B. subtilis* was more related to *Actinomadura sp. R39.* These results suggest that the biological role of PBP4 in Gram-positives may be conserved in the mycobacterial DD-CPase homologues, a hypothesis we assessed further by studying the localization of DD-CPases in *M. smegmatis*.

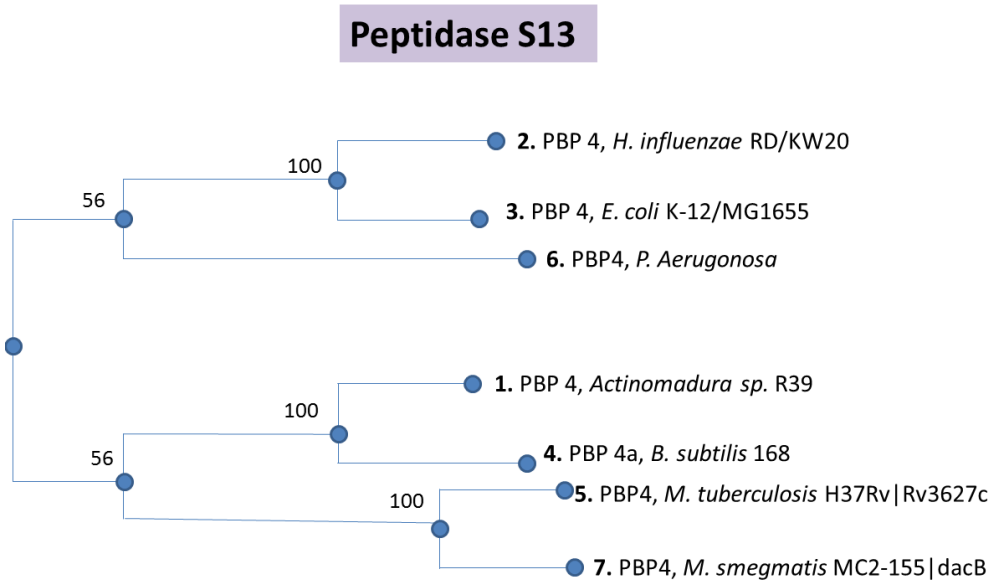


Figure 3.3: Phylogenetic tree showing divergence of PBP4 across rod-shape bacteria. Shown is the maximum-likelihood tree of Peptidase_S13 from various Actinobacteria, *Actinomadura sp*., *H. influenza*, *E. coli*, *B. subtilis*, *M. tuberculosis*, *P. aerugonosa*, and *M. smegmatis*. Numbers 1 to 7 in bold represent the order in which the data was added on the list prior alignment. Higher values of maximum likelihood (i.e. 100) represent maximum support and/or evidence of sequences clustering together and a lower value suggests the opposite.

Section B: Cellular localization of DD-CPases and cell wall remodelling enzymes in wild-type *M. smegmatis* cells

To localize DD-CPases, relative to other components of the cell division and elongation machinery, we created reporter genes to evaluate the function(s) of these proteins during mycobacterial cell division and cell growth. The reporter genes used in this study were created using three way cloning (for example, the genes for DacB or the other DD-CPases were ligated into the pMV306H vector together with the gene for GFP, see Methods section 2.12.1 on how exactly this was done). Controls (or reference strains containing just the reporter gene) were created using standard cloning process (e.g. GFP ligated into pMV306H vector). The former constructs were generated to track the location of proteins of interest in *M. smegmatis* cells, while the latter were used as reference strains to ensure that localization observed is not a representation of the tag alone. The location of fusion proteins in the cell were measured based on the fluorescent intensity of foci using light microscopy. Plasmid constructs carrying all reporter fusions used in the study were confirmed with restriction enzyme mapping and DNA sequencing prior to introduction in *M. smegmatis* cells.

Please note: All gel electrophoresis pictures of the PCR data showing correct or successfully amplified DNA of the inserts (genes of interest and fluorescent reporter proteins), in addition to PCRs that confirm the integration of the vectors in *M. smegmatis* are listed in the appendices section. Additionally, maps of the plasmids used to create these constructs with their restriction enzyme (RE) profiles are also listed in the appendices section as well. The detailed restriction analysis or profiles confirming the genetic integrity of the plasmids are included in this section.

3.2 Identification of gene location and transcription units for the DD-CPases in *M. smegmatis* prior cloning

Prior to cloning, we first confirmed that cloning strategy to produce fused proteins that are in-frame by using ExPASy at the SIB Bioinformatics Resource Portal. This allowed for translation of in silico genetic fusions and the results obtained confirmed that fusions were in-frame. We then investigated if the LMW PBPs (DD- CPases) used in this study are singularly transcribed or co-transcribed with other genes. For this, we identified and evaluated the operonic regions of these genes using the BioCyc Collection of Pathway/Genome Databases to identify the transcriptional units and operonic structures (if present). Results showed that the gene encoding *dacB* or MSMEG_6113 (Rv3627c in *M. tuberculosis*) appeared to be co-transcribed with a conserved hypothetical protein MSMEG_6112 (Rv3626c) and thus formed an Rv3627c-Rv3626c operon, Figure 3.4. However, since MSMEG_6112 (Rv3626c) is first gene of the operon, 150 bp upstream of this gene, which presumably contained the promoter region, was selected for cloning. A similar approach was adopted with the other genes. The remaining DD-CPases; Rv2911 (MSMEG_2433 and MSMEG_2432) and Rv3330 (MSMEG_1661) were also analyzed and results showed that they are singularly transcribed (Figure 3.4B and 3.4C).

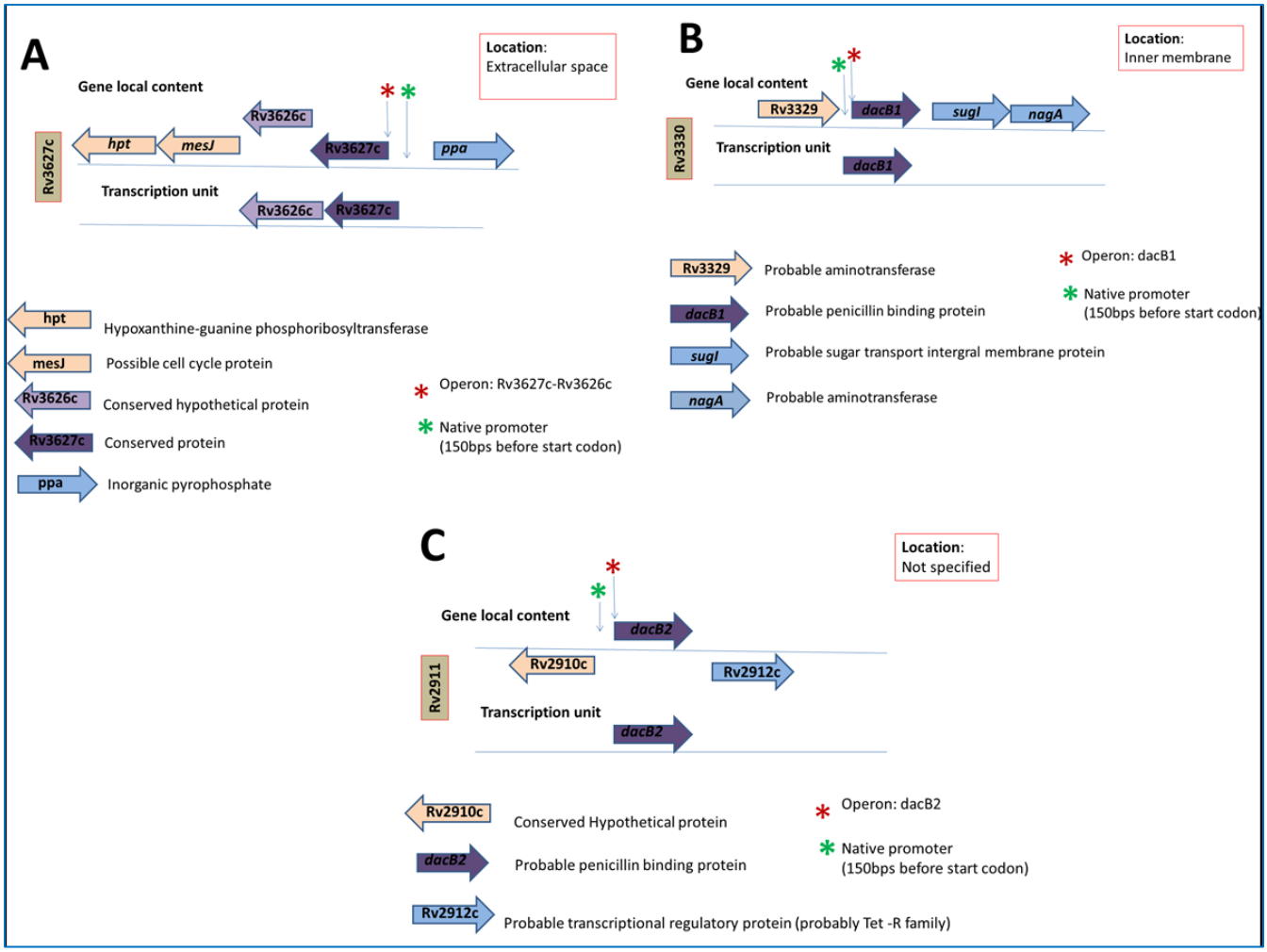


Figure 3.4: Illustration showing gene loci that encode DD-CPases in mycobacteria. **(A)** Gene local content and transcription units of DacB (Rv3627c in *M. tuberculosis*). **(B)** Gene local content and transcription units of MSMEG_1661 (Rv3330 in *M. tuberculosis*). **(C)** Gene local content and transcription units of MSMEG_2433 (Rv2911 in *M. tuberculosis*). The dark purple arrow represents gene of interest in this study and the lighter purple or violet represents the possible operonic gene/s. Genes occurring upstream or downstream of operon are coded with colours other that the purple/violet. Genes of the same colour represents members in the same operon. In the case of genes listed the top and at bottom of the strand, these represent genes transcribed in opposite direction. The start of operon is represented by red star (*) and the native promoter region, which is taken to lie within 150 bp before the gene/operon start, is represented by the green star (*). Shown in the red box is the predicted location of the DD-CPases, with DacB2, it was unclear **Note**: Figures are not according to scale.

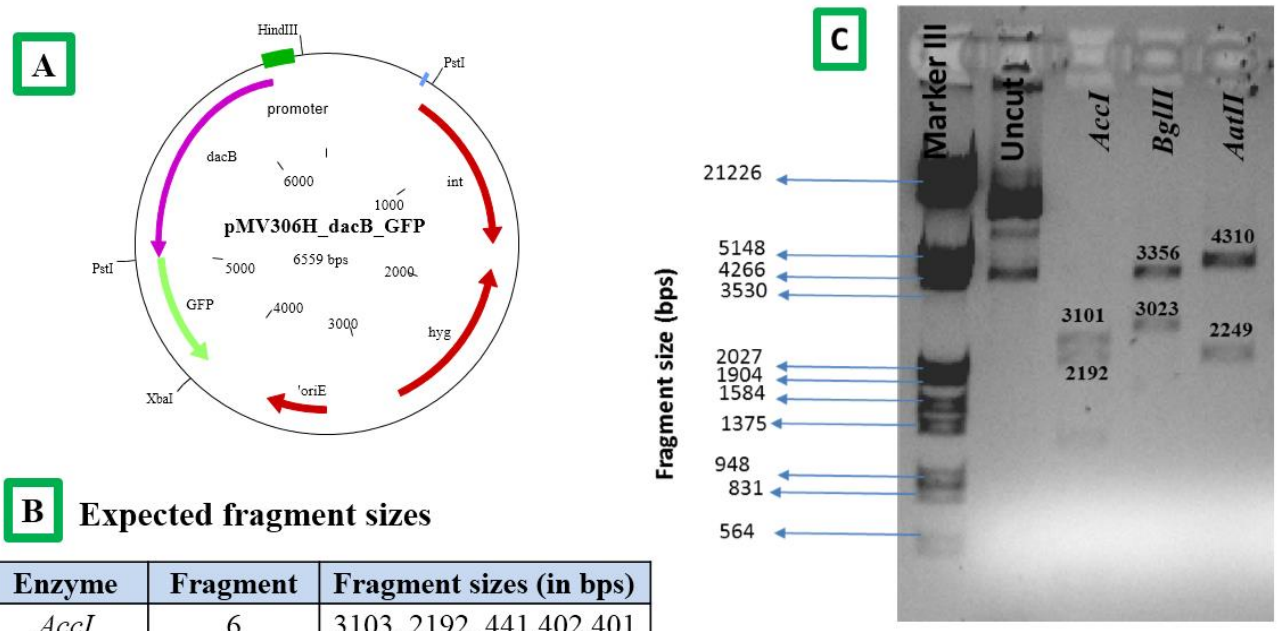
3.2.1 Subcellular localization of the DacB in wild-type *M. smegmatis* cells

Construction of the pMV306H_dacB_GFP plasmid using three-way cloning

To create integration vectors for chromosomal expression of fluorescent derivatives of *M. smegmatis* DD-CPases, we constructed integrative plasmids expressing these proteins from their native chromosomal promoters in *M. smegmatis*. These fluorescently-tagged proteins

carried either a green (Figure 3.5), Red, mCherry or Turquoise fluorescent protein at the C-terminus (Appendix G). To create such constructs, we first extracted genomic DNA from mc2155 strain (wild-type *M. smegmatis*) using CTAB method (as described on methods section 2.4.2.2) and plasmid DNA containing the gene of the fluorescent protein of interest (for example, pGMEH-P38-mRFP to obtain mRFP) using mini/maxi-prep DNA extraction (as described in methods section 2.4.1). Genomic DNA was used to amplify DD-CPases or mycobacteria genes of interest using PCR with primers listed in Table 2.3 and amplified products are shown in the Appendix D, Figure D1.

Primers used for DNA amplification were designed in such a way that they would have complementary restriction sites at each end when ligated in order to have one in-frame gene. This was done by introducing amino acid linkers and restriction enzymes at both ends of the genes and both ends of the tags (for example *dacB*, *HindIII/ Pst*I and GFP, *Pst*I*/Xba*I, sites were included, therefore *dacB* and GFP joins at the *PstI* site). Different ratios were used for ligation purposes (1:1:1 to 4:4:1 → gene: reporter tag: vector). The recombinant DNA molecules were then transformed into *E. coli* and the transformed cells were streaked onto LB Agar medium containing respective antibiotics. A minimum of 20 colonies or clones that grew on these plates were selected, inoculated, the plasmid DNA extracted using mini/maxi-prep and profiled using restriction enzymes (data not shown). The DNA for one correct clone was then prepared in bulk and this was followed by restriction analysis, shown in Figure 3.5 for the pMV306H_dacB_GFP plasmid. All cloned fragments were also sequenced to ensure that no mutations were introduced during PCR (data not shown). Other constructs including pMV306H_dacB_mTurq and pMV306H_dacB_mRFP in attempt to create vectors for co-localization studies with other cell wall remodelling enzymes listed in the sections below. The final restriction analysis for these plasmids is given in Appendix G (Figure G2.1 and Figure G2.2). After confirmation, plasmids were electroporated into *M. smegmatis* cells and integration of plasmid at the L5 *attB* site was confirmed by PCR (data not shown due to space limitations). Fluorescent intensities and representative localization patterns were determined for about 100 cells per experiment and each experiment was conducted three times for each strain.



B **Expected fragment sizes**

Enzyme	Fragment	Fragment sizes (in bps)
AccI	6	3103, 2192, 441,402,401 and 21
BglII	2	3356, 3023
AatII	2	4310, 2249

Figure 3.5: Restriction enzyme profiling of the pMV306H_dacB_GFP construct **(A)** Represents the pMV306H_dacB_GFP construct (Derivative of DacB carrying an in-frame C-terminal GFP tag) and the enzmyes used for creating the construct are; DacB (*HindIII* and *PstI*), GFP (*PstI* and *XbaI)* and pMV306H (*HindIII* and *XbaI*). To confirm this construct is correct, restriction profiling was done and the expected fragment sizes **(B)** were compared to those observed **(C)** on the agarose gel. The expected sizes matched observed and this indiated that construct created was correct. This plasmid was used to track the localization pattern of DacB in *M. smegmatis* cells.

Cellular localization of DacB-GFP in *M. smegmatis*

To determine the subcellular localization patterns of DacB in wild-type *M. smegmatis* cells, we created a reporter DacB-GFP fusion and the localization was visualized under a fluorescence microscope. Different localization patterns were observed and these varied from unipolar, mid-cell to bipolar. A total of nine localization patterns [(i) Sub-polar and mid-cell, (ii) Mid-cell and bipolar, (iii) Bipolar, (iv) multiple mid-cell and bipolar, (v) Subpolar, (vi) Unipolar and mid-cell, (vii) Mid-cell, (viii) Unipolar, (ix) Punctate] were observed (Figure 3.6A). However, in majority of the cells, the most frequent (top three) observed localization patterns were bipolar, when cell were between the lengths 1.5 µm – 3.8 µm (newly divided and non-diving cells), followed by mid-cell and bipolar localization when cells were between cell lengths 2.0 µm – 3.9 µm (elongating cells and cell that are about to divide), and unipolar

localization in cells with lengths between 1.8 μm – 3.5 μm (Figure 3.6B). We also found that two foci-containing cells consisted of cells with bipolar, unipolar and mid-cell, and subpolar and unipolar localization patterns (Figure 3.6A iii, vi and i). Three foci cells consisted of cells with mid-cell localization pattern (Figure 3.6A ii). Four foci cells consisted of cells with multiple mid-cell and bipolar and punctate localization patterns (Figure 3.6A iv and ix) and five foci cells were represented by punctate localization. Most of the cells (44 %) contained two foci and one foci (20 %) and rest had either three (19 %), four (15 %) or five foci (4 %) during exponential growth phase. As mycobacterial cells elongate at their poles(Singh *et al*., 2013), these patterns suggest that DacB is involved in the elongation. The septal localization patterns suggest that DacB is also involved in PG remodeling during cell division.

Next, we compared foci observed in single cells of *M. smegmatis* carrying the DacB-GFP fusion, Figure 3.6C. Cells with one focus included those with mid-cell and unipolar localization patterns (Figure 3.6A v, vii and viii) from both rod and V-shaped cells (Figure 3.6C). Rod-shape bacteria are presumed to be undergoing elongation or have just divided. Mycobacterial cells separate after cytokinesis using V-snapping mechanism (Thanky *et al*., 2007, Kieser and Rubin, 2014). Hence, the V-shaped cells are presumed to be undergoing cell division. One to four foci were found in both rod-shape and V-shaped cells, their localization patterns is shown in Figure 3.6C. Five foci were only found in Rod-shape bacteria. It should be noted that only a small proportion of cells viewed has a V-shaped morphology, Figure 3.6D. This is to be expected as the actual cell division event is occurring asynchronously in broth culture, hence only a small proportion of cells will be dividing at any given time. Most will have just divided or will be in the process of extending.

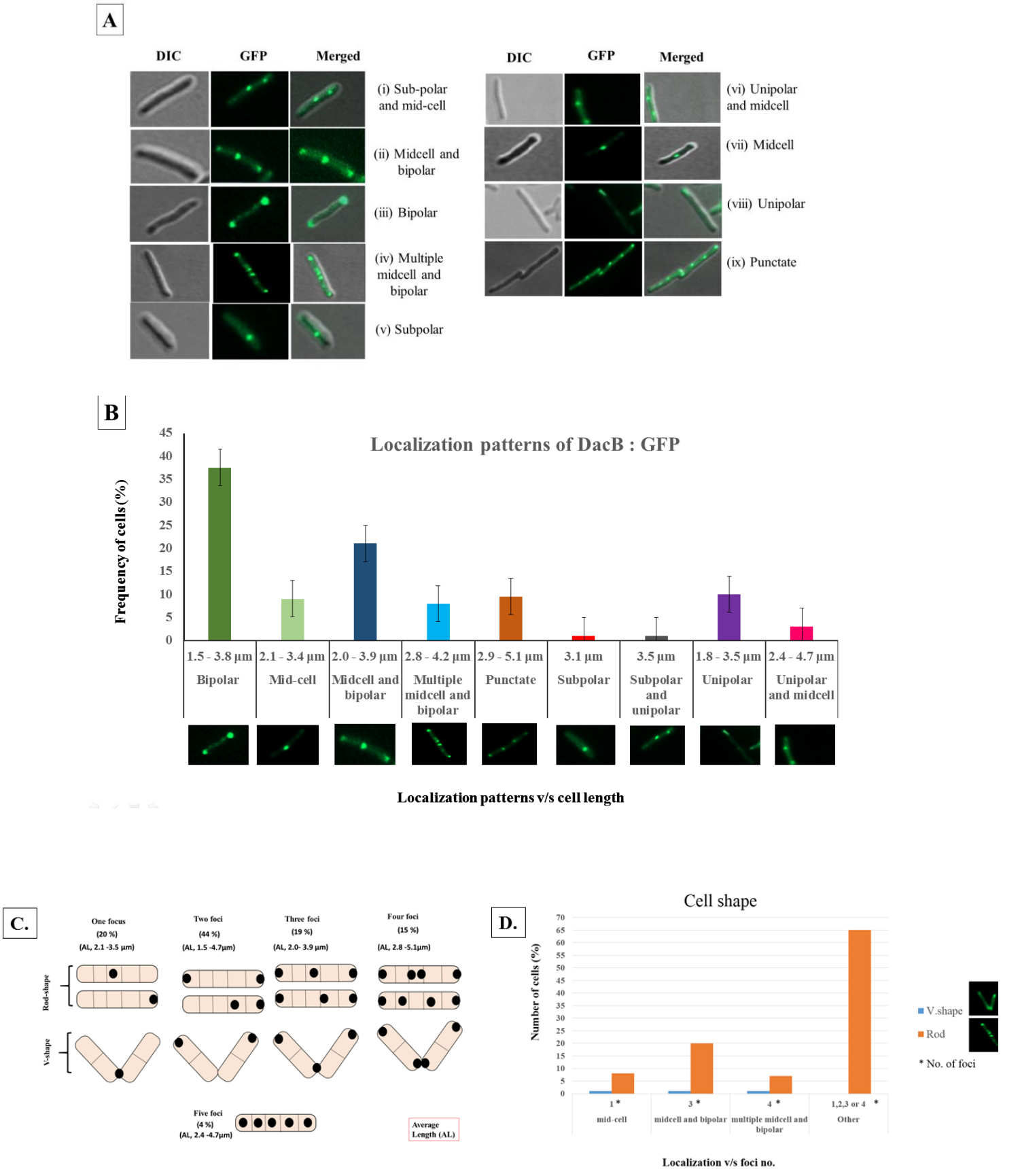


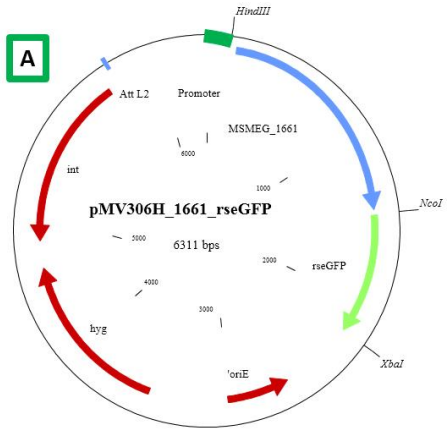
Figure 3.6: Subcellular localization patterns of DacB-GFP in wild-type *M. smegmatis* cells. **(A)** Numbers (i) to (ix) represent different patterns observed [(i) Sub-polar and mid-cell, (ii) Mid-cell and bipolar, (iii) Bipolar,

(iv) multiple mid-cell and bipolar, (v) Subpolar, (vi) Unipolar and mid-cell, (vii) Mid-cell, (viii) Unipolar, (ix) Punctate]. Scale used to measure cells is 5 µm. **(B)** Quantitation of the localization patterns observed in (A) of DacB in wild-type *M. smegmatis*. The histogram represents the frequency of cells with specific localization patterns in relation to cell length. The experiment was done in triplicate (n= 100 cells, per biological repeat, data represents at least two biological repeats, some data had to excluded from certain biological repeats due to poor microscopy data). **(C)** Cartoons representing wild-type *M. smegmatis* cells with one to five DacB-GFP foci. On each cartoon, is a representation of number foci, percentage of cells with that foci and the average cell length (AL). Also shown is localization in the two different shapes observed, rod-shape and V-shape. **(D).** Total percentage in which the various cell shapes were observed**.**

3.2.2. Subcellular localization MSMEG_1661 in wild-type *M. smegmatis* cells

Construction of the pMV306H_MSMEG_1661_GFP plasmid using three way cloning

For localization of the MSMEG_1661-encoded DD-CPase, a plasmid that allowed for the production of a MSMEG_1661-GFP fusion was created as for DacB described previously. The genetic integrity of the plasmid was confirmed by restriction mapping, Figure 3.7, and sequencing, data not shown. Restriction digest with the plasmid, pMV306H_MSMEG_1661_rseGFP yielded the expected banding patterns, Figure 3.7 and hence, this plasmid was taken forward for localization studies. The plasmid was electroporated into wild-type *M. smegmatis* and incorporation of the vector was confirmed by PCR.



B **Expected fragment sizes**

Enzyme	Fragment (no.)	Fragment size (base pairs)
AccI	4	2941, 2191,885,294
BamHI	2	4445, 1866
BglII	2	3288,3023

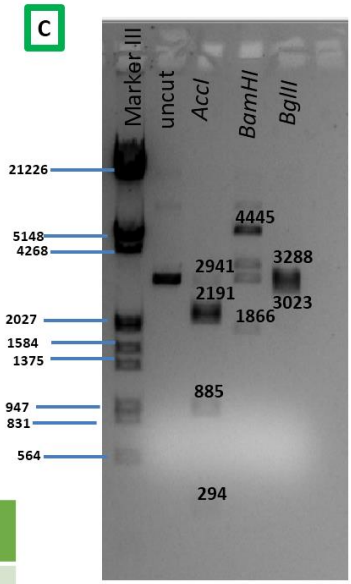


Figure 3.7: Restriction enzyme profiling of the pMV306H_MSMEG_1661_GFP construct. **(A)** Represents the map of pMV306H_MSMEG_1661_GFP construct (Derivative of MSMEG_1661 carrying an in-frame C-terminal GFP tag). During restriction profiling, the expected fragment sizes **(B)** were compared to those observed **(C)** on the agarose gel. The expected sizes matched the observed, thus confirming that the plasmid was correct and could be used to track localization patterns of MSMEG_1661 in *M. smegmatis* cells. Please note: the extra two bands seen in *BamHI* around3500 bp are none specific and could have resulted partial digestion, however, the plasmid was sent for sequencing and the construct was correct.

Localization of MSMEG_1661 in wild-type *M. smegmatis* single cells

The subcellular localization patterns of MSMEG_1661 during cell growth and division in wild-type *M. smegmatis* cells were tracked using a reporter strain expressing MSMEG_1661 -GFP. Different localization patterns observed varied from multiple mid-cell and bipolar to just bipolar. About six localization patterns [(i) Multiple mid-cell and bipolar, (ii) Punctate, (iii) Subpolar and mid-cell, (iv) Unipolar, (v) Mid-cell and (vi) Bipolar] were observed, Figure 3.8A. As with DacB, varying localization patterns were observed in rod-shape and V-shaped cells, Figure 3.8B. The two most frequent localization patterns observed in these cells were bipolar (in cell with lengths between 2.0 μm – 5.1 μm) and multiple-mid-cell/mid-cell and bipolar (in cells with lengths between 2.9 μm – 5.0 μm), Figure 3.8C. These results suggested that MSMEG_1661 is also involved in cell elongation during mycobacterial cell division and growth. The bipolar-multiple-mid-cell localization may represent the last stage of cell division, where daughter cells are about to divide and the bipolar only localization may represent cells at birth before they elongate.

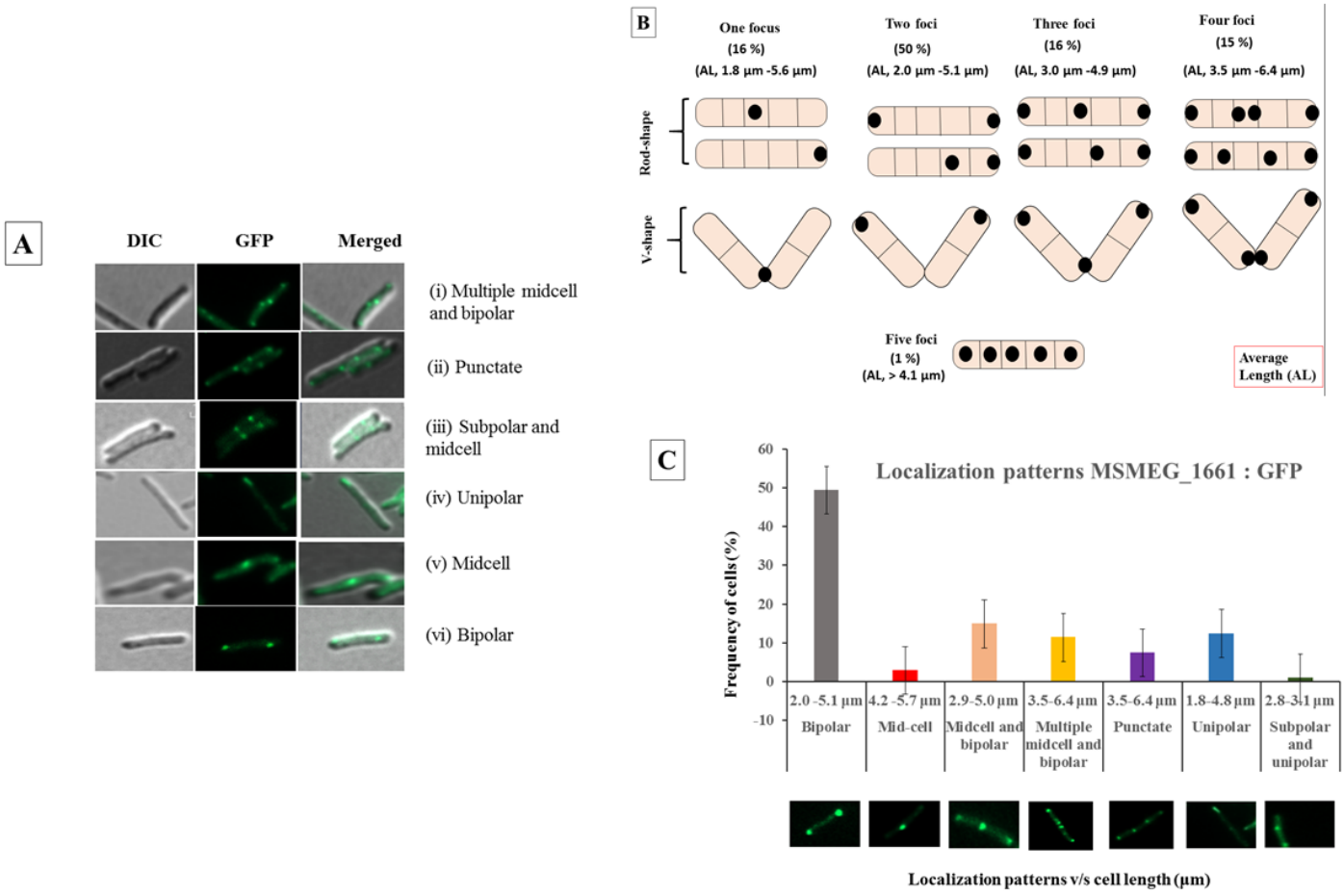


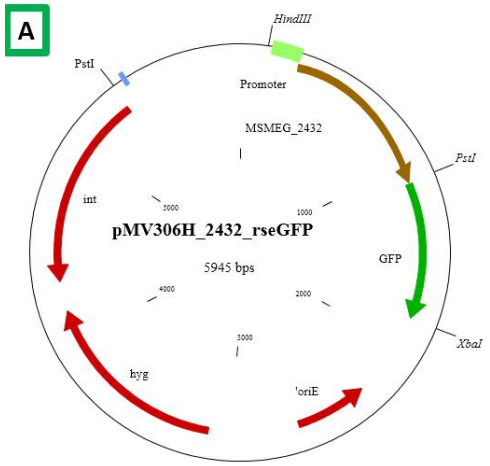
Figure 3.8: Subcellular localization patterns of MSMEG_1661_GFP in wild-type *M. smegmatis* cells. (A) Numbers 1 to 6 represent different patterns observed [1: Multiple mid-cell and bipolar, 2: Punctate,

3: Sub-polar and mid-cell, 4: unipolar, 5: Mid-cell and 6: Bipolar]. Scale used to measure cells is 5 µm. **(B)** Quantitation of the localization patterns observed (A) of MSMEG_1661 in wild-type *M. smegmatis*. The histogram represents the frequency of cells with specific localization patterns in relation to cell length. The experiment was done in triplicates (n= 100 cells, per repeat). **(C)** Cartoons representing wild-type *M. smegmatis* cells with one to five MSMEG_1661-GFP foci. On top of each cartoon, is a representation of number foci, percentage of cells with that foci and the average cell length (AL) in which the foci was observed. The two different shapes observed in these cells rod-shape and V-shape.

3.2.3. Subcellular localization of the MSMEG_2432 in wild-type *M. smegmatis* cells

Construction of the pMV306H_MSMEG_2432_GFP plasmid using three way cloning

Using an approach that was similar to that employed for the two DD-CPases discussed previously, a vector expressing an MSEMG_2432-GFP fusion was created. Restriction analysis of the pMV306H_MSMEG_2432_GFP plasmid yielded the correct banding patterns, Figure 3.9, and sequencing confirmed that no mutations were introduced during PCR. This plasmid was electroporated into *M. smegmatis* wild-type for localization studies.



B

Expected fragment sizes

Enzyme	Fragment (no.)	Fragment size (base pairs)
AccI	2	3754, 2191
MscI	3	3816, 1344, 785
NotI	2	4389, 1556
XbaI	1	5945

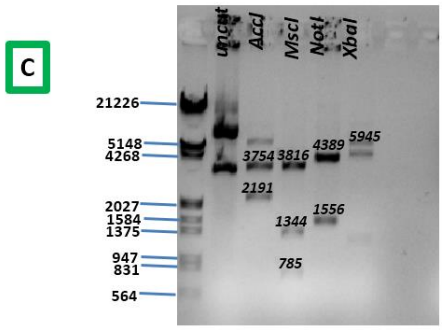


Figure 3.9: Restriction profiling of the pMV306H_MSMEG_2432_GFP construct **(A)** Represents the pMV306H_MSMEG_2432_GFP construct (Derivative of MSMEG_2432 carrying an in-frame C-terminal GFP tag)/ The enzymes used for creating the construct are; MSMEG_2432 (*HindIII* and *PstI*) GFP (*PstI* and *XbaI)* and pMV306H (*HindIII* and *XbaI*). To confirm that this construct is correct, restriction profiling was done and the expected fragment sizes **(B)** were compared to those observed **(C)** on the agarose gel. The expected sizes matched observed thus confirming that the plasmid created was correct and could be used to track the localization pattern of MSMEG_2432 in *M. smegmatis* cells. Please note: the faint bands or extra bands in *AccI* (above the 3754 bp band) and *XbaI* (band below the 5945 bp fragment) may have resulted from star activity of the enzyme or due to partial restriction. However, other restriction enzymes were also used to confirm this clone in addition to DNA sequencing.

Unlike DacB-GFP and MSMEG_1661-GFP, which localized in varying patterns, the subcellular localization patterns of MSMEG_2432-GFP in wild-type *M. smegmatis* cell were mainly polar and polar-mid-cell. Six localization patterns [(i) Unipolar, (ii) Multiple mid-cell and bipolar, (iii) Punctate, (iv) Mid-cell and bipolar, (v) Bipolar and (vi) Mid-cell] were observed, Figure 3.10A. The most frequent localization patterns observed were bipolar, in cells with lengths of 1.5 μm – 5.4 μm and bipolar-mid-cell, in cells with lengths of 2.3 μm – 6.0 μm, respectively, Figure 3.10B and C. This suggests that MSMEG_2432 may also be in involved in cell elongation during mycobacterial cell division and growth. Unpublished data from our lab (C. Ealand) indicated that MSMEG_2432 is expressed in very low abundance and as a result, it was difficult to localize.

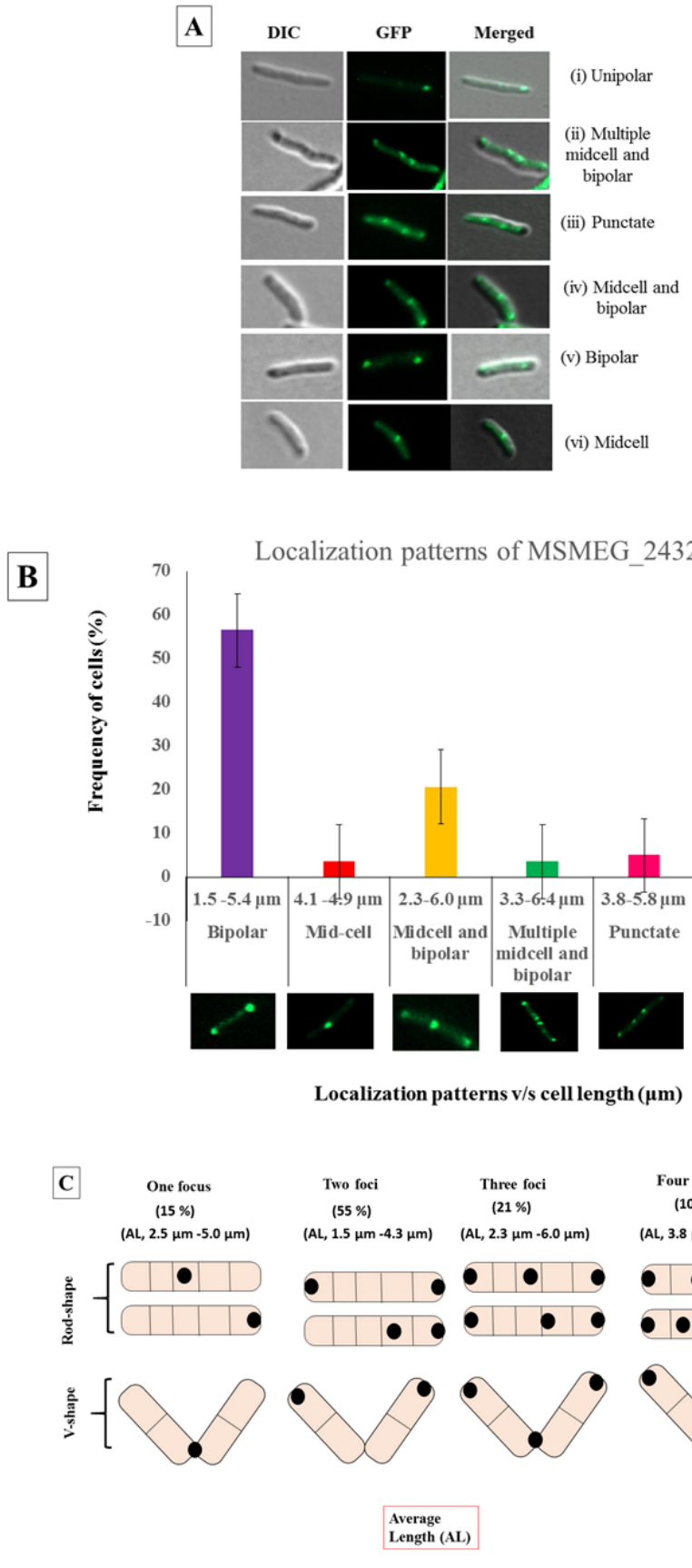
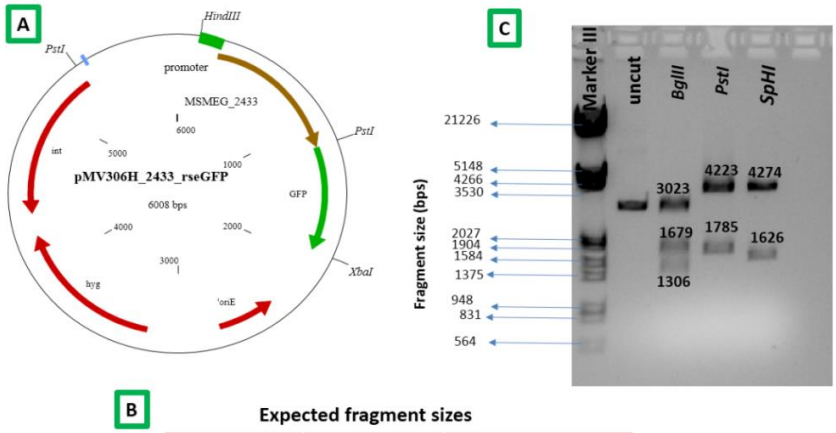


Figure 3.10: Subcellular localization patterns of MSMEG_2432_GFP in wild-type *M. smegmatis* cells. (A) Numbers (i) to (vi) represent different patterns observed [(i) Unipolar, (ii) Multiple mid-cell and bipolar, (iii) Punctate, (iv) Mid-cell and bipolar, (v) Bipolar and (vi) Mid-cell]. (B) Quantitation of the localization patterns observed (A) of MSMEG_2432 in wild-type *M. smegmatis*. The histogram represents the frequency of cells with specific localization patterns in relation to cell length. The experiment was done in triplicates. Data represents at least two biological repeats. (C) Cartoons representing wild-type *M. smegmatis* cells with one to five MSMEG_2432-GFP foci. On top of each cartoon, is a representation of number foci, percentage of cells with that foci and the average cell length (AL) in which the foci was observed. Two different shapes observed in these cells are rod-shape and V-shape.

3.2.4. Subcellular localization of the MSMEG_2433 in wild-type *M. smegmatis* cells

Construction of the pMV306H_MSMEG_2433_GFP plasmid using three way cloning

As with the other DD-CPases, a plasmid was constructed that allowed for expression of a MSMEG_2433-GFP fusion protein and that could be used to determine the localization of this protein. Restriction analysis of the pMV306H_MSMEG_2433_GFP plasmid, Figure 3.11, yielded the expected banding pattern and sequencing yielded no mutations (data not shown).



B

Expected fragment sizes

Enzyme	Fragment (no.)	Fragment size (base pairs)
BglII	3	3023,1679,1306
PstI	2	4223,1785
SpHI	3	4274,1626,108

Figure 3.11: Restriction enzyme profiling of the pMV306H_MSMEG_2433_GFP construct **(A)** Represents the pMV306H_MSMEG_2433_GFP construct (Derivative of MSMEG_2433 carrying an in-frame C-terminal GFP tag). The enzymes used for creating the construct are MSMEG_2433 (*HindIII* and *PstI*) GFP (*PstI* and *XbaI)* and pMV306H (*HindIII* and *XbaI*). Restriction profiling was done and the expected fragment sizes **(B)** were compared to those observed **(C)** on the agarose gel. The expected sizes matched observed thus confirming that construct created was correct and could be used to track the localization pattern of MSMEG_2433 in *M. smegmatis.*

Localization of MSMEG_2433-GFP in *M. smegmatis* wild-type

Different localization patterns were also observed MSMEG_2433-GFP as with all other DD-CPases analyzed in this study. Patterns varied from sub-polar, bipolar to multiple mid-cell and bipolar. Seven localization patterns [(i) Unipolar, (ii) Punctate, (iii) Multiple mid-cell and bipolar, (iv) Bipolar, (v) Mid-cell, (vi) Sub-polar and mid-cell, (vii) Mid-cell-polar], Figure 3.12A .

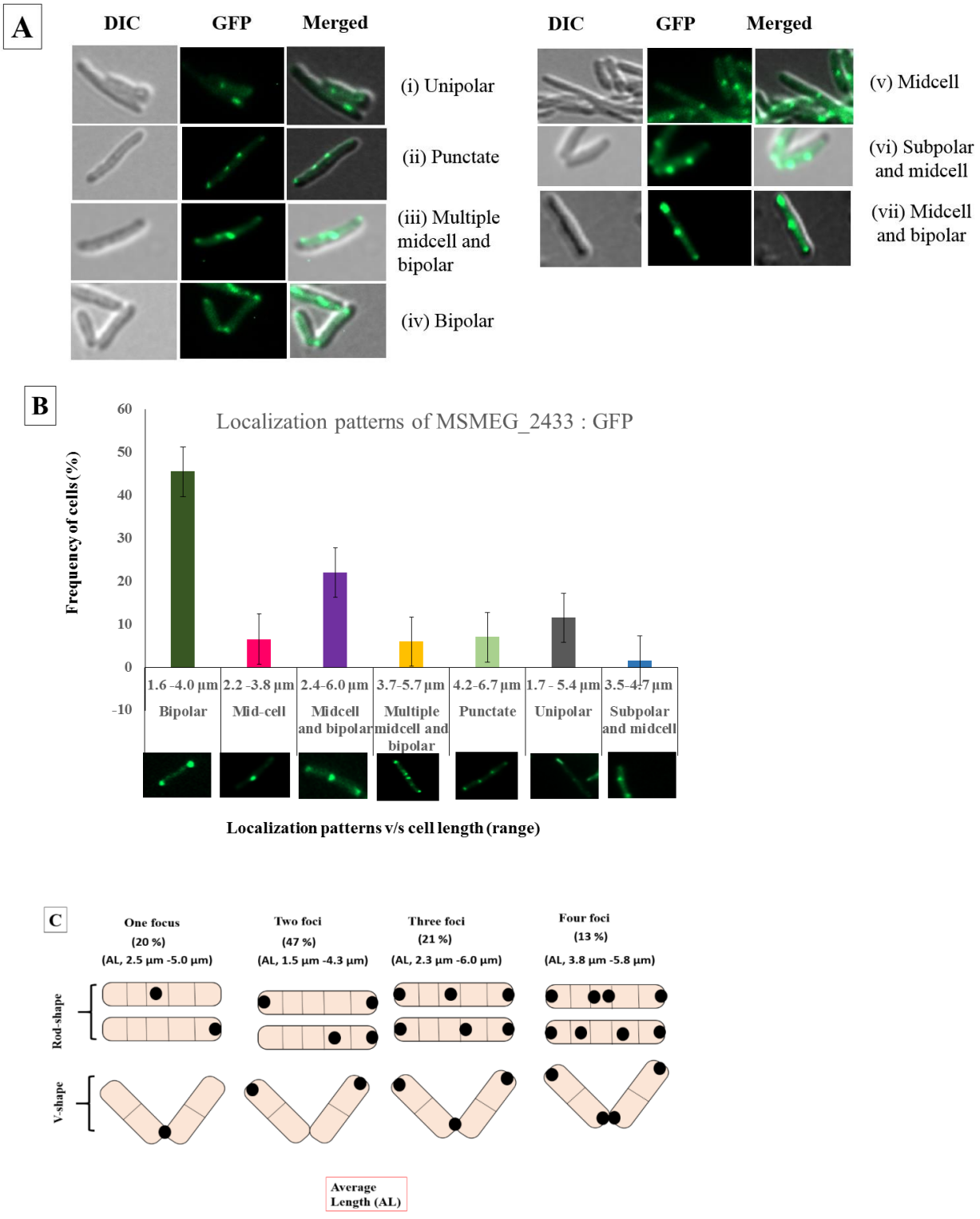


Figure 3.12: Subcellular localization patterns of MSMEG_2433 in wild-type *M. smegmatis*. **(A)** Numbers (i) to (vii) represent each pattern observed [(i) Unipolar, (ii) Punctate, (iii) Multiple mid-cell and bipolar, (iv) Bipolar, (v) Mid-cell, (vi) Sub-polar and Mid-cell, (vii) Mid-cell-polar]. **(B)** Quantitation of the localization patterns observed in (A) of MSMEG_2433-GFP in wild-type *M. smegmatis*. The histogram represents the frequency of cell with specific localization patterns in relation to cell length. Data represents at least two biological repeats. **(C)** Cartoons representing wild-type *M. smegmatis* cells with one to five MSMEG_2433-GFP foci. On top of each cartoon, is a representation of number foci, percentage of cells with that foci and the average cell length (AL) in which the foci was observed. Two different shapes observed in these cells are rod-shape and V-shape.

displayed mostly mid-cell and bipolar localization of MSEMG_2433-GFP. Bipolar localization was observed in cells with lengths between 1.6 μm – 4.0 μm. Mid-cell localization was observed in cells with lengths between 2.2 μm – 3.8 μm, Figure 3.12 B and C. As with the others proteins, these patterns suggest that MSMEG_2433 is involved in mycobacterial cell division and elongation.

3.2.5. Subcellular localization of PonA2 in wild-type *M. smegmatis*

To correlate the dynamics of DD-CPase localization with that of other cell division enzymes, the localization pattern of PonA2, a HMW PBP was assessed. The PBP1a (PonA2 in *M. smegmatis*) is hypothesized to be involved in the last stage of PG synthesis (Trojanowski *et al*., 2015). To identify the subcellular localization patterns of PonA2 in *M. smegmatis*, PonA2-GFP patterning was tracked in wild-type *M. smegmatis* cells. The restriction profiling for the plasmid created to express PonA2-GFP is given in the AppendixG, Figure 2.4. PonA2-GFP localized in various positions [(i) Mid-cell, (ii) Multiple mid-cell and bipolar, (iii) punctate, (iv) mid-cell and bipolar, (v) bipolar, (vi) unipolar, (vii) sub-polar and (viii) sub-polar and mid-cell], Figure 3.13A. Similar to DacB, PonA2 localization in the majority of the cells was mainly to both poles followed by mid-cell and bipolar and mid-cell localization, respectively, Figure 3.13B. In cells with cell lengths between 2.5 μm – 5.8 μm, 2.3 μm – 4.6 μm and 1.6 μm – 4.5 μm, mid-cell and bipolar, mid-cell, and bipolar localization patterns were observed respectively, Figure 3.13 B and C. The mid-cell and bipolar localization observed here may represent the last stage of cell division, just before the daughter cell separate. This statement can be supported by the observation that when the cell reaches the longest length (for example ± 5.8 μm), mid-cell-bipolar localization patterning occurs. The results observed here suggest that PonA2 is involved in cell elongation in mycobacterial cell division. Moreover, as DacB-GFP localized in the similar manner as PonA2, these data also suggest that DacB may also be involved in cell elongation.

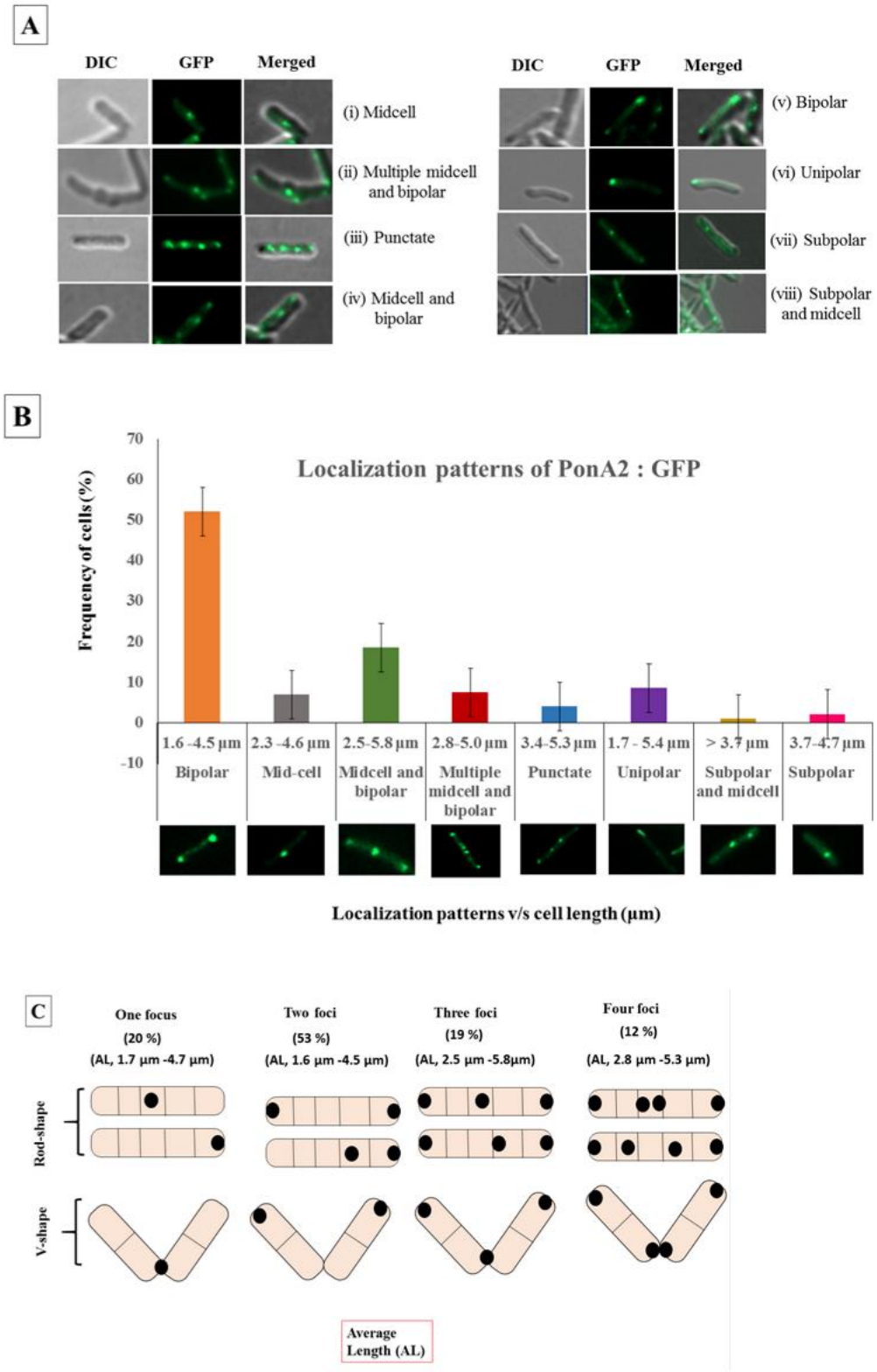


Figure 3.13: Subcellular localization patterns of PonA2 in wild-type *M. smegmatis*. (A) Numbers (i) to (viii) represent the patterns [(i) Mid-cell, (ii) Multiple mid-cell and bipolar, (iii) punctate, (iv) mid-cell and bipolar, (v) bipolar, (vi) unipolar, (vii) sub-polar and (viii) sub-polar and mid-cell]. (B) Quantitation of the localization patterns observed (A) for PonA2 in wild-type *M. smegmatis*. The histogram represents the frequency of cells with specific localization patterns in relation to cell to cell length. Data represents at least two biological repeats. (C) Cartoons representing wild-type *M. smegmatis* cells with one to five MSMEG_2432-GFP foci. On top of

each cartoon, is a representation of number foci, percentage of cells with that foci and the average cell length (AL) in which the foci was observed. Two different shapes are observed, namely rod-shape and V-shape.

3.2.6. Cellular localization of cell wall machinery (FtsZ and DivIVA/Wag31) in wild-type *M. smegmatis*

To further assess the localization pattern of DD-CPases relative to other cell division proteins, plamids to express FtsZ-GFP and DivIVA-GFP were created. The restriction profile of these plasmids is given in the Appendix. As in *E. coli*, *B. subtilis* and other rod-shape bacteria, the *M. smegmatis* cell division initiating protein, FtsZ localizes to the septum (mid-cell) and the late division and/or cell elongation protein (DivIVA) localized at both poles, Figure 3.14. In order to confirm the localization pattern of cell division proteins (FtsZ and DivIVA) based on cell length, the intensities of fluorescent foci were using Fiji software. FtsZ localizes exactly at the septum as expected with the fluorescence intensity observed at 2 μm of the 4 μm-long *M. smegmatis* cell, Figure 3.14. In the case of DivIVA, although two bipolar peaks occurred, uneven intensities were observed suggesting that the old pole (represented by highest peak/ fluorescence intensity) grows faster than the new pole (represented by lowest peak/ fluorescence intensity). In order to compare DacB localization in relation to FtsZ and DivIVA, the fluorescent intensity for this protein was traced in wild-type *M. smegmatis* cells (Figure 3.14C). DacB displayed a more similar pattern of localization to that of DivIVA. This suggests that DacB localizes with the elongasome complex and that it may play a role in cell elongation.

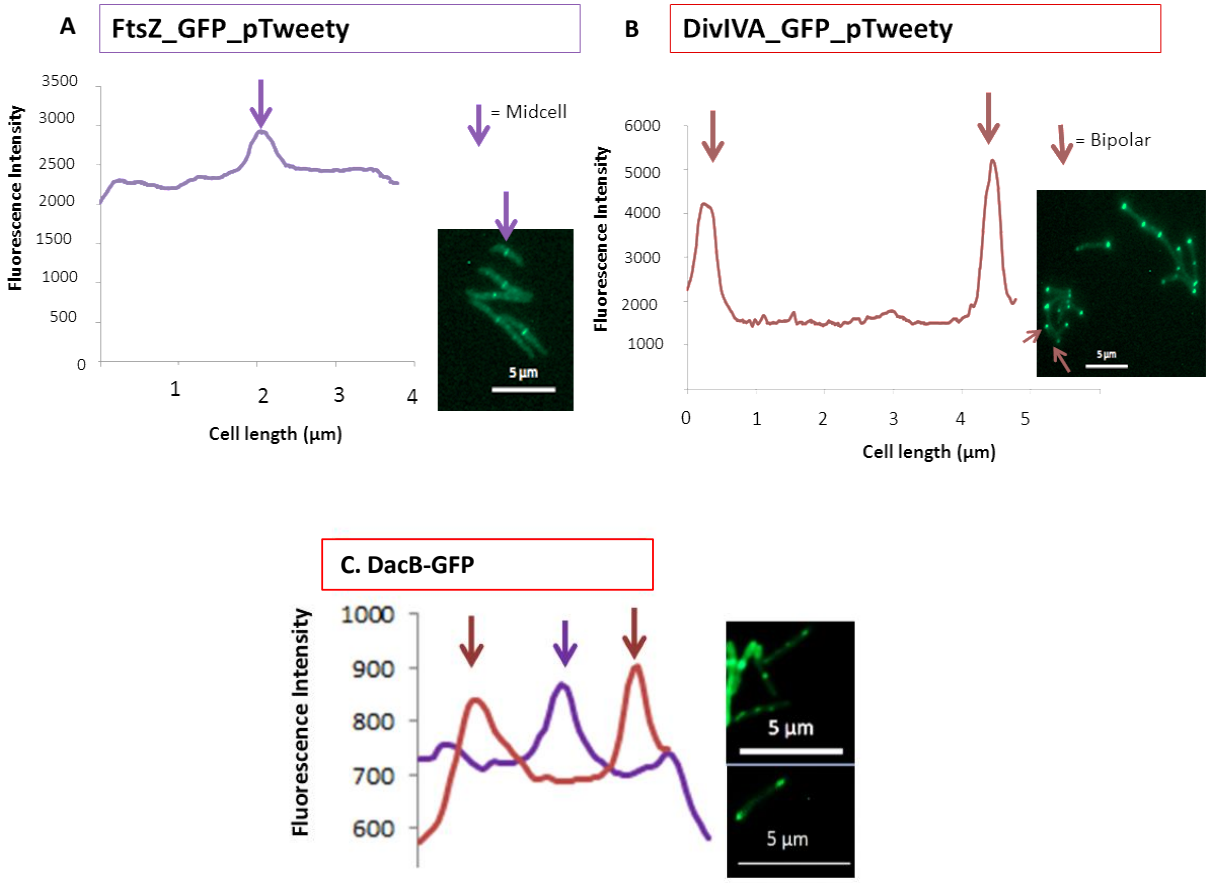


Figure 3.14: Subcellular localization patterns of FtsZ (left) and DivIVA (right) in wild-type *M. smegmatis* cells. **(A)** and **(B)** Localization patterns for FtsZ and DivIVA. Peaks observed represent the fluorescence intensity. (**C**) Localization comparison between DacB (red line) and FtsZ (purple line).

3.3. Localization of cell wall remodelling and cell division enzymes in mutants defective for DD-CPases

3.3.1. Cellular localization dynamics of FtsZ and DivIVA in wild-type and mutants defective for DD-CPases.

Deletion of two or more LMW PBP in *E. coli* has been associated with cells that display extensive morphological diversity (Potluri *et al*., 2012). To investigate the connection between cell division and cell shape in mycobacteria, we investigated the localization dynamics of FtsZ, DivIVA, DacB and PonA2 in *M. smegmatis* wild-type and in mutants defective for DD-CPases. Of the four DD-CPases, studied herein, we focused only on DacB in

this section of the MSc as DacB has been annotated as essential (C. Ealand, unpublished). Cellular localization of these proteins was conducted in strains that harboured different combinations of double gene deletions in DD-CPases (Δ1661 Δ2432, Δ2433 Δ1661 and Δ2433 Δ2432). For this, we first introduced the FtsZ-GFP reporter gene in both wild-type as well as mutant strains. In *E. coli,* localization of the septal protein FtsZ in mutants lacking two or more LMW PBPs results in improper oriented septa or mis-localized FtsZ. As a result of this, cell shape becomes altered and the uniform rod cell shape is disturbed, with a change from rod-shape to spiral (Potluri *et al*., 2012).

Consistent with this, localization of FtsZ in *M. smegmatis* was indeed altered in DD-CPases mutants as FtsZ failed to maintain its septum (mid-cell) patterning in some of the mutants lacking two DD-CPases. These include the △1661 △2432 and △2433 △2432 strains, Figure 3.15. However, cell shape in these mutants was not affected as they continued to grow in their usual rod-shape, Figure 3.15. In the △2433 △1661 double mutant, FtsZ localization was not affected as it localized directly to the septum (mid-cell) as in the wild-type strain.

Next, we studied the localization dynamics of DivIVA in wild-type *M. smegmatis* as well as mutants defective for combinations of DD-CPases. In both wild-type and mutant strains, DivIVA localization to the poles was maintained, suggesting that cell extension processes continued irrespective of the presence of DD-CPases (Figure 3.16).

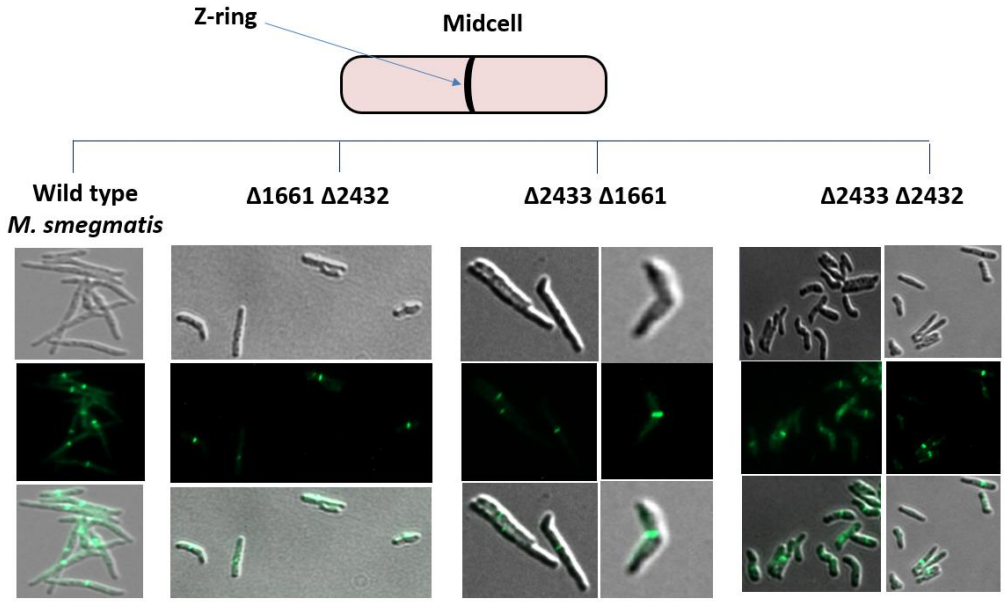


Figure 3.15: Subcellular localization of a cell division protein, FtsZ, in wild-type *M. smegmatis* and DD-CPases deficient mutants. The double gene knockout combinations of DD-CPases: MSMEG_1661, MSMEG_2432 and MSMEG_2433 were: Δ1661 Δ2432, Δ2433 Δ1661 and Δ2433 Δ2432. The cartoon shows the Z-ring at mid-cell.

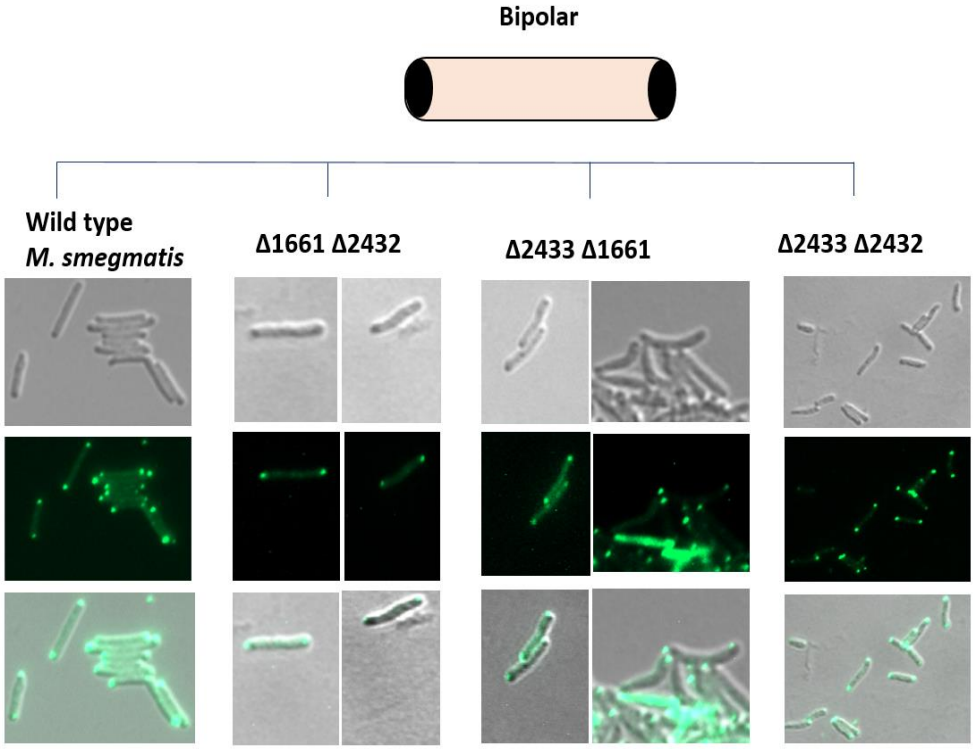


Figure 3.16: Illustration showing subcellular localization of a cell elongation protein, DivIVA (wag31), in wild-type *M. smegmatis* single cells and the double gene knockout mutants of DD-Cpase MSMEG_1661, MSMEG_2432 and MSMEG_2433 in combinations (Δ1661 Δ2432, Δ2433 Δ1661 and Δ2433 Δ2432). Number 1 represents the localization pattern of FtsZ in both wild-type and mutant strains. Scale bar, 5 µm.

3.3.2. Cellular localization of DacB in the DD-CPases double mutants (Δ1661 Δ2432, Δ2433 Δ1661 and Δ2433 Δ2432)

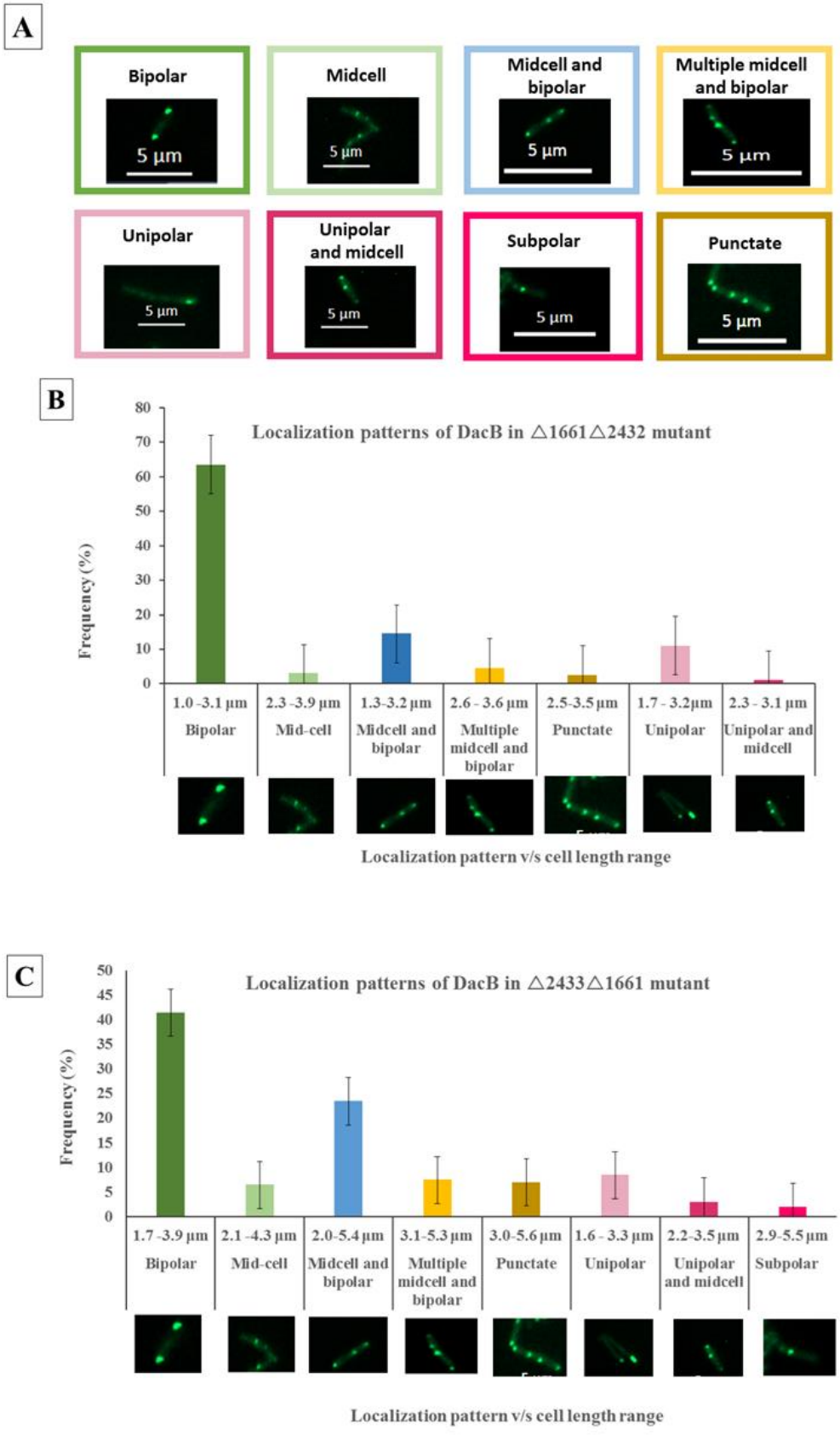
To determine if localization of DacB is affected in mutants defective for other DD-CPases, we compared the localization patterns DacB in *M. smegmatis* mutants lacking the previously-mentioned combinations of DD-CPases. Overall localization patterns observed in these strains included; bipolar, mid-cell, mid-cell and bipolar, multiple mid-cell and bipolar, unipolar, unipolar and mid-cell, subpolar, and subpolar and mid-cell (Figure 3.17A). For all comparisons to wild-type patterns, please refer to Figure 3.6 for the wild-type data. For comparison, a compilation is given in Figure 3.17E.

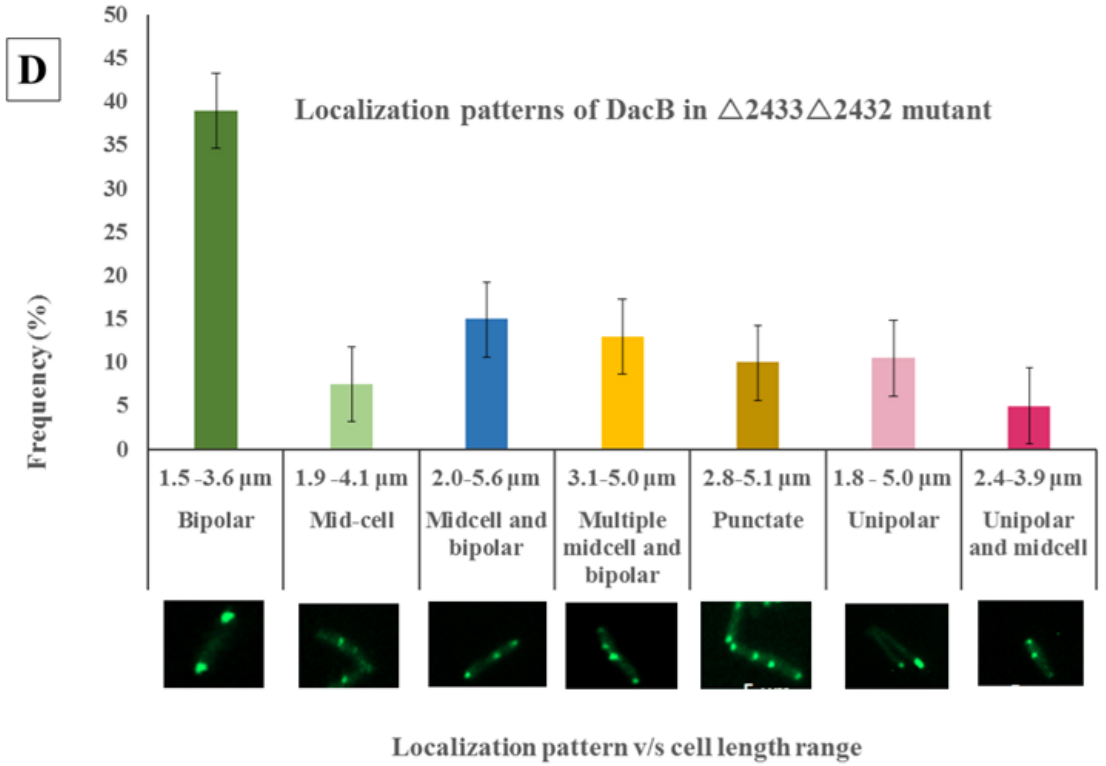
First, we examined the localization pattern of DacB in the Δ1661 Δ2432 mutant. The results revealed no changes in patterning compared to the localization of DacB in wild-type *M. smegmatis* (Figure 3.6), except an increase in polar localization of DacB in the majority of the cells in Δ1661 Δ2432 mutant (Figure 3.17B). The increase of DacB bipolar localization was from 38 % in wild-type (Figure 3.6) to 64 % in the double deletion mutant (Figure 3.17B and E). Another phenotype observed in these strains was the reduction in mid-cell and bipolar localization of DacB in this mutant. Decrease in DacB bipolar localization was from 21 % in wild-type to 15 % in mutant.

We next looked at the localization of DacB in the absence of MSMEG_1661 and MSMEG_2433 (the Δ2433 Δ1661 mutant), Figure 3.17 C. The results showed that as with Δ1661 Δ2432, localization of DacB in Δ2433 Δ1661 mutant localized mostly at the poles regions, bipolar to be specific with percentage difference of 38 % in wild-type to 42 % in the mutant, Figure 3.17E. This difference was marginal and not considered as signficant. Unlike in the Δ1661Δ2432 mutants, proportions of cells with mid-cell and bipolar localization patterning was maintained, 21 % and 24 % in wild-type and mutant strains respectively.

Lastly, we studied the localization patterns of DacB in the Δ2433 Δ2432 mutant. This mutant had to be created in this study. Details on how this mutant was created and its characterization are explained in Section C of the results. In this mutant, no difference was observed in terms of the localization patterning of DacB. Bipolar localization patterning remained the same (38 % and 39 % in wild-type and mutant strains respectively, Figure 3.17D and E). However there was a slight difference in mid-cell- bipolar localization of

DacB, with the proportion of cells with this pattern being 21 % and 15 % for the wild-type and mutant strains respectively (Figure 3.17 D and E).





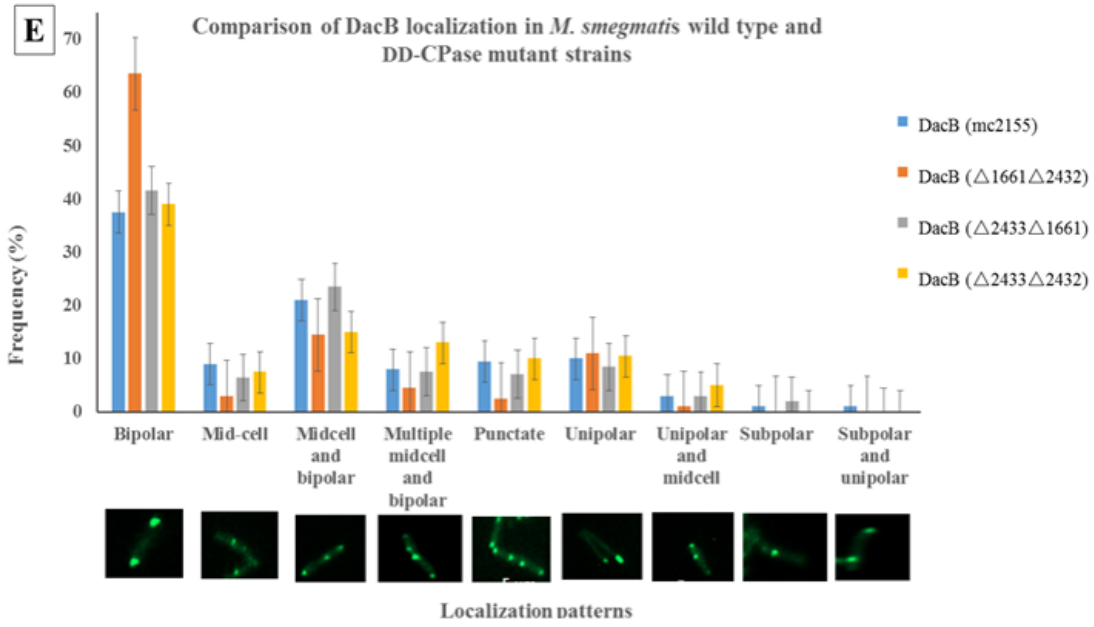


Figure 3.17: DacB localization in wild-type and DD-CPase knockouts. Shown are the subcellular localization patterns of DacB in the DD-CPase double gene knockout mutants (Δ1661 Δ2432, Δ2433 Δ1661 and Δ2433 Δ2432). **(A)** Different localization patterns. **(B)** Quantitation of localization patterns of DacB-GFP in the Δ1661 Δ2432 mutant. **(C)** Quantitation of localization patterns of DacB-GFP in the Δ2433 Δ1661 mutant. **(D)** Quantitation of localization patterns of DacB-GFP in Δ2433Δ2432 mutant. (**E**) Comparison of all mutants in one graph to visualize the pattern of localization relative to wild-type. Error bars used are standard error bars. [Please note: Figure 3.17 (A), (B) and (C) are on the previous page, page 86]

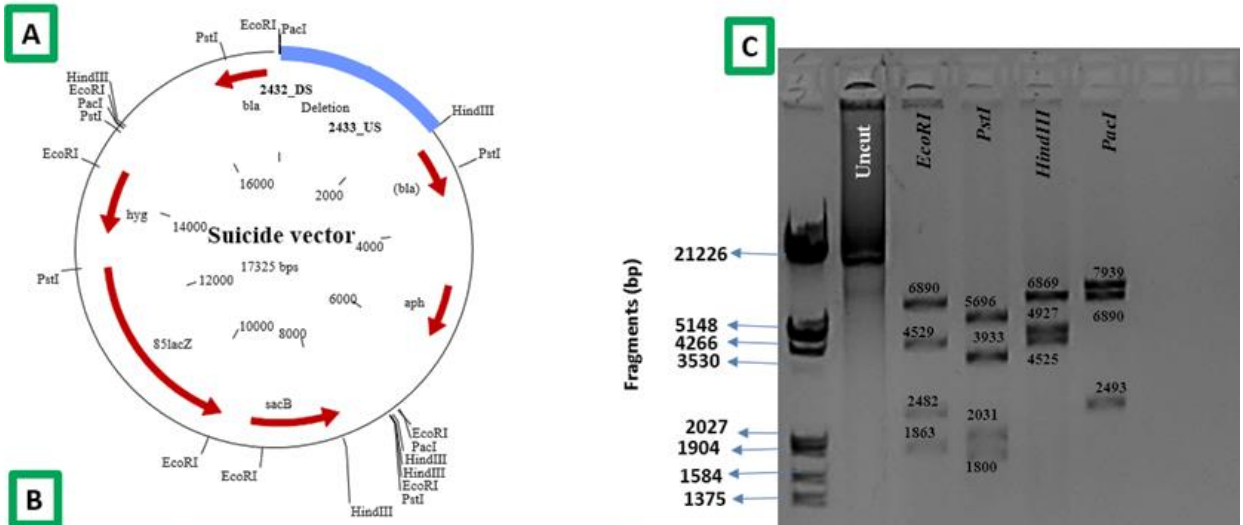
Section C: Gene knockout studies.

3.4 Knockout MSMEG_2433 and MSMEG_2432 in combination

As seen in previous section, three double gene knockout mutants were used to determine the localization patterning of DacB in *M. smegmatis* wild-type and DD-CPase mutant strains. Two of the three mutants (Δ1661 Δ2432 and Δ2433 Δ1661) were created in a previous study by a colleague and the details and description of these mutants are found in the list of strains (Table 2.2). The third combinatorial mutant was not made and had to be constructed and phenotyped in this MSc. From this section onwards, we explain how the mutant lacking two DD-CPases ΔMSMEG_2433 and ΔMSMEG_2432 was created, together with some analysis deciphering it role in PG remodelling.

Construction of the suicide vector p2NIL_2433_2432::pG19

The MSMEG_2433 and MSEMG_2432 mutants occur in an operon in *M. smegmatis* and were targeted for simultaneous deletion. The gene knockout method used involves allelic exchange using a suicide plasmid. For this, a plasmid carrying an in-frame unmarked deletion of these two *M. smegmatis* DD-CPases was created by another MSc student (Z. Ismail). In this MSc, the marker genes were cloned into his pre-existing plasmid, which was done by digesting p2NIL_2433_2432 and pGOAL_19 with *PacI*, followed by ligation of the marker gene cassette liberated from pGOAL_19 to the linearized p2NIL_2433_2432. This suicide vector was then confirmed by restriction profiling (Figure 3.18) and the vector was sent in for DNA sequencing (data not shown). Once the vector was confirmed as correct, transformed into *E. coli* and post selection of potential clones, sucrose sensitivity testing) was carried out as this suicide vector contained a *sacB* gene. This gene is a counter selectable marker which confers sucrose sensitivity. A full detail on how this test was done is explained in methods section 2.14.1 and an example of a positive test is shown in the Appendix F, Figure F2. One of the potential clones which passed this test was then cultured and the resulting DNA obtained was electroporated into *M. smegmatis* to create the ΔMSMEG_2433 ΔMSMEG_2432 (Δ2433 Δ2432) mutant by two-step allelic exchange using homologous recombination as described by Gordhan and Parish (2001) and briefly explained in section 2.14. Potential mutants were confirmed with PCR.



B

Enzyme	Fragment	Fragment size (bps)
EcoRI	7	7026, 4539, 2481, 1863, 766, 635, 14
PstI	5	5696, 4543, 3255, 2031, 1800
HindIII	5	7107, 6879, 2573, 739, 27
PacI	3	7939, 6890, 2493

Figure 3.18: Restriction analysis of the suicide plasmid, p2NIL_2433_2432::pG19, created in this study. **(A)** Represents the suicide vector and restriction enzymes that were used to confirm the vector. **(B)** Shows the table of enzymes used for profiling and the expected fragment sizes. **(C)** Shows the observed fragment sizes on an agarose gel. Expected fragment sizes matched the observed thereby confirming that the construct created was correct.

3.4.1 Confirmation of the DD-CPases double gene knockout mutant (ΔMSMEG_2433 ΔMSMEG_2432) using PCR

Using a PCR strategy to confirm the mutant, a minimum of ten white colonies were picked from the 7H10 media plate supplemented with sucrose and X-gal and DNA was extracted from these colonies using the colony boil method for small scale genomic DNA extraction. The three primers that were used to amplify DNA using PCR are labeled primer 1, 2 and 3 on Figure 3.19 and listed as as K.O_conf_2433_R2‡, K.O_conf_2432_R1† and K.O_conf_2433_F1‴, respectively on the list of confirmation primers for mutants (Table 2.4), respectively. Amplification of the single crossover (SCO) or wild-type will produce two bands, one corresponding to the mutant allele (263 bp) and corresponding to the wild-type (1.2 kb/ 1200 bp), Figure 3.18. Once the mutants were confirmed the genotypes were further analysed with Southern blot analysis.

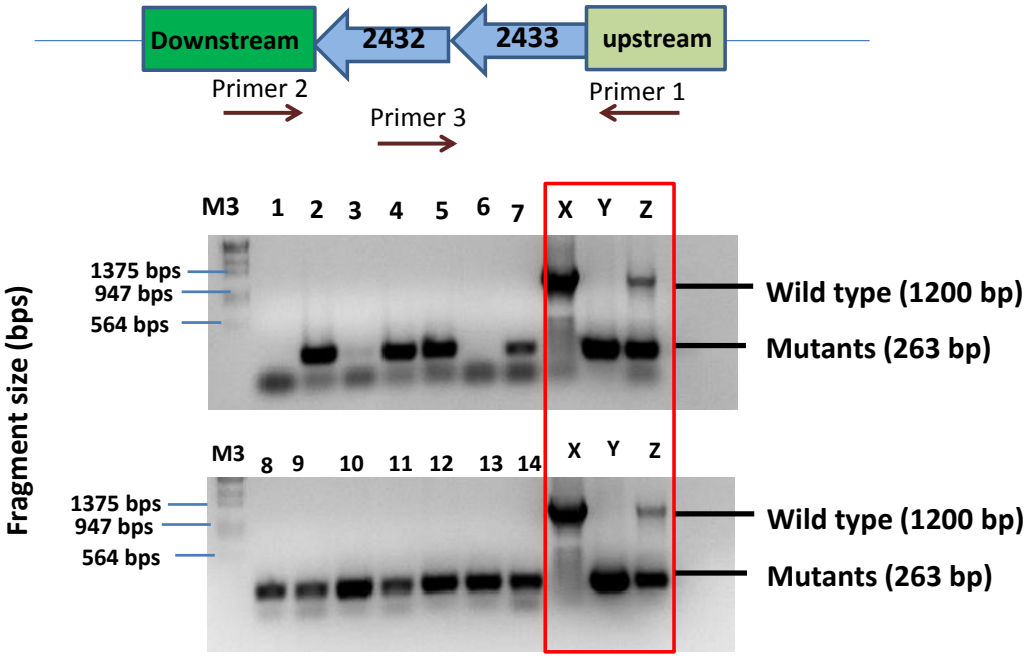


Figure 3.19: PCR confirmation of the Δ2433 Δ2432 double mutant. Shown is the way in which primers to confirm the mutants were designed. Primer1 referred to as KO_conf_2433 US_F1 primer in the primer list binds 100 bp before the start of the MSMEG_2433, Primer 2 referred to as KO_conf_2432 DS_R2 binds 100 bp after the stop codon of MSMEG_2432 and Primer 3 referred to as KO_conf_2433 US_R1 is found in the middle of the operon. All three primers were added to a single PCR reaction. Shown below the map is the PCR screen for mutants. Lane 1 in each gel: M3, represents Roche Marker 3, Lane 1-14 represents potential mutants (Double crossover), Lane X, Y, Z represents the controls: X is the wild-type *M. smegmatis*, Y is the suicide vector and Z is the single cross over.

3.4.2. Confirmation of the DD-CPases double gene knockout mutant (Δ2433 Δ2432) using southern blot

Post PCR confirmation of the mutant, three colonies of potential mutants were taken further for genotypic analysis using Southern Blot. Two other colonies (wild-type and SCO) were also included in the experiment and were used as references or controls. For this, genomic DNA was extracted using the CTAB method or large scale genomic DNA extraction method (as described on section 2.4.22 of the methods section). Two to five micrograms (µg) of the extracted DNA was digested with *PstI* yielding a smear or partial digestion which represented large numbers of fragments. Using Southern blot, specific DNA fragments were detected from these digests and these were represented by a 6675 bp fragment in wild-type *M. smegmatis* and a 4936 bp fragment in the mutants (Figure 3.20). The probe that was used was

the MSMEG_2433 upstream region that was designed for homologous recombination and is represented by an orange block on Figure 3.20 A. These results proved that both Δ2433 Δ2432 were successfully deleted. Once the correct mutants were obtained and following confirmation with PCR and Southern blotting technique, they were then phenotypically analysed.

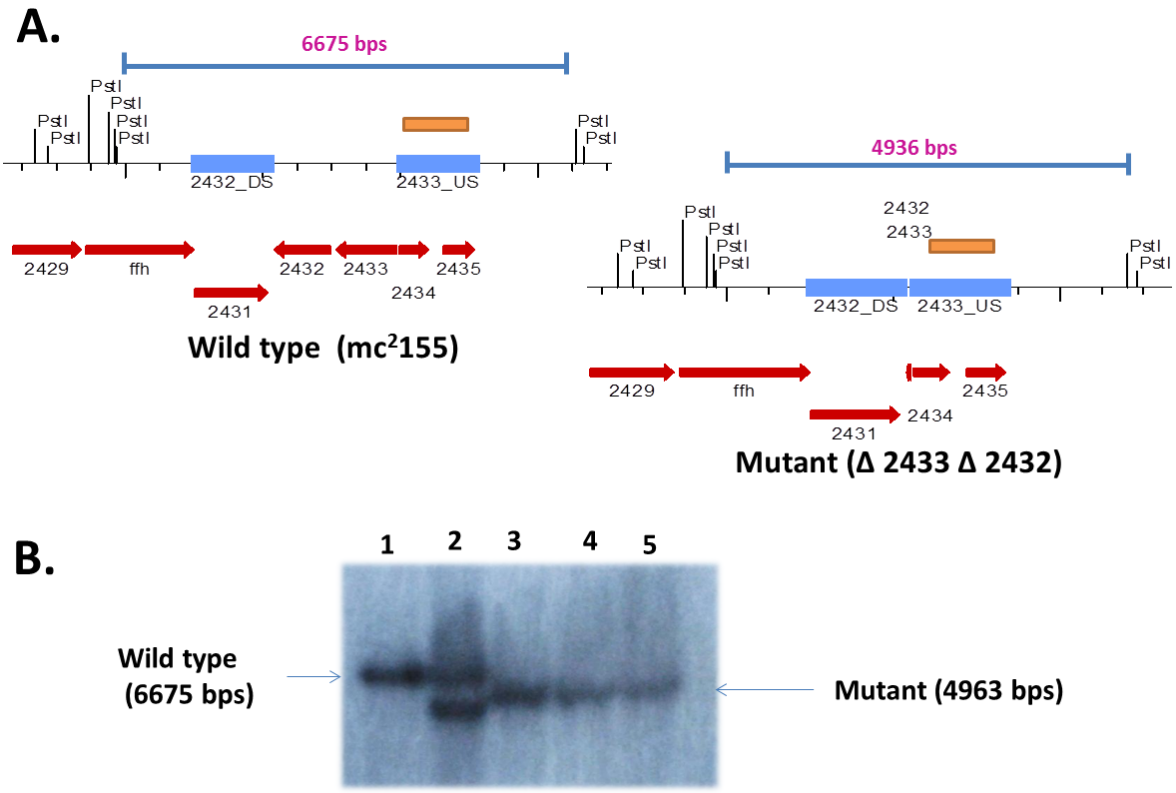


Figure 3.20: Southern Blot confirmation of the Δ2433 Δ2432 double mutant. **(A)** Genomic map and organization of wild-type and mutant strains in *M. smegmatis*. The probe used for Southern Blot is shown by the orange box **(B)** Genotypic characterization of Δ 2433 Δ 2432 strains using Southern blot. Genomic DNA of wild-type *M. smegmatis* (mc^2155), Lane 1; single cross-over (SCO), Lane 2; and mutants/double crossovers (DCOs), Lane 3-5 The DCO and wild-type strains showed single hybridizing fragment sizes of 4937 bp and 6675 bp, respectively when digested with *PstI*.

3.4.3. Growth kinetics of the Δ2433 Δ2432 mutant

To determine if the DD-CPase double gene knockout mutant, Δ2433 Δ2432, displays any growth defects, a growth curve was carried out. The mutant was also genetically

complemented with either the MSMEG_2433 or MSMEG_2432 genes. These plasmids were created in another study (C. Ealand, unpublished) and their details and description are listed in the list of plasmids (Table 2.1). Growth analysis was measured by growth curves determined by optical density (OD) measurements at different time points (3 hours intervals). The growth kinetics experiment was conducted in triplicates using different 7H9 batches, with different freezer stocks per strain. Results, Figure 3.21, reveal that the mutant displayed no growth defects in broth culture when compared to the wild-type. Hence, these two DD-carboxypeptidases in *M. smegmatis* are collectively dispensable for growth.

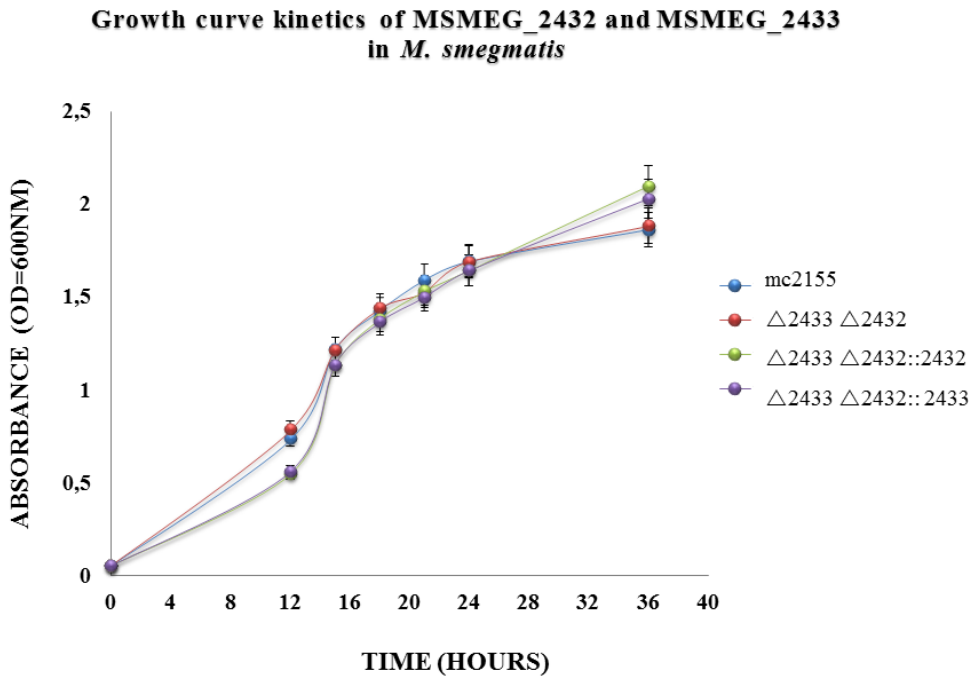


Figure 3.21: Growth rate comparison between wild-type (mc2155), mutant (Δ 2432 Δ2433) and complementation strains (Δ 2432 Δ2433::2432 and Δ 2432 Δ2433::2433). Growth curves were determined by optical density (OD). Strains were grown in 7H9 media supplemented with Glucose salts and Glycerol. Deletion of the two DD- carboxypeptidases in *M. smegmatis* is dispensable for growth.

3.4.4 Biofilm formation in the △2433 △2432 mutant.

Environmental and/or non-pathogenic mycobacteria including *M. smegmatis, M. avium, M. marinum* are known to form biofilm. Formation of these biofilm in mycobacteria is associated with reduction in antibiotic susceptibility (Chen *et al*., 2006). In *E. coli* it has also

been shown that mutants that lack LMW PBP 4, 5, 7 and/or all these PBPs in combinations have defects in the biofilm formation (Gallant *et al*., 2005). To examine the role of DD-CPases in *M. smegmatis* in biofilm formation, we measured the pellicle formation of wild-type, mutant and the complemented strains on the surface of liquid cultures (Figure 3.22). Results, Figure 3.22, illustrated that the △2433 △2432 double knockout mutant produced a biofilm with a smooth surface (represented by purple arrows, Figure 3.22) and thick cords (represented by green arrows, Figure 3.22) compared to wild-type *M. smegmatis*. However, these differences were very marginal and were difficult to capture in photographs. For further confirmation, biofilm formation was quantified using the Crystal violet assay.The biofilm-associated crystal voilet dye was extracted with ethanol and was measured using the spectophotometer at OD_{600nm}. In Figure 3.23, biofilm formation in all strains tested was not different to the wild-type.

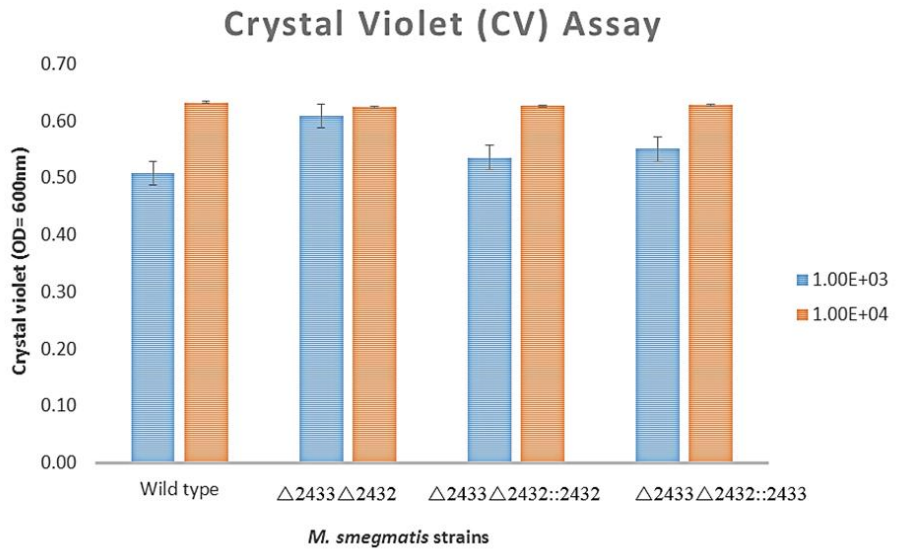


Figure 3.23: Quantification of biofilm formation of *M. smegmatis* using crystal violet. Images shown above are representatives of three biological repeats. Serial dilutions were made for this experiment where biofilms were established for dilutions from 10^1 to 10^6. However, images shown in the illustration above are for serial dilutions; 10^3 (represented by 1.00E+03) and 10^4 (represented by1.00E+04) only. Bars represents standard error bars.

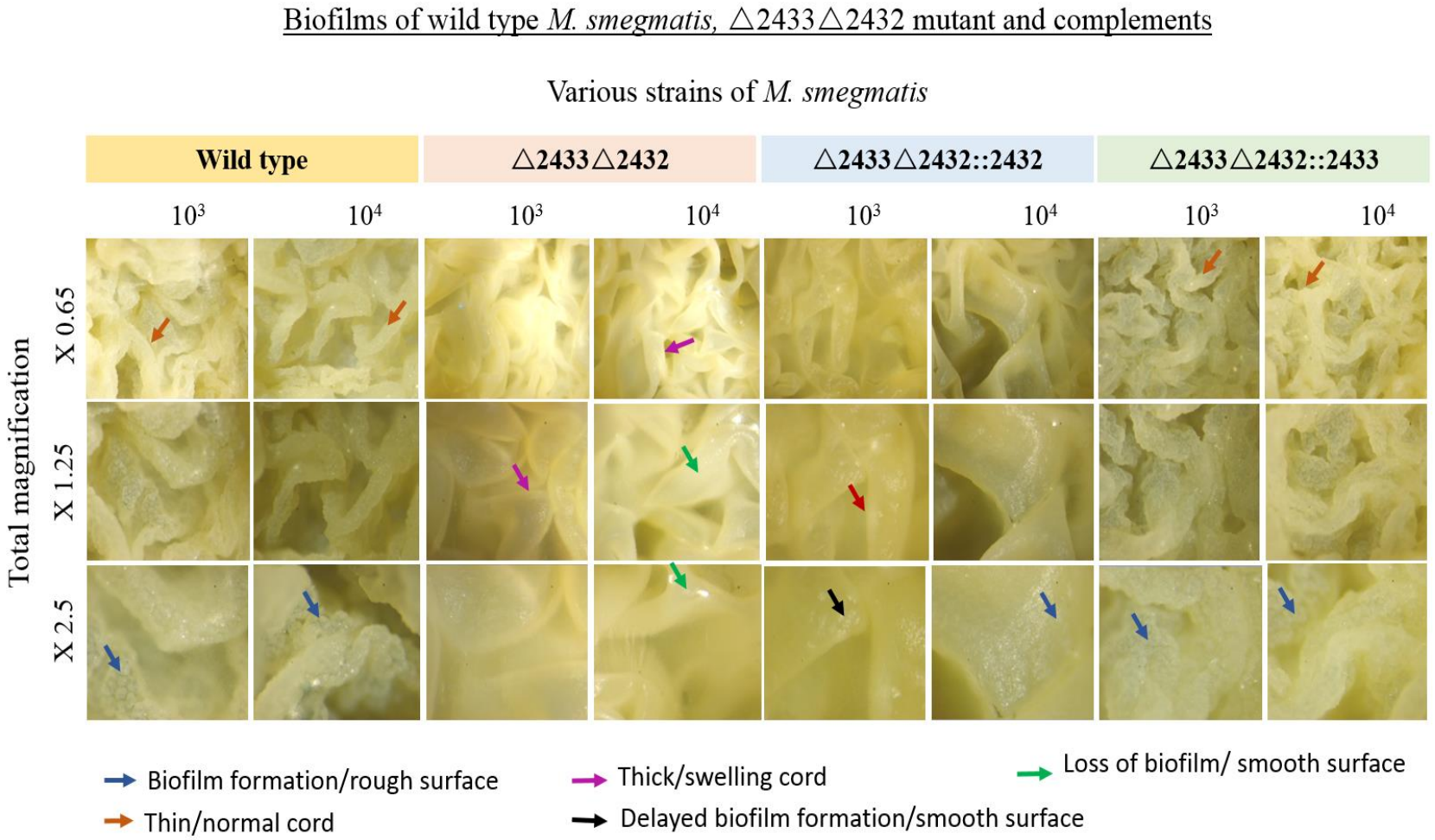


Figure 3.22: Biofilm formation in the △2433 △2432 mutant. Images shown above are representatives of three biological repeats. Serial dilution were made for this experiment were from 10^1 to 10^6, however, images shown in the illustration above are 10^3 and 10^4. Red arrows indicate rough patches on the biofilm. Blue arrows represent normal or thin cording on the biofilm. Green arrows represent the smooth cording on the biofilms. Black arrows on the biofilm represent delayed biofilm formation. Purple arrows show the thickening or swelling on the biofilm.

3.4.5 Click chemistry analysis of the Δ2433 Δ2432 mutant

To investigate the effect of deleting DD-CPases on PG synthesis, we employed Copper Click Chemistry, with D-alanine analogue, which allowed labelling of the PG. Basically, this method facilitates spatial and temporal resolution of PG dynamics by determining where the new PG is inserted or synthesized (Siegrist *et al*., 2013, Hett and Rubin, 2008). Mycobacteria are known to insert PG at the newly formed septa and at the pole (Hett and Rubin, 2008). Our analysis revealed six common localization patterns observed in among wild-type, mutant and complemented strains namely (a) unipolar represented by one bright /green spot at one end/pole of the cell, (b) mid-cell represented by a Z-ring in the middle of the cell, (c) unipolar and mid-cell represented by a spot at the end end/pole of the cell and a Z-ring at the mid-cell of the cell, (d) bipolar represented by two green spots at the ends of the poles of the cell, (e) bipolar and mid-cell represented by two green spots at the end of both poles and a Z-ring in the middle of the cell, (f) multiple mid-cell and unipolar represented by a green spot at the end of one pole and multiple Z-rings throughout the cell (Figure 3.24A). The observed localization patterns were quantified and results were represented by a histogram in Figure 3.24 B. No significant differences were observed between localization patterns of new PG in the wild-type and mutant strains. In general, bipolar localization was the highest observed localization pattern in all strains.

We also measure lengths of cells used in this analysis to ensure that the click chemistry analogue did not affect growth. As shown in Figure 3.24C, no significant differences were observed in cell lengths.

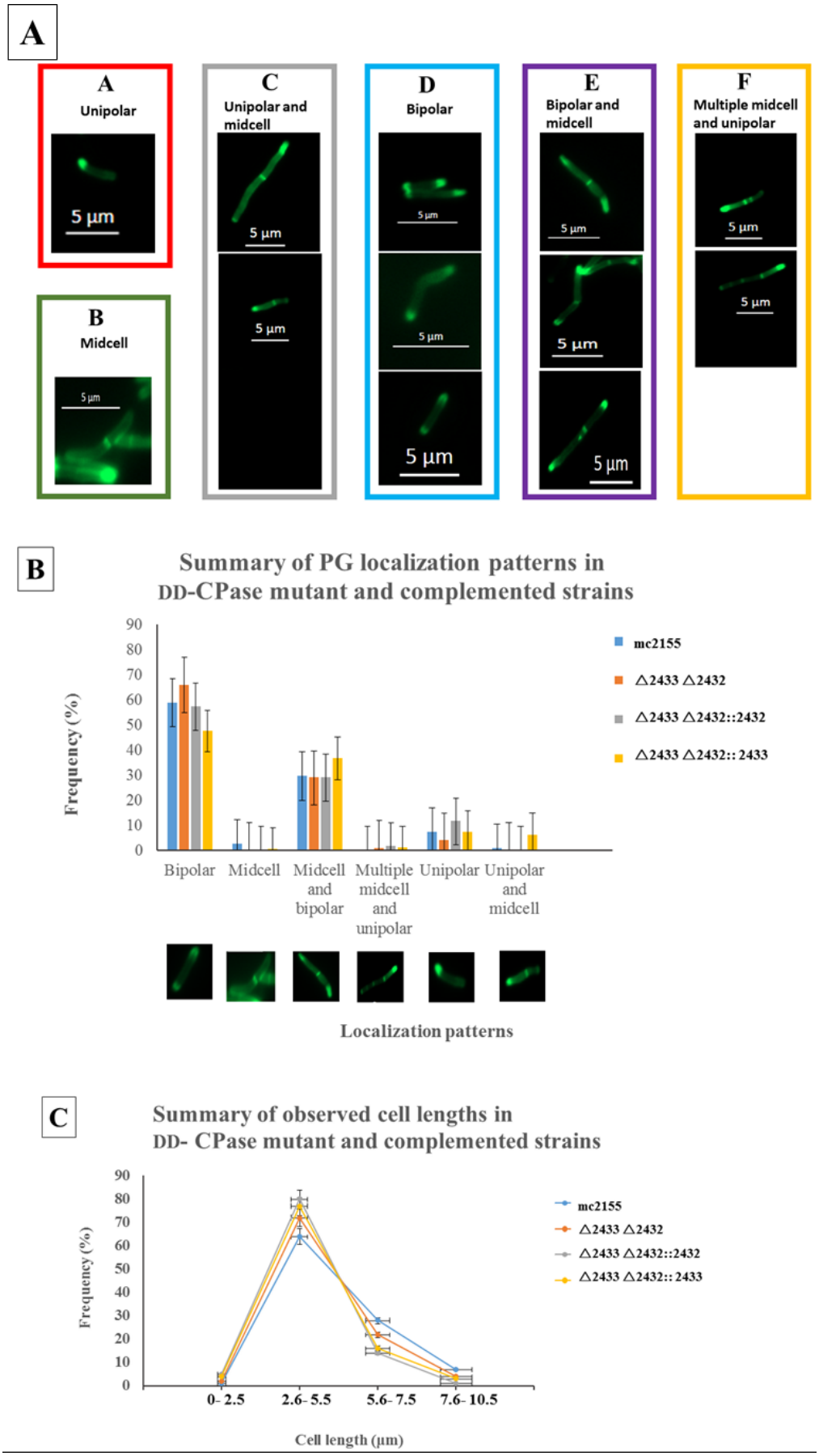


Figure 3.24: Localization of new peptidoglycan synthesis in wild-type and the DD-CPases mutant strains using click chemistry. **(A)** Illustration showing different localization patterns that represent where the nascent PG is inserted. Localization patterns include [A: Unipolar. B: Mid-cell, C: Unipolar and mid-cell, D: Bipolar, E: Bipolar and mid-cell, F: Multiple mid-cell and unipolar]. Scale bar, 5 µm. (B) Quantitation of the localization patterns. (C) Quantitation of cell length distribution of wild-type, mutant and complemented *M. smegmatis* strain (n=100 per repeat, per strain). Data represent three independent experiments. Error bars represent standard error bars.

CHAPTER 4: DISCUSSION

The emergence of drug resistance, the increase of mortality rates due to HIV co-infection and the potential for disease reactivation makes TB the top killer disease from a bacterial infection (WHO, 2016). In addition, the consequences of lengthy and complex treatment regimens together with adverse side effects of anti-TB treatment further complicates the problem by contributing to the poor patient compliance and disease containment. Ultimately, the spread and transmission of untreatable drug-resistant forms of TB poses a great risk to global health (Laurenzi *et al*., 2007). In this regard, it is necessary to develop novel drugs that are more efficient and that can be co-administered with current antiretroviral therapy. In order to do achieve this goal, a detailed understanding of key biological processes which modulate different disease states is required. In the context of this project, processes operating during cell division and PG remodeling served as a starting point for the identification and validation of new TB drugs.

The processes of cell growth and division are critical for bacterial proliferation (Cava *et al*., 2013). Coordination of these processes involves multienzyme protein complexes called the "elongasome" (required for bacterial elongation) and the "divisome" (required for cell division) (Chien *et al*., 2012, Peters *et al*., 2016). Proper coordination of these processes ensures that, under any given environmental condition, cells grow to an appropriate size and/or shape and that viability is maintained (Chien *et al*., 2012, Cava *et al*., 2013). In this context, the regulation of cell wall turnover in *M. tuberculosis* is speculated to serve as an attractive drug target since disruption of any vital process will result in cell death (Peters *et al*., 2016). Proteins targeted by the β-lactam class of antibiotics, the PBPs, play an essential role in PG synthesis and thus are vulnerable to inhibition by antibiotics. DD-CPases Class C LMW PBPs, trim the stem peptide to abolish substrate availability for HMW PBP, thereby regulating the amount of PG cross-linking (Peters *et al*., 2016).

In previous studies from the laboratory (C. Ealand, unpublished data), strains that lacked individual DD-CPases were constructed in *M. smegmatis*, These mutants, ΔMSMEG_1661, ΔMSMEG_2432 and ΔMSMEG_2433, did not display any growth defects. The fourth gene, *dacB*, could not be deleted and was shown to be essential *in vitro*. Based on these findings,

the function of DacB was investigated via a gene knockdown approach. Over-expression of DacB resulted in elongated cells whereas a reduction in gene expression was associated with the loss of PG precursor staining on one growth pole. Moreover, cells were shorter, relative to the wild-type strain, supporting a role of DacB in mycobacterial cell elongation and/or growth.

Expression of the *M. smegmatis* DD-CPases homologues was assessed at various growth phases (i.e. lag, exponential/log and stationary phase). There was a clear distinction in the transcript levels for each gene, i.e. transcript abundances (highest to lowest) were as follows: MSMEG_2433, MSMEG_1661, DacB and MSMEG_2432. This pattern was evident across all growth phases assessed (C. Ealand, unpublished data). The relatively reduced abundance of DacB was surprising considering its apparent essentiality. This suggests a high specific activity for the enzyme that is sufficient to fulfill its biological role when present in low abundance. An alternative hypothesis is that the low amounts of DacB play a regulatory role in the cell. Collectively, these preliminary results suggest that DacB, in combination with other PBPs, plays a significant role in PG biosynthesis and remodeling. Considering this, we reasoned that it would be advantageous to elucidate the role of these proteins by experimentally investigating their localization patterns in the cell.

In this project, we sought to identify the cellular localization patterns of all four DD-CPase homologues in *M. smegmatis*, i.e. DacB, MSMEG_1661, MSMEG_2432 and MSMEG_2433, a model organism for *M. tuberculosis*. Each gene was fused to C-terminal fluorescent tags, including green fluorescent protein (GFP), mRFP (red), mTurqoise mCherry. Due to time constraints, only the data for the GFP fusions are reported in the results section. The Appendix G section has further details on construction of other fusion protein tags, which now require further biological study. In addition, we also localized other cell division proteins, i.e. DivIVA, FtsZ and PonA2 relative to DacB in wild-type and three double gene knockout mutants defective for DD-CPases.

Bioinformatics analyses to predict functions of LMW PBPs and other proteins involved in cell growth and division

Using a bioinformatics approach, we were able to predict the tertiary structures of all four *M. smegmatis* DD-CPase homologues, namely, MSMEG_1661, MSMEG_2432, MMEG 2433

and DacB. In addition, we modelled the bifunctional, mycobacterial homologue of PonA2. All PBP assessed maintained the three essential catalytic residues or signature motifs required for activity, i.e. S*XXK, SXN and KTG. These motifs are essential for the acylation and deacylation of enzyme substrates. The organization of these motifs was similar, except for DacB, possibly reflective of divergent function. Additionally, and consistent with a study done by Bansal *et a*l (2015) that predicted an omega-loop like region required for determining the β-lactamase activity in MSMEG_2433, our study showed that the KTG resided around this region in the three DD-CPases that had a similar structure (Bansal *et al*., 2015).

Moreover, *E. coli* PBP5, a DD-CPase shown to be necessary for maintenance of cell shape, contains a membrane anchor that is important for its function. It has also been shown to have an extended β-lactam binding domain (amino acid residues **200 to 219** surrounding the KTG motif) (Peters *et al*., 2016). These features and positioning of the KTG motif (amino acid residues **212 to 214**) were similar MSMEG_2433 suggesting that MSMEG_2433 may play a similar role in cell shape maintenance, despite being dispensable for growth.

In the case of DacB, in addition to the typical motifs found in DD-CPases, an additional S*XXK motif and a β-lactamase RSG motif were detected. Our analyses further shows that the RSG motif occurs within the PASTA domain of PonA2. This domain is hypothesized to be involved in interaction with the unlinked PG peptides of the terminal D-ala D-ala; detection of PG pentapeptide precursors; determination of dividing/non dividing cells and involvement in cell survival under non-replicating conditions (Patru and Pavelka, 2010). Since both PonA2 and DacB displayed structures with similar localization patterning of the three conserved PBP motifs there could be a potential protein-protein interaction between them. Based on these bioinformatics analyses, we predicted that MSMEG_1661, MSMEG_2432 and MSMEG_2433 would localize similarly during cell growth and division. However as DacB is more similar to PonA2, it would localize at the bacterial poles as PonA2 has an established role in the polar growth of mycobacterial cells (Kieser *et al*., 2015, Aldridge *et al*., 2012, Santi *et al*., 2013)

Prediction of subcellular localization of DacB using phylogenetics

The phylogeny of DacB, together with other DD-CPase homologues, was compared. We selected the following organisms in our analyses: *Actinomadura sp. R39*, *H. influenza*, *E. coli*, *B. subtilis*, *M. tuberculosis*, *P. aerugonosa*, and *M. smegmatis*. The PBP4 homologue of *M. smegmatis* was most closely related to *M. tuberculosis*, *B. subtilis* and *Actinomadura sp. R39* homologues. In *B. subtilis*, PBP4a plays a role in lateral cell wall synthesis and is localized to the mid-cell. It has also been shown co-localize with PBP3 (Sauvage *et al*., 2008). In *E. coli* and *C. crescentus*, PBP4 is required for the transitioning of growth from cell elongation to cell division at mid-cell. Recruitment of this protein to this site enables PG synthesis and cell division by constriction and/or septation (Kysela *et al*., 2013). Based on these observations, DacB could also play central roles in cell elongation and division.

The DD-CPase homologues of *M. smegmatis* localize predominantly at cell poles

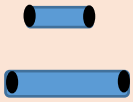
GFP fusions were created with all four DD-CPase homologues and the bifuntional PBP (PonA2) in order to investigate cellular localization in wild-type *M. smegmatis*. All proteins assessed localized at spatially restricted zones, i.e. predominantly at both poles and in some cases, at the septa. Polar localization was expected as mycobacteria grow by polar elongation / apical growth (Singh *et al*., 2013). The localization patterns from all experiments are summarized in Table 4.1. Localization patterns appeared to be similar suggesting a similar role (for example, cell elongation) during cell growth. The frequency of localization patterns for all proteins assessed occurred in the following order: bipolar (B) → mid-cell and bipolar (MB) → unipolar (U) or mid-cell (M) → punctate (P)→ multiple mid-cell and bipolar (MMB). The appearance of two foci at both ends/poles of a cell were referred to as bipolar, at one end (unipolar), in the middle of the cell or septum (mid-cell), two foci in the middle of the cell and two at both ends/poles (multiple mid-cell and bipolar), and multiple foci throughout the cell (punctate). Next, we associated localization patterns with cell growth by using cell length and shape as an arbiter of growth stage. Long, Rod-shape bacteria represent cells that are elongating. Short Rod-shape bacteria represent newly born cells and V-shaped cells represent cells undergoing division and separation. As before, no differences were observed between the DD-CPases, however, a trend did emerge. Shorter cells were predominantly characterized by bipolar localization (B) and were associated with cells that had already undergone a division cycle and/or were about the elongate. In cells undergoing

the process of elongating, localization patterns of "MB" (mid-cell and bipolar), "U" (unipolar), and "M" (mid-cell) were observed. These patterns make sense in the context of cell growth and could resemble cytokinesis, septation or the initiation of constriction leading up to cell division. When cells were at their longest, "P" (punctate) and "MMB" (multiple mid-cell and bipolar) localization patterns occurred. These patterns reflect the dynamic nature of these proteins during cell elongation and division. Despite being largely dispensable for growth, their actions seem to finely tune and regulate PG biosynthesis.

In our subsequent analysis, we focused only the localization of DacB, as it is the only essential homologue and therefore requires further characterization. To address this, we assessed the localization patterns of DacB in mutant strains lacking at least two other DD-CPase homologues in various combinations, i.e. Δ1661 Δ2432; Δ2433 Δ1661; and Δ2432 Δ2433. Having established the localization patterning of DacB in wild-type *M. smegmatis* which was polar and not much different to that of other DD-CPases, we then wanted to examine how DacB would localize in mutants defective for the DD-CPases. Localization dynamics of DacB were compared between the various double gene deletion mutants (Δ 1661 Δ 2432/ Δ 2433 Δ 1661/ Δ 2433 Δ 2432). Four interesting phenotypes observed were based on DacB localization in mutants (Figure 3.17). One, bipolar localization was the highest with mid-cell localization being lowest in the presence of MSMEG_2433 suggesting that it is a cell shape maintaining protein and its involvement in the cell elongation. Two, the absence of MSMEG_2432 in any of the mutants resulted in a mid-cell-associated localization, suggesting it may also be involved in septal formation and/or polar localization. Three, all mutants followed a similar localization patterning when mid-cell-associated localization (mid-cell/mid-cell and bipolar/multiple mid-cell) occurred with Δ 2433 Δ 2432 being highest and Δ 1661 Δ 2432 being lowest, suggesting either MSMEG_2432 or MSMEG_2433 are involved in septal localization/polar localization. Lastly in the absence of MSMEG_1661 in various mutants, cells were more associated with mid-cell localization, whereas in its absence cell were more polar localized.

Biosynthesis and remodelling of PG during cell growth and division must be carefully at specific times and locations to maintain the cell viability. Proteins such as DivIVA, tubulin like proteins (e.g. FtsZ), PG synthases (e .g. PonA2) and PG hydrolases (e.g. DD-CPases) all have different and important roles to play (Randich and Brun, 2015). It is known mycobacterial PG synthesis is spatially regulated by DivIVA (Meniche *et al*., 2014) at sub-polar regions and that initiation of cell division is mediated by FtsZ (Bi and Lutkenhaus, 1991). These proteins were thus selected as markers for elongation and division. In actively growing cells, FtsZ localized at mid-cell which represented the initiation of the cell division process. This was consistent with the findings of (Joyce *et al*., 2012). In contrast, DivIVA localized as two fluorescing foci on the cell poles, again, consistent with previous reports (Meniche *et al*., 2014). Interestingly, intensities of polar localized DivIVA were disproportional and represented the potential differential growth rates of the two growing poles (Dworkin, 2009). When compared to FtsZ and DivIVA, DacB consistently localized at cell poles suggesting that it functions in the cell elongation process as part of the elongasome complex. Based on these observations, we propose a model for mycobacterial growth with an emphasis on DacB, Figure 4.1, and suggest that this protein localizes to the cell pole during mycobacterial growth.

Table 4.1: Spatial and temporal organization of the DD-CPases during cell division and cell growth based on the localization patterns of these proteins observed in this study

Protein		**Sequential cell growth process based on localization patterning (Most frequent = 1 to Least frequent=5)**				
		1	**2**	**3**	**4**	**5**
DD-CPases (LMW PBP)	DacB	B	MB	U/M	P	MMB
	MSMEG_1661	B	MB	U	MMB	P
	MSMEG_2432	B	MB	U	P	MMB
	MSMEG_2433	B	MB	U/M	P	MMB
HMW PBP	PonA2	B	MB	U	P	MMB
Stages during cell division :		**Non-dividing / Elongation** 	**Cytokinesis/ Septation/ Initiation of constriction** 		**Cell division/ Physical separation of daughter cell by binary fission** 	

Keys/Abbreviation	**Full name**	**Keys/Abbreviation**	**Full name**
B	Bipolar	**DD-CPases**	DD-Carboxypeptidases
M	Mid-cell	**LMW PBP**	Low-molecular-weight penicillin-binding proteins
MB	Mid-cell and Bipolar	**HMW PBP**	High-molecular-weight penicillin-binding proteins
U	Unipolar		
MMB	Multiple mid-cell and bipolar		
P	Punctate		

DacB co-localizes with DivIVA (an elongasome protein) in *M. smegmatis*

The role of FtsZ and DivIVA in the mutants

In addition to assessing the localization patterns of DacB, DivVIA and FtsZ in wild-type *M. smegmatis*, we assessed it in mutant strains lacking combinations of DD-CPase homologues. In the Δ1661 Δ2432 and Δ2433 Δ1661 double mutant strains, localization of FtsZ was not altered. In all cases, FtsZ localized to the mid-cell reflective of its role in cell division. DacB and DivIVA localized similarly relative to wild-type strain (i.e. bipolar) suggesting that interaction with the other DD-CPases is not required for correct localization and function. Interestingly, localization of FtsZ was affected in the Δ2433 Δ2432 double mutant strain. Mislocalization also affected how DacB localized but what this means with respect to the mechanism of cell division remains to be elucidated because DivIVA localization remained unchanged (i.e. bipolar).

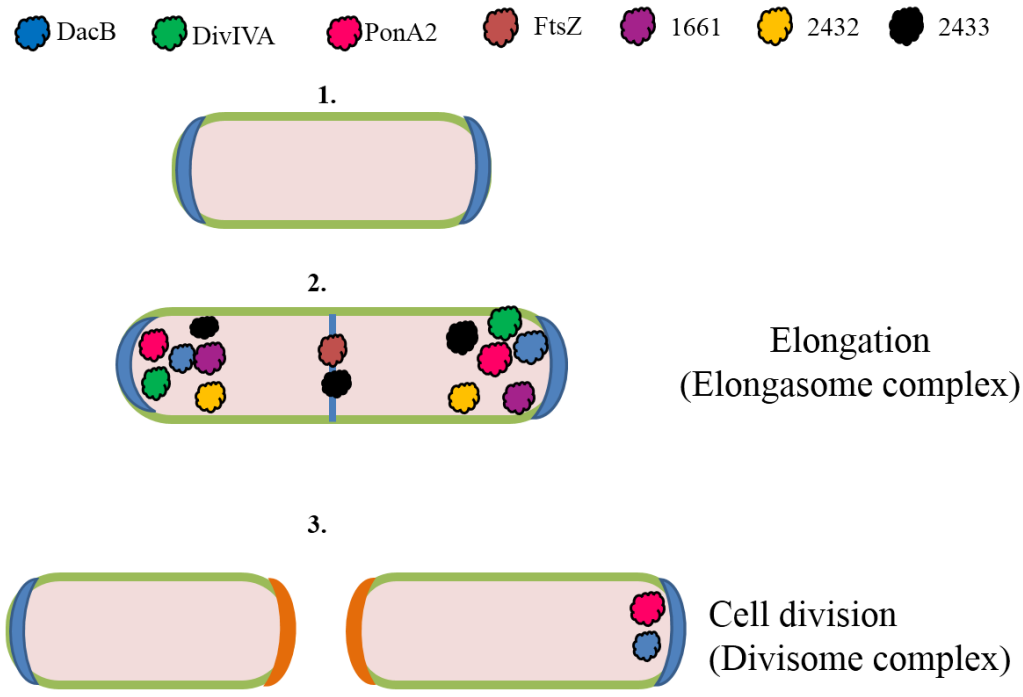


Figure 4.1 Model representing the role of DacB in mycobacterial cell elongation. (1) non-diving cells (cell elongation), (2) elongating cells, protein recruitment to the division sites (Z-ring formation) and (3) cells post division.

Phenotypic characterization of the ΔMSMEG_2432 ΔMSMEG_3433 double mutant strain

It has previously been shown that three out of the four DD-CPase homologues in *M. smegmatis* are dispensable for growth (C. Ealand, unpublished data). In this study, the double deletion mutant (Δ2433 Δ2432) was constructed using allelic exchange and confirmed using PCR and Southern hybridization. A growth kinetics analysis revealed that, relative to the wild-type strain, the mutant strain grew at an equal rate. Similarly, the ability to form pellicle biofilms at the liquid-air interface was not negatively affected. As per the wild-type strain, biofilms of the mutant exhibited the characteristic ruffling and texture associated with mycobacterial biofilms. Moreover, biomass of the mutant strain (as determined by its ability to retain crystal violet) was statistically indistinguishable from the wild-type. These results were not surprising as DD-CPase homologues are individually dispensable with no obvious morphological phenotypes.

PG biosynthesis in the mutant strain (together with the wild-type and complemented strains) was assessed using a D-alanine analogue (Siegrist *et al*., 2013). During growth, cells take up the analogue from the media and incorporate it into PG. Via a chemical reaction (fluorescent probe reaction dependent on copper), areas of analogue incorporation can be visualised via a fluorescent signal. In the wild-type strain, the predominant pattern of incorporation corresponded to bipolar staining. The second most frequent pattern observed was that of mid-cell and bipolar. There was no difference in the spatial patterns of PG localization between the wild-type and Δ2333 Δ2432 mutant, confirming that these two DD-CPases were dispensable for PG remodelling. Cell lengths in the mutant were comparable to the wild-type.

CHAPTER 5: CONCLUSION

Conclusions

Collectively, our localization studies confirm that the four DD-CPases in *M. smegmatis* localise predominantly to sites of new PG synthesis, namely the cell pole and septum. The localization pattern for DacB, the only essential DD-CPase, was more similar to that of the HMW PBP, PonA2, as it was found predominantly at the cell pole. These observations suggest an essential role for DacB in mycobacterial cell elongation. The divergent localization pattern of DacB, relative to the other three DD-CPases found in *M. smegmatis*, was consistent with our predictions of its three-dimensional structure and evolutionary origin. Using two-step allelic exchange mutagenesis, we confirm that MSMEG_2342 and MSMEG_2433 are collectively dispensable for growth and spatial localization of PG in *M. smegmatis*.

Limitations and Future Studies

The research conducted in this MSc opens up several avenues for future research. Using some of the novel fluorescent reporters generated herein, co-localization with other HMW PBP and cell division apparatus proteins is now possible and will form part of future work. Single-cell time-lapse microscopy can be conducted to track localization of DD-CPases in bacteria are they are elongating and dividing. The dispensability of MSMEG_2342 and MSMEG_2433 is suggestive of redundant function amongst the DD-CPases in *M. smegmatis*. To test this, a triple mutant lacking all the non-essential DD-CPases will be constructed and analysed as part of the future outlook for this project.

CHAPTER 6: REFERENCES

AHMAD, S. (2010) Pathogenesis, immunology, and diagnosis of latent *Mycobacterium tuberculosis* infection. *Clinical and developmental immunology*, 2011, 1-17.

AHUJA, S.D., ASHKIN, D., AVENDANO, M., BANERJEE, R., BAUER, M., BAYONA, J.N., BECERRA, M.C., BENEDETTI, A., BURGOS, M., CENTIS, R. AND CHAN, E.D. (2012) Multidrug-resistant pulmonary tuberculosis treatment regimens and patient outcomes: an individual patient data meta-analysis of 9,153 patients. *PLoS medicine*, 9, 1-16.

ALDRIDGE, B. B., FERNANDEZ-SUAREZ, M., HELLER, D., AMBRAVANESWARAN, V., IRIMIA, D., TONER, M. & FORTUNE, S. M. (2012) Asymmetry and aging of mycobacterial cells lead to variable growth and antibiotic susceptibility. *Science*, 335**,** 100-104.

BALTUSSEN, R., FLOYD, K. & DYE, C. (2005) Cost effectiveness analysis of strategies for tuberculosis control in developing countries. *British medical journal*, 331**,** 1-6.

BANSAL, A., KAR, D., MURUGAN, R. A., MALLICK, S., DUTTA, M., PANDEY, S. D., CHOWDHURY, C. & GHOSH, A. S. (2015) A putative low-molecular-mass penicillin-binding protein (PBP) of *Mycobacterium smegmatis* exhibits prominent physiological characteristics of DD-carboxypeptidase and beta-lactamase. *Microbiology*, 161**,** 1081-1091.

BASU, J., CHATTOPADHYAY, R., KUNDU, M. & CHAKRABARTI, P. (1992) Purification and partial characterization of a penicillin-binding protein from *Mycobacterium smegmatis*. *Journal of bacteriology*, 174 **,** 4829-4832.

BASU, J., MAHAPATRA, S., KUNDU, M., MUKHOPADHYAY, S., NGUYEN-DISTECHE, M., DUBOIS, P., JORIS, B., VAN BEEUMEN, J., COLE, S. T. & CHAKRABARTI, P. (1996) Identification and overexpression in *Escherichia coli* of a *Mycobacterium leprae* gene, *pon1*, encoding a high-molecular-mass class A penicillin-binding protein, PBP1. *Journal of bacteriology*, 178**,** 1707-1711.

BERTSCHE, U., MAYER, C., GOTZ, F. & GUST, A. A. (2015) Peptidoglycan perception-sensing bacteria by their common envelope structure. *International journal of medical microbiology*, 305**,** 217-223.

BHATTACHARJEE, M. K. (2016) Chapter 3.Antibiotics that inhibit cell wall synthesis. *Chemistry of antibiotics and related drugs*. doi:10.1007/978-3-319-40746-3,_3, 49- 94.

BHATT, K. & SALGAME, P. (2007) Host innate immune response to *Mycobacterium tuberculosis*. *Journal of clinical immunology*, 27, 347-362.

BI, E. & LUTKENHAUS, J. (1991) FtsZ ring structure associated with division in *Escherichia coli*. *Nature*, 354**,** 161-164.

BOURAI, N., JACOBS, W. R., JR. & NARAYANAN, S. (2012) Deletion and overexpression studies on DacB2, a putative low-molecular mass penicillin-binding protein from *Mycobacterium tuberculosis* H_{37}Rv. *Microbial pathogenesis*, 52**,** 109-116.

BUTCHER, P., HUTCHINSON, N., DORAN, T. & DALE, J. (1996) The application of molecular techniques to the diagnosis and epidemiology of mycobacterial diseases. *Journal of applied bacteriology*, 81, 53S–71S.

BUYNAK, J. D. (2007) Cutting and stitching: The cross-linking of peptidoglycan in the assembly of the bacterial cell wall. *ACS chemical biology*, 2**,** 602-605.

CADENA, A.M., FLYNN, J.L. & FORTUNE, S.M. (2016) The importance of first impressions: early events in *Mycobacterium tuberculosis* infection influence outcome. *American society for microbiology*. *mBio*, 7, 1-9.

CAMERON, T. A., ZUPAN, J. R. & ZAMBRYSKI, P. C. (2015) The essential features and modes of bacterial polar growth. *Trends microbiol*ogy, 23, 347-353.

CAVA, F., KURU, E., BRUN, Y. V. & DE PEDRO, M. A. (2013) Modes of cell wall growth differentiation in rod-shape bacteria. *Current opinion in microbiology*, 16**,** 731-737.

CHANG, F. & HUANG, K. C. (2014) How and why cells grow as rods. *Biomed central biology*, 12**,** 1-11.

CHEN, J. M., GERMAN, G. J., ALEXANDER, D. C., REN, H., TAN, T. & LIU, J. (2006) Roles of Lsr2 in colony morphology and biofilm formation of *Mycobacterium smegmatis*. *Journal of bacteriology,* 188**,** 633-641.

CHIEN, A.C., HILL, N. S. & LEVIN, P. A. (2012) Cell size control in bacteria. *Current biology,* 22**,** R340-R349.

CLARK-CURTISS, J.E. & HAYDEL, S.E. (2003) Molecular genetics of *Mycobacterium tuberculosis* pathogenesis. *Annual reviews in microbiology,* 57, 517-549.

COOPER, A.M. (2009) Cell-mediated immune responses in tuberculosis. *Annual review of immunology,* 27, 393-422.

CORRALES, R.M., MOLLE, V., LEIBA, J., MOUREY, L., DE CHASTELLIER, C. & KREMER, L.(2012) Phosphorylation of mycobacterial PcaA inhibits mycolic acid cyclopropanation. Consequences for intracellular survival and for phagosome maturation block. *Journal of Biological Chemistry*, 287, 26187-26199

DANIEL, R.A. & ERRINGTON, J. (2003) Control of cell morphogenesis in bacteria: two distinct ways to make a rod-shaped cell. *Cell*, 113, 767-776.

DUTTA, N. K. & KARAKOUSIS, P. C. (2014) Latent tuberculosis infection: myths, models, and molecular mechanisms. *Microbiology and molecular biology reviews,* 78**,** 343-371.

DWORKIN, J. (2009) Cellular polarity in prokaryotic organisms. *Cold spring harbor perspectives in biology,* 1**,** 1-24.

EGAN, A. J. & VOLLMER, W. (2013) The physiology of bacterial cell division. *Annals of the New York academy of sciences,* 1277**,** 8-28.

EUROPEAN BIOINFORMATICS INSTITUTE (EMBL-EBI). (2016) Peptidase S11, D-alanyl-D-alanine carboxypeptidase A (IPR018044). Available from https://www.ebi.ac.uk/interpro/entry/IPR018044 [Accessed: 10 June 2016]

EUROPEAN BIOINFORMATICS INSTITUTE (EMBL-EBI). (2016) Peptidase S13, D-Ala-D-Ala carboxypeptidase C (IPR000667). Available from https://www.ebi.ac.uk/interpro/entry/IPR000667 [Accessed: 10 June 2016]

EVANS, T. G., SCHRAGER, L. & THOLE, J. (2016) Status of vaccine research and development of vaccines for tuberculosis. *Vaccine,* 34**,** 2911-2914.

FISHER, J. F. & MOBASHERY, S. (2014) The sentinel role of peptidoglycan recycling in the β-lactam resistance of the gram-negative Enterobacteriaceae and *Pseudomonas aeruginosa*. *Bioorganic chemistry,* 56**,** 41-48.

FLEURIE, A., CLUZEL, C., GUIRAL, S., FRETON, C., GALISSON, F., ZANELLA-CLEON, I., DI GUILMI, A.M. & GRANGEASSE, C. (2012) Mutational dissection of the S/T-kinase StkP reveals crucial roles in cell division of *Streptococcus pneumoniae*. *Molecular microbiology,* 83**,** 746-758.

FLORES, A. R., PARSONS, L. M. & PAVELKA JR, M. S. (2005) Genetic analysis of the β-lactamases of *Mycobacterium tuberculosis* and *Mycobacterium smegmatis* and susceptibility to β-lactam antibiotics. *Microbiology,* 151**,** 521-532.

FRIRDICH, E. & GAYNOR, E. C. (2013) Peptidoglycan hydrolases, bacterial shape, and pathogenesis. *Current opinion in microbiology,* 16**,** 767-778.

GALLANT, C. V., DANIELS, C., LEUNG, J. M., GHOSH, A. S., YOUNG, K. D., KOTRA, L. P. & BURROWS, L. L. (2005) Common β- lactamases inhibit bacterial biofilm formation. *Molecular microbiology,* 58**,** 1012-1024.

GENGENBACHER, M. & KAUFMANN, S. H. (2012) *Mycobacterium tuberculosis*: success through dormancy. *FEMS microbiology reviews,* 36**,** 514-532.

GHOSH, A. S., CHOWDHURY, C. & NELSON, D. E. (2008) Physiological functions of D-alanine carboxypeptidases in *Escherichia coli*. *Trends in microbiology,* 16**,** 309-317.

GOFFIN, C. & GHUYSEN, J.M. (1998) Multimodular penicillin-binding proteins: an enigmatic family of orthologs and paralogs. *Microbiology and molecular biology reviews,* 62**,** 1079-1093.

GOFFIN, C. & GHUYSEN, J.M. (2002) Biochemistry and comparative genomics of SxxK superfamily acyltransferases offer a clue to the mycobacterial paradox: presence of penicillin-susceptible target proteins versus lack of efficiency of penicillin as therapeutic agent. *Microbiology and molecular biology reviews,* 66**,** 702-738.

GORDHAN, B. G. & PARISH, T. (2001) Gene Replacement using Pretreated DNA. *Mycobacterium tuberculosis protocols,* 54**,** 77-92.
GRZEGORZEWICZ, A. E., DE SOUSA-D'AURIA, C. L., MCNEIL, M. R., HUC-CLAUSTRE, E., JONES, V., PETIT, C. C., KUMAR ANGALA, S., ZEMANOVÃ, J. L., WANG, Q. & BELARDINELLI, J. M. (2016) Assembling of the *Mycobacterium tuberculosis* cell wall core. *Journal of biological chemistry,* 291**,** 18867-18879.
GUIRADO, E. & SCHLESINGER, L.S. (2013) Modeling the *Mycobacterium tuberculosis* granuloma–the critical battlefield in host immunity and disease. *Frontiers in immunology,* 4, 1-7.
HUANG, K.C., EHRHARDT, D.W. &SHAEVITZ, J.W. (2012) The molecular origins of chiral growth in walled cells. *Current opinion in microbiology,* 15, 707-714.
HENRIQUES, M. X., CATALÃO, M. J. O., FIGUEIREDO, J., GOMES, J. O. P. & FILIPE, S. R. (2013) Construction of improved tools for protein localization studies in *Streptococcus pneumoniae*. *PLoS one,* 8**,** 1-9.
HETT, E. C., CHAO, M. C. & RUBIN, E. J. (2010) Interaction and modulation of two antagonistic cell wall enzymes of mycobacteria. *PLoS pathogen,* 6**,** 1-14.
HETT, E. C. & RUBIN, E. J. (2008) Bacterial growth and cell division: a mycobacterial perspective. *Microbiology and molecular biology reviews,* 72**,** 126-156.
HOAGLAND, D. T., LIU, J., LEE, R. B. & LEE, R. E. (2016) New agents for the treatment of drug-resistant *Mycobacterium tuberculosis*. *Advanced drug delivery reviews,* 102, 55-72.
HOPPE, L. E., KETTLE, R., EISENHUT, M. & ABUBAKAR, I. (2016) Tuberculosis-diagnosis, management, prevention, and control: summary of updated NICE guidance. *British medical journal,* 352**,** 71-74.
HOUSTON, A. & MACALLAN, D.C. (2014) Extra-pulmonary tuberculosis. *Medicine,* 42, 18-22.
JANKUTE, M., COX, J. A., HARRISON, J. & BESRA, G. S. (2015) Assembly of the mycobacterial cell wall. *Annual review of microbiology,* 69**,** 405-423.
JOYCE, G., WILLIAMS, K. J., ROBB, M., NOENS, E., TIZZANO, B., SHAHREZAEI, V. & ROBERTSON, B. D. (2012) Cell division site placement and asymmetric growth in mycobacteria. *PLoS one,* 7**,** 1-8.
KANG, C.M., NYAYAPATHY, S., LEE, J.Y., SUH, J.W. & HUSSON, R. N. (2008) Wag31, a homologue of the cell division protein DivIVA, regulates growth, morphology and polar cell wall synthesis in mycobacteria. *Microbiology,* 154**,** 725-735.
KAPLAN, G., POST, F. A., MOREIRA, A. L., WAINWRIGHT, H., KREISWIRTH, B. N., TANVERDI, M., MATHEMA, B., RAMASWAMY, S. V., WALTHER, G. & STEYN, L. M. (2003) *Mycobacterium tuberculosis* growth at the cavity surface: a microenvironment with failed immunity. *Infection and immunity,* 71**,** 7099-7108.
KIESER, K. J., BARANOWSKI, C., CHAO, M. C., LONG, J. E., SASSETTI, C. M., WALDOR, M. K., SACCHETTINI, J. C., IOERGER, T. R. & RUBIN, E. J. (2015) Peptidoglycan synthesis in *Mycobacterium tuberculosis* is organized into networks with varying drug susceptibility. *Proceedings of the national academy of sciences,* 112**,** 13087-13092.
KIESER, K. J. & RUBIN, E. J. (2014) How sisters grow apart: mycobacterial growth and division. *Nature reviews microbiology,* 12**,** 550-562.
KONAKLIEVA, M. I. (2014) Molecular targets of β-lactam-based antimicrobials: Beyond the usual suspects. *Antibiotics,* 3**,** 128-142.
KONG, K., SCHNEPER, L. & MATHEE, K. (2010) Beta-lactam antibiotics: from antibiosis to resistance and bacteriology. *Apmis,* 118**,** 1-36.
KUMAR, P. (2016) Adult pulmonary tuberculosis as a pathological manifestation of hyperactive antimycobacterial immune response. *Clinical and translational medicine,* 5**,** 1-7.
KYSELA, D. T., BROWN, P. J., HUANG, K. C. & BRUN, Y. V. (2013) Biological consequences and advantages of asymmetric bacterial growth. *Annual review of microbiology,* 67**,** 417-435.
LADDOMADA, F., MIYACHIRO, M. M. & DESSEN, A. (2016) Structural insights into protein-protein interactions involved in bacterial cell wall biogenesis. *Antibiotics,* 5**,** 1-14.
LAURENZI, M., GINSBERG, A. & SPIGELMAN, M. (2007) Challenges associated with current and future TB treatment. *Infectious disorders-drug targets (Formerly current drug targets-infectious disorders),* 7**,** 105-119.

LARSEN, M. H. (2000) Appendix 1. In HATFUL, G. F., JACOBS, W. R., JR. (ed.) Molecular genetics of mycobacteria. ASM Press Washington, D.C., 313-321.
LAXMINARAYAN, R., BHUTTA, Z., DUSE, A., JENKINS, P., O'BRIEN, T., OKEKE, I., PABLO-MENDEZ, A. & KLUGMAN, K. (2006) Chapter 55: Drug-resistance. *Disease control priorities in developing countries*. 2nd edition. 1031-1052
LEDERER, E., ADAM, A., CIORBARU, R., PETIT, J.F. O. & WIETZERBIN, J. (1975) Cell walls of Mycobacteria and related organisms; chemistry and immunostimulant properties. *Molecular and cellular biochemistry,* 7**,** 87-104.
LODDENKEMPER, R., LIPMAN, M. & ZUMLA, A. (2016) Clinical aspects of adult tuberculosis. *Cold spring harbor perspectives in medicine,* 6**,** 1-26.
LYBARGER, S. R. & MADDOCK, J. R. (2001) Polarity in action: asymmetric protein localization in bacteria. *Journal of bacteriology,* 183**,** 3261-3267.
MACHOWSKI, E. E., SENZANI, S., EALAND, C. & KANA, B. D. (2014) Comparative genomics for mycobacterial peptidoglycan remodelling enzymes reveals extensive genetic multiplicity. *Biomed central microbiology,* 14**,** 1-12.
MANOSUTHI, W., WIBOONCHUTIKUL, S. & SUNGKANUPARPH, S (2016) Integrated therapy for HIV and tuberculosis. *AIDS research and therapy,* 13**,** 1-12.
MATHEWS, C. K., VAN HOLDE, K. E. & AHERN, K. G. (2000) Biochemistry. 3rd edition (International Edition). Pearsons Addison-Wesley Publishing Company.
MCLAREN, Z. M., MILLIKEN, A. A., MEYER, A. J. & SHARP, A. R. (2016) Does directly-observed-therapy improve tuberculosis treatment? More evidence is needed to guide tuberculosis policy. *Biomed central infectious diseases,* 16**,** 1-4.
MENICHE, X., OTTEN, R., SIEGRIST, M. S., BAER, C. E., MURPHY, K. C., BERTOZZI, C. R. & SASSETTI, C. M. (2014) Subpolar addition of new cell wall is directed by DivIVA in mycobacteria. *Proceedings of the national academy of sciences,* 111**,** E3243-E3251.
MOLL, A., DORR, T., ALVAREZ, L., DAVIS, B. M., CAVA, F. & WALDOR, M. K. (2015) AD, DD-carboxypeptidase is required for *Vibrio cholerae* halotolerance. *Environmental microbiology,* 17**,** 527-540.
MORANDI, M., SALI, M., MANGANELLI, R. & DELOGU, G. (2013) Exploiting the mycobacterial cell wall to design improved vaccines against tuberculosis. *The journal of infection in developing countries,* 7**,** 169-181.
OGU, C. C. & MAXA, J. L. (2000) Drug interactions due to cytochrome P450. *Proceedings (Baylor university. Medical center),* 13, 421-423.
OSBORN, M.J. & ROTHFIELD, L. (2007) Cell shape determination in *Escherichia coli. Current opinion in microbiology*, 10, 606-610.
PARISH, T. & STOKER, N. G. (2000) Use of a flexible cassette method to generate a double unmarked *Mycobacterium tuberculosis tlyA plcABC* mutant by gene replacement. *Microbiology,* 146**,** 1969-1975.
PATRU, M. M. & PAVELKA, M. S. (2010) A role for the class A penicillin-binding protein PonA2 in the survival of *Mycobacterium smegmatis* under conditions of nonreplication. *Journal of bacteriology,* 192**,** 3043-3054.
PETERS, K., KANNAN, S., RAO, V. A., BIBOY, J., VOLLMER, D., ERICKSON, S. W., LEWIS, R. J., YOUNG, K. D. & VOLLMER, W. (2016) The redundancy of peptidoglycan carboxypeptidases ensures robust cell shape maintenance in *Escherichia coli*. *American society for microbiology*. *mBio,* 7, 1-14.
PHAM, T.T., JACOBS-SERA, D., PEDULLA, M.L., HENDRIX, R.W. & HATFULL, G.F. (2007) Comparative genomic analysis of mycobacteriophage Tweety: evolutionary insights and construction of compatible site-specific integration vectors for mycobacteria. *Microbiology*, 153, 2711-2723
PHAM, D.D., FATTAL, E. & TSAPIS, N. (2015) Pulmonary drug delivery systems for tuberculosis treatment. *International journal of pharmaceutics,* 478, 517-529
PLOCINSKI, P., ARORA, N., SARVA, K., BLASZCZYK, E., QIN, H., DAS, N., PLOCINSKA, R., ZIOLKIEWICZ, M., DZIADEK, J., KIRAN, M. & GORLA, P. (2012) *Mycobacterium tuberculosis* CwsA interacts with CrgA and Wag31, and the CrgA-CwsA complex is involved

in peptidoglycan synthesis and cell shape determination. *Journal of bacteriology*, 194, 6398-6409.
POTLURI, L. P., DE PEDRO, M. A. & YOUNG, K. D. (2012) *Escherichia coli* low-molecular-weight penicillin-binding proteins help orient septal FtsZ, and their absence leads to asymmetric cell division and branching. *Molecular microbiology*, 84**,** 203-224.
PROMEGA. Protocols and Applications Guide. 3rd edition (1996), 45-46.
RAMKISSOON, S., MWAMBI, H.G. & MATTHEWS, A.P. (2012) Modelling HIV and *MTB* co-infection including combined treatment strategies. PloS one, 7, 1-18.
RANDICH, A. M. & BRUN, Y. V. (2015) Molecular mechanisms for the evolution of bacterial morphologies and growth modes. *Frontiers in microbiology*, 6**,** 1-13.
RAWLINGS, N. D. & BARRETT, A. J. (1993) Evolutionary families of peptidases. *Biochemical journal*, 290**,** 205-218.
RIOSERAS, B., YAGUE, P., LOPEZ-GARCIA, M. T., GONZALEZ-QUINONEZ, N., BINDA, E., MARINELLI, F. & MANTECA, A. (2016) Characterization of SCO4439, a D-alanyl-D-alanine carboxypeptidase involved in spore cell wall maturation, resistance, and germination in *Streptomyces coelicolor*. *Scientific reports*, 6, 1-15.
ROSSI, C. G. A., GOMEZ-PUERTAS, P. & SERRANO, J. A. A. (2016) *In vivo* functional and molecular characterization of the penicillin-binding protein 4 (DacB) of *Pseudomonas aeruginosa*. *Biomed central microbiology*, 16**,** 234.
RUSSELL, D.G., CARDONA, P.J., KIM, M.J., ALLAIN, S. & ALTARE, F. (2009) Foamy macrophages and the progression of the human tuberculosis granuloma. *Nature immunology*, 10, 943-948.
SANTI, I., DHAR, N., BOUSBAINE, D., WAKAMOTO, Y. & MCKINNEY, J. D. (2013) Single-cell dynamics of the chromosome replication and cell division cycles in mycobacteria. *Nature communications*, 4, 1-11.
SAUVAGE, E., KERFF, F., TERRAK, M., AYALA, J. A. & CHARLIER, P. (2008) The penicillin-binding proteins: structure and role in peptidoglycan biosynthesis. *FEMS microbiology review*, 32**,** 234-258.
SCHEFFERS, D.J. (2005) Dynamic localization of penicillin-binding proteins during spore development in *Bacillus subtilis*. *Microbiology*, 151**,** 999-1012.
SCHEFFERS, D.J. & PINHO, M. G. (2005) Bacterial cell wall synthesis: new insights from localization studies. *Microbiology and molecular biology reviews*, 69**,** 585-607.
SCHNIPPEL, K., BERHANU, R. H., BLACK, A., FIRNHABER, C., MAITISA, N., EVANS, D. & SINANOVIC, E. (2016) Severe adverse events during second-line tuberculosis treatment in the context of high HIV co-infection in South Africa: a retrospective cohort study. *Biomed central infectious diseases*, 16**,** 593 (1-10).
SCOLLARD, D. M., DACSO, M. M. & ABAD-VENIDA, M. L. (2015) Tuberculosis and leprosy: classical granulomatous diseases in the twenty-first century. *Dermatologic clinics*, 33**,** 541-562.
SHARMA, N., SINGH, R. & SHARMA, P. (2016) Molecular mycobacteriology and expansion in disease diagnosis. *Indian journal of clinical biochemistry*, 31**,** 138-147.
SIEGRIST, M. S., WHITESIDE, S., JEWETT, J. C., ADITHAM, A., CAVA, F. & BERTOZZI, C. R. (2013) D-amino acid chemical reporters reveal peptidoglycan dynamics of an intracellular pathogen. *American chemical society chemical biology*, 8**,** 500-505.
SILVA MIRANDA, M., BREIMAN, A., ALLAIN, S., DEKNUYDT, F. & ALTARE, F. (2012) The tuberculous granuloma: an unsuccessful host defense mechanism providing a safety shelter for the bacteria? *Clinical and developmental immunology*, 2012, 1-14.
SINGH, B., NITHARWAL, R. G., RAMESH, M., PETTERSSON, B., KIRSEBOM, L. A. & DASGUPTA, S. (2013) Asymmetric growth and division in *Mycobacterium spp.*: compensatory mechanisms for non-medial septa. *Molecular microbiology*, 88**,** 64-76.
SMITH, I. (2003) *Mycobacterium tuberculosis* pathogenesis and molecular determinants of virulence. *Clinical microbiology reviews*, 16**,** 463-496.
SMITH, T., WOLFF, K. A. & NGUYEN, L. (2012) Molecular biology of drug resistance in *Mycobacterium tuberculosis*. *Pathogenesis of Mycobacterium tuberculosis and its interaction with the host organism*. 374, 53-80.

STAFSTROM, J. P. & STAEHELIN, L. A. (1986) Cross-linking patterns in salt-extractable extensin from carrot cell walls. *Plant physiology,* 81**,** 234-241.
STATISTICS SOUTH AFRICA (2014) Mortality and causes of death in South Africa, 2014: Findings from death notification. Available from http://www.statssa.gov.za/publications/P03093/P030932014. [Accessed: 15 January 2017]
STEWART, G.C. (2005) Taking shape: control of bacterial cell wall biosynthesis. *Molecular microbiology*, 57, 1177-1181.
STOVER C.K, DE LA CRUZ V.F, FUERST T.R, BURLEIN J.E, BENSON L.A, BENNETT L.T, BANSAL G.P, YOUNG J.F, LEE M.H, HATFULL G.F et al. (1991) New use of BCG for recombinant vaccines. *Nature* 351, 456-460.
STROBEL, W., MOLL, A., KIEKEBUSCH, D., KLEIN, K. E. & THANBICHLER, M. (2014) Function and localization dynamics of bifunctional penicillin-binding proteins in *Caulobacter crescentus*. *Journal of bacteriology*,196**,** 1627-39.
SULIS, G., CENTIS, R., SOTGIU, G., D'AMBROSIO, L., PONTALI, E., SPANEVELLO, A., MATTEELLI, A., ZUMLA, A. & MIGLIORI, G. B. (2016) Recent developments in the diagnosis and management of tuberculosis. *NPJ primary care respiratory medicine,* 26**,** 1-8.
SZWEDZIAK, P. & LOWE, J. (2013) Do the divisome and elongasome share a common evolutionary past? *Current opinion in microbiology,* 16**,** 745-751.
THANKY, N. R., YOUNG, D. B. & ROBERTSON, B. D. (2007) Unusual features of the cell cycle in mycobacteria: polar-restricted growth and the snapping-model of cell division. *Tuberculosis,* 87**,** 231-236.
TORRELLES, J.B. & SCHLESINGER, L.S. (2017) Integrating lung physiology, immunology, and tuberculosis. *Trends in microbiology,* 1-10. Available from : https://doi.org/10.1016/j.tim.2017.03.007 [Accessed 15 June 2017]
TROJANOWSKI, D., GINDA, K., PIORO, M., HOLOWKA, J., SKUT, P., JAKIMOWICZ, D. & ZAKRZEWSKA-CZERWINSKA, J. (2015) Choreography of the Mycobacterium replication machinery during the cell cycle. *American society for microbiology mBio,* 6**,** 1-12.
VAN CREVEL, R., OTTENHOFF, T.H. & VAN DER MEER, J.W. (2002) Innate immunity to *Mycobacterium tuberculosis*. *Clinical microbiology reviews,* 15, 294-309.
VARMA, A. & YOUNG, K. D. (2004) FtsZ collaborates with penicillin-binding proteins to generate bacterial cell shape in *Escherichia coli*. *Journal of bacteriology,* 186**,** 6768-6774.
WANG, S., FURCHTGOTT, L., HUANG, K.C. & SHAEVITZ, J.W. (2012) Helical insertion of peptidoglycan produces chiral ordering of the bacterial cell wall. *Proceedings of the national academy of sciences,* 109, E595-E604.
WHALEN, C.C. (2006) Failure of directly observed treatment for tuberculosis in Africa: a call for new approaches. *Clinical infectious diseases*, 42, 1048-1050
WHO. Global tuberculosis report 2014,World Health Organization, Geneva. (2014). Available from: http://www.who.int/tb/publications/global_report/en/ [Accessed:30 March 2015]
WHO. Global tuberculosis report 2016 (2016) http://www.who.int/tb/publications/global_report/en/ [Accessed: 5 December 2016]
WIVAGG, C. N., BHATTACHARYYA, R. P. & HUNG, D. T. (2014) Mechanisms of β-lactam killing and resistance in the context of *Mycobacterium tuberculosis*. *The journal of antibiotics,* 67**,** 645-654.
XIAO, J. & GOLEY, E. D. (2016) Redefining the roles of the FtsZ-ring in bacterial cytokinesis. *Current opinion in microbiology,* 34**,** 90-96.
YANG, W.F., HAN, F., ZHANG, X.H., ZHANG, P. & CHEN, J.H. (2013). Extra-pulmonary tuberculosis infection in the dialysis patients with end stage renal diseases: case reports and literature review. *Journal of Zhejiang university. Science. B (Biomedicine & Biotechnology)*, 14, 76-82
ZHANG, D., WANG, Y., LU, J. & PANG, Y. (2016) *In vitro* activity of β-lactams in combination with β-lactamase inhibitors against multidrug-resistant *Mycobacterium tuberculosis* isolates. *Antimicrobial agents and chemotherapy*, 60**,** 393-399.
ZUMLA, A., RAVIGLIONE, M., HAFNER, R. & VON REYN, C.F. (2013) Current concepts. *New england journal of medicine,* 368, 745-755.

ZUMLA, A., NAHID, P. & COLE, S.T. (2013) Advances in the development of new tuberculosis drugs and treatment regimens. *Nature reviews drug discovery*, 12, 388-404.

CHAPTER 7: APPENDICES

Appendix A: Genetic code and amino acids

Table A1: Representation of Table of codons or the genetic code

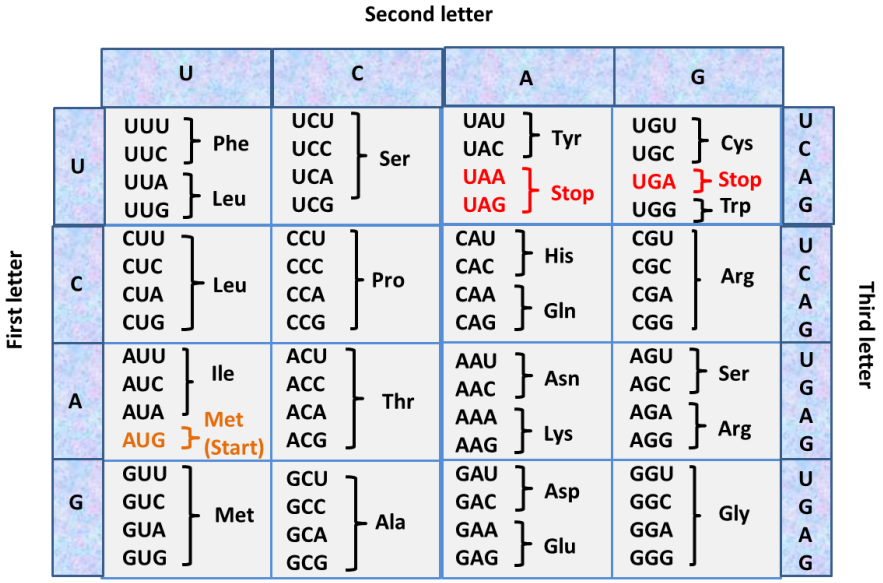


Table A2: Representation of table of Amino acids and their abbreviations

SYMBOLS		
1-Letter	**3-Letter**	**Amino Acids**
Y	Tyr	Tyrosine
G	Gly	Glycine
F	Phe	Phenylalanine
M	Met	Methionine
A	Ala	Alanine
S	Ser	Serine
I	Ile	Isoleucine
L	Leu	Leucine
T	Thr	Threonine
V	Val	Valine
P	Pro	Proline
K	Lys	Lysine
H	His	Histidine
Q	Gln	Glutamine
E	Glu	Glutamic acid

Z	Glx	Glu and/or Gln
W	Trp	Tryptophan
R	Arg	Arganine
D	Asp	Aspartic acid
N	Asn	Asparagine
B	Asx	Asn and/or Asp
C	Cys	Cysteine
X	Xaa	Unknown or other

Appendix B: Media and solutions

Table B1: Media used for bacterial growth

Medium	**Component (for 1 Litre)**	**Dissolvent**	**pH**	**Autoclave (A) (121 °C for 10 min) or Filter sterilize (FS)**
LB	10 g tryptone, 10 g NaCl, 5 g yeast extract	dH_2O		A
LB agar	10 g tryptone, 5 g NaCl. 5g yeast extract, 15 g agar	dH_2O		A
7H9	4.7 g 7H9, 100 ml OADC or 10 ml 100× G N, 2 ml glycerol, 2 ml 25% Tween80 **(F.S)**	dH_2O		A
7H10	19 g 7H10, 10 ml 100× G N, 5 ml glycerol	dH_2O		A
2xTY	20 g tryptone, 10 g NaCl, 10 g yeast extract	dH_2O		A
Sautons	4 g asparagine, 0.5 g MgSO4, 2 g citric acid, 0.5 g KH2PO4, 0.05 g ammonium ferric citrate, 60 ml glycerol	dH_2O	7.2 (with ammonia)	A

Table B2: Media supplementation

Supplement	**Components**	**Dissolvent**	**Autoclave (A) (121 °C for 10 min) or Filter sterilize (FS)**
Glucose salts (100X)	20 g glucose, 8.5 g NaCl	100 ml dH_2O	A
Tween80 (25 %)	10 ml Tween80 dissolved	40 ml dH_2O	FS
Sucrose (75 %)	75 g sucrose	100 ml dH_2O	A
X-gal (2 %)	1 g X-gal in	50 ml deionized DMF	
Hygromycin B (50mg/ml)	Purchased as a ready-made product from Roche 4 °C		
Kanamycin (50mg/ml)	Dissolve powder in sterile distilled water and store at 4 °C	sterile dH_2O	FS

Table B3: Solutions for transformation and preparation of chemically competent cells

Solution	**Recipe/ Description**	**Dissolvent**	**pH**	**Autoclave (A) (121 °C for 10 min) or Filter sterilize (FS)**
TfbI	30 mM Potassium acetate, 100 mM Rubidium chloride, 10 mM Calcium chloride, 50 mM Manganese chloride, 15 % v/v Glycerol made up in dH_2O	dH_2O	5.8 (with dilute acetic acid)	FS
TfbII	10 mM MOPS, 75 mM Calcium chloride, 10 mM Rubidium chloride, 15 % v/v Glycerol made up in dH2O	dH_2O	6.5 (with dilute NaOH)	FS
Glycerol (10%)	10 ml glycerol made up to 100 ml with dH2O	dH_2O		A

Table B4: Solutions for genomic DNA Extraction

Solution	**Recipe\ Description**	**Dissolvent**	**Autoclave (A) (121 °C for 10 min) or Filter sterilize (FS)**
CTAB/NaCl	4.1 % NaCl, 10 % N-cetyl-N,N, N-trimethyl ammonium bromide	dH_2O	FS
TE buffer	10 mM Tris-HCl (pH 8), 10 mM EDTA	dH_2O	A
NaCl	5 M NaCl	dH_2O	A
SDS (10 %)	10 g SDS	100 ml dH_2O	FS

Table B5: Solutions for plasmid DNA Extraction

Solution	**Recipe/ Description**	**Dissolvent**	**Autoclave (A) (121 °C for 10 min) or Filter sterilize (FS)**
Solution I	50mM Glucose, 25mM Tris-HCl (pH 8), 10 mM EDTA	dH_2O	A
Solution II	1 % SDS, 0.2 M NaOH	dH_2O	
Solution III	3 M Potassium acetate, 11.5% Acetic acid	dH_2O	
RNaseA (10 mg/ml)	10 mg RNaseA	1ml sdH_2O	

Table B6: Solutions for DNA Precipitation

Solution	**Recipe/ Description**	**Dissolvent**	**pH**	**Autoclave (A) (121 °C for 10 min) or Filter sterilize (FS)**
Chloroform: Isoamyl alcohol	24 ml chloroform, 1 ml isoamyl alcohol	dH_2O		-
Sodium acetate	3M sodium acetate	dH_2O	5.2	A

Table B7: Solutions for DNA electrophoresis

Solution	**Recipe/ Description**	**Dissolvent**
TAE	(50x stock solution): 242 g Tris base, 57.1 ml glacial acetic acid, 100 ml 0.5 M EDTA (pH 8) make up to 1L in dH2O (1x working solution contains 40 mM Tris-acetate and 1 mM EDTA)	dH_2O
Ethidium bromide (EtBr)	10 mg/ml	sdH_2O

Table B8: Solutions for DNA Precipitation

Solution	**Recipe/ Description**	**Dissolvent**	**pH**
Denaturation solution	0.5 M NaOH, 1.5 M NaCl	dH_2O	
Depurination solution	0.25M HCl	dH_2O	
TBE (5X)	Tris-Borate-EDTA powder (Sigma)	2l dH_2O	
SSC (20X)	3M NaCl, 0.3M sodium citrate	dH_2O	
Solution I	2X SSC, 0.1% SDS	dH_2O	
Solution II	0.5X SSC, 0.1% SDS	dH_2O	
Maleic acid buffer	1M Maleic acid, 1.5M NaCl	dH_2O	7.5 (with NaOH pellets)
Wash buffer	0.1M Maleic acid buffer, 0.3 % Tween20	dH_2O	
Blocking solution (Roche)	1X blocking solution in maleic acid buffer	dH_2O	
Detection buffer	0.1M Tris-HCl, 0.1M NaCl	dH_2O	9.5
Antibody solution(Roche)	Dilute 1 in 10 000 in blocking solution	dH_2O	
CSPD (Roche)	Disodium 2-chloro-5-(4-methoxyspiro (2-dioxetane-3,2 (2-dioxetane-3,2'-(5'-chloro)-tricyclo[3.3.1.1. 3, 7.]decan(-. 4-yl)-1-phenyl phosphate	dH_2O	

Table B9: Reagents for click chemistry

Solution	Recipe/ Description	Dissolvent	pH
CuSO4	1 mM CuSO4 from 50mM stock	dH_2O	
TBTA (Sigma)	128 Um from 6.4 mM TBTA stock	DMSO	
Sodium ascorbate	1.2 mM sodium ascorbate from the 60mM stock	dH_2O	
Azido-PEG488 (azido probe)	20Um from the 1mM azido probe	DMSO	
PBS (Sigma)	1 tablet in 200 mL water (Yield: 137 mM NaCl, 2.7 mM KCl and 10 mM PBS)	dH_2O	7.4 (at 25 °C)
PBSTB	PBS, 0.05 % BSA, 0.01 % Tween 20		
Alkaline-D-alanine	1 mM Alkaline-D-alanine (For mycobacteria, a final concentration of 0.5Mm was used)	dH_2O	

Table B10: Reagents for crystal violet assay

Solution	Recipe/ Description	Dissolvent	Autoclave (A) (121 °C for 10 min) <u>or</u> Filter sterilize (FS)
Crystal Violet (1mg/mL)	For ≥ 90 % dye content (dark purple) : 5 mg crystal powder and 5 mL dH_2O	dH_2O	FS
99 % Ethanol	99 mL 100 % ethanol and 1 mL dH_2O	dH_2O	FS

Appendix C: Molecular weight markers

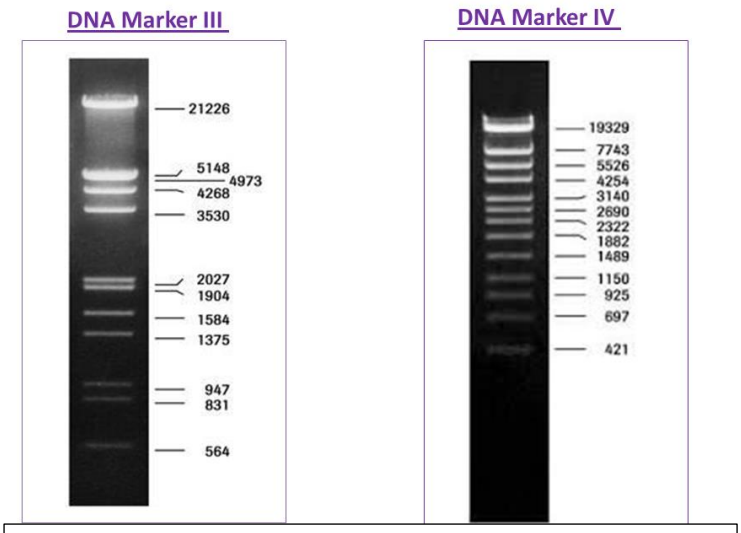


Figure C1: Molecular weight markers used in this study

Appendix D: DNA amplification of DD-CPases and other cell wall remodelling enzymes used in this study

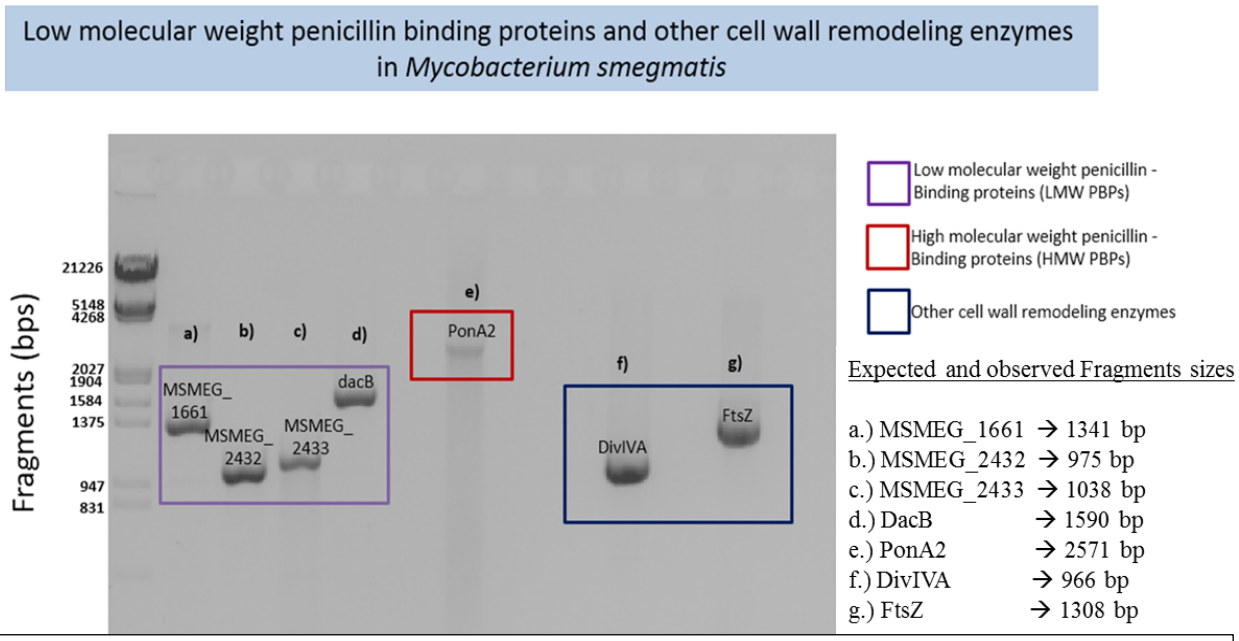


Figure D1: Gel electrophoresis of PCR products. Shown are the PCR amplicons for all enzymes that were cloned in this study. The purple box represents the low-molecular-weight penicillin-binding proteins (or DD-CPases). The red box represents a high-molecular-weight penicillin-binding proteins (PonA2). The blue box represents cell division proteins (FtsZ and DivIVA). All sizes were correct and these fragments were further used for cloning purposes.

Appendix E: Proteins tagged with monomeric red fluorescent tag (mRFP)

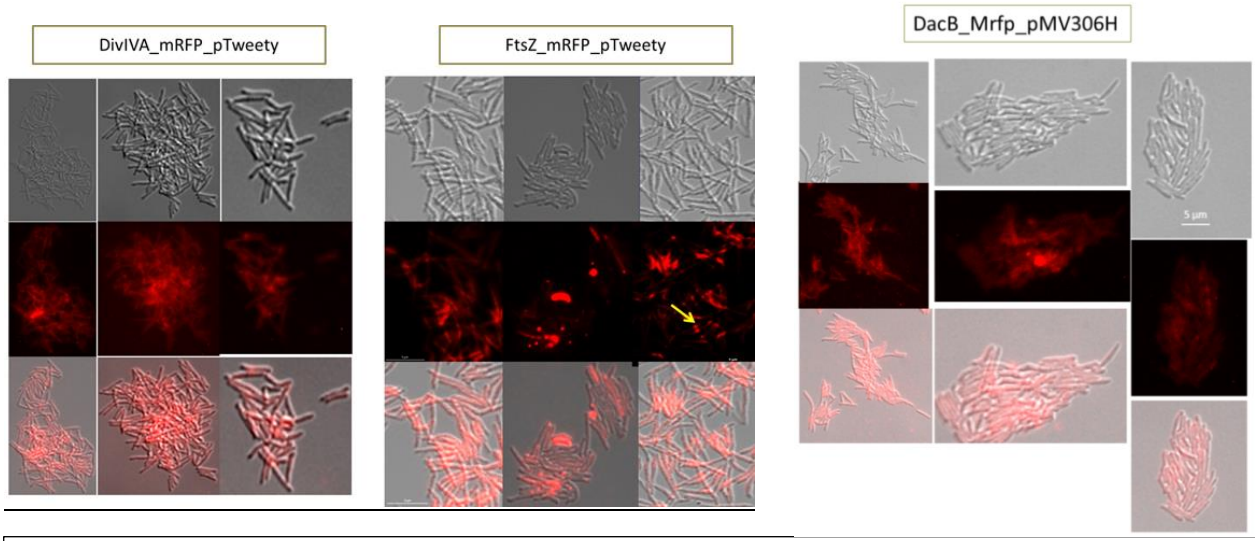
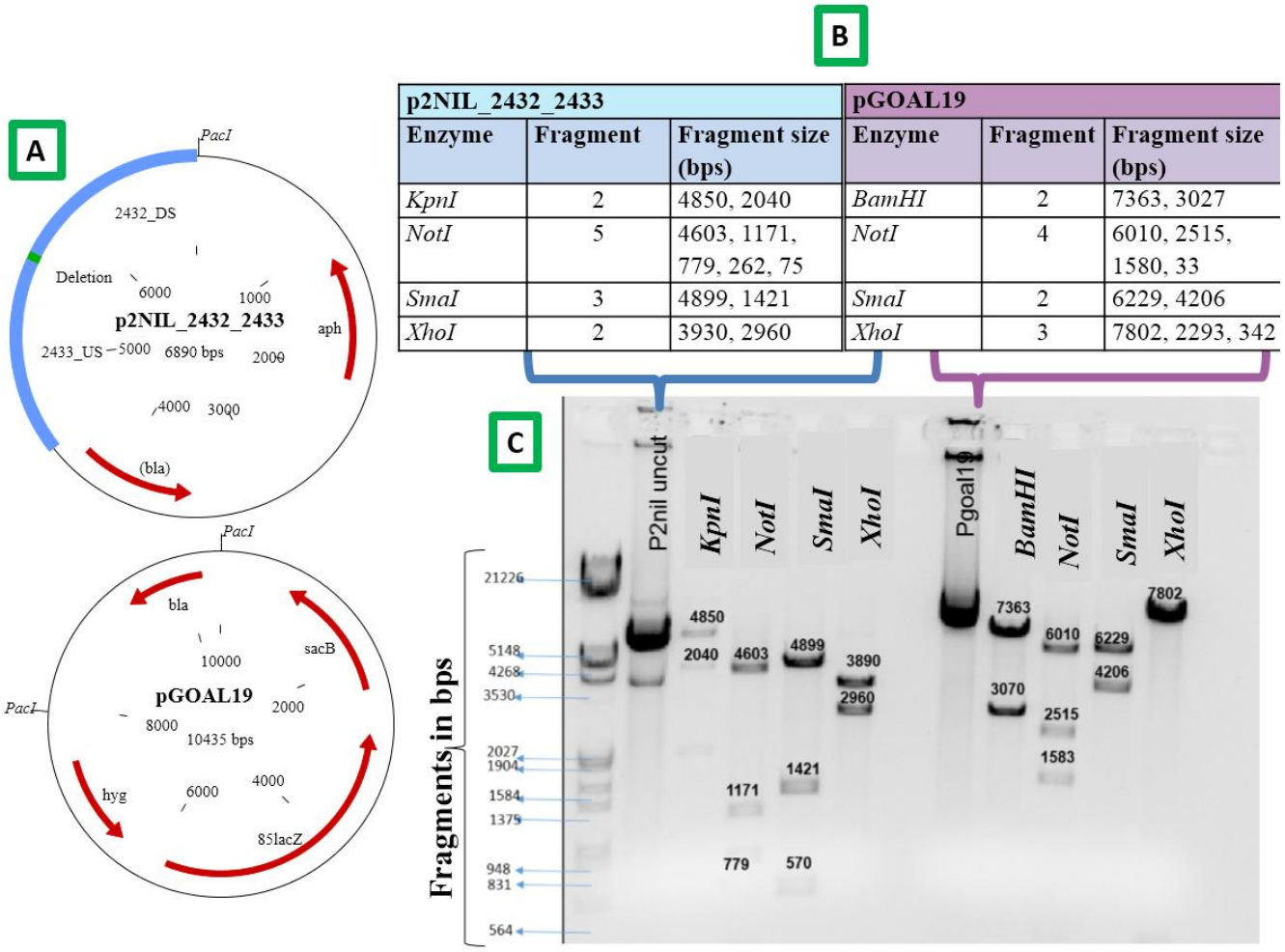


Figure E1: Failed localization with mRFP proteins. Shown are the diffused localization patterns obtained when mRFP was used as a fluorescent tag for DacB, FtsZ and DivIVA. Some focused localization for FtsZ was observed (yellow arrow) but this was not sufficient for advancement in this study. All restriction maps for these plasmids yielded the correct banding pattern (shown in figures hereafter) and sequencing confirmed the in-frame nature of the fusion. Hence, it is unclear why these fusions did not work. As a result, none of these fusions were pursued further.

Appendix F

Appendix F: Plasmids used to create the suicide vector



p2NIL_2432_2433			pGOAL19		
Enzyme	**Fragment**	**Fragment size (bps)**	**Enzyme**	**Fragment**	**Fragment size (bps)**
KpnI	2	4850, 2040	*BamHI*	2	7363, 3027
NotI	5	4603, 1171, 779, 262, 75	*NotI*	4	6010, 2515, 1580, 33
SmaI	3	4899, 1421	*SmaI*	2	6229, 4206
XhoI	2	3930, 2960	*XhoI*	3	7802, 2293, 342

Figure F1: Restriction enzyme profiling of the p2NIL_2433_2432 and pGOAL_19 constructs to create a suicide vector (p2NIL_2433_2432::pG19). **(A)** Represents the plasmids used to create the suicide vector and the enzyme that was used to digest the plasmid for cloning purposes. The enzyme used for digesting both vectors was *PacI*. To confirm the clones obtained are correct, the expected fragment sizes **(B)** were compared to those observed **(C)** on the gel electrophoresis. The expected fragment sizes matched observed therefore plasmids were correct and could be used for cloning

Appendix F: Sucrose sensitivity testing for the double mutant created in this study

Sucrose sensitivity testing

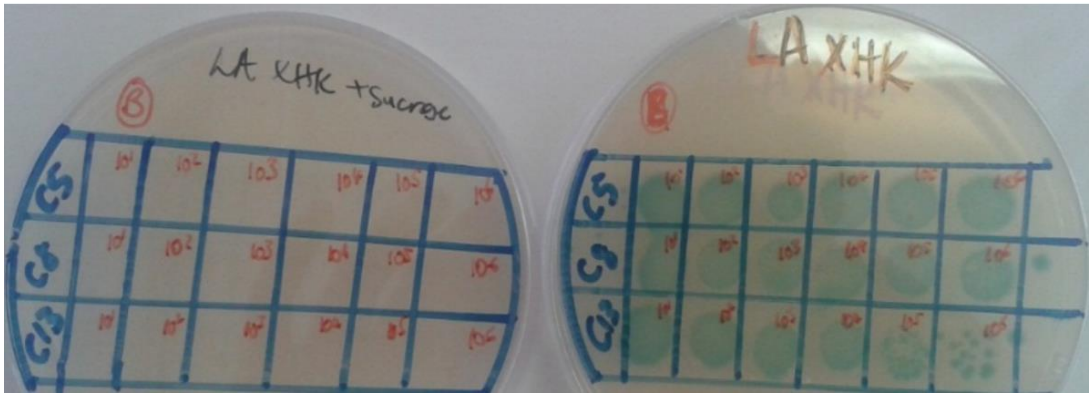
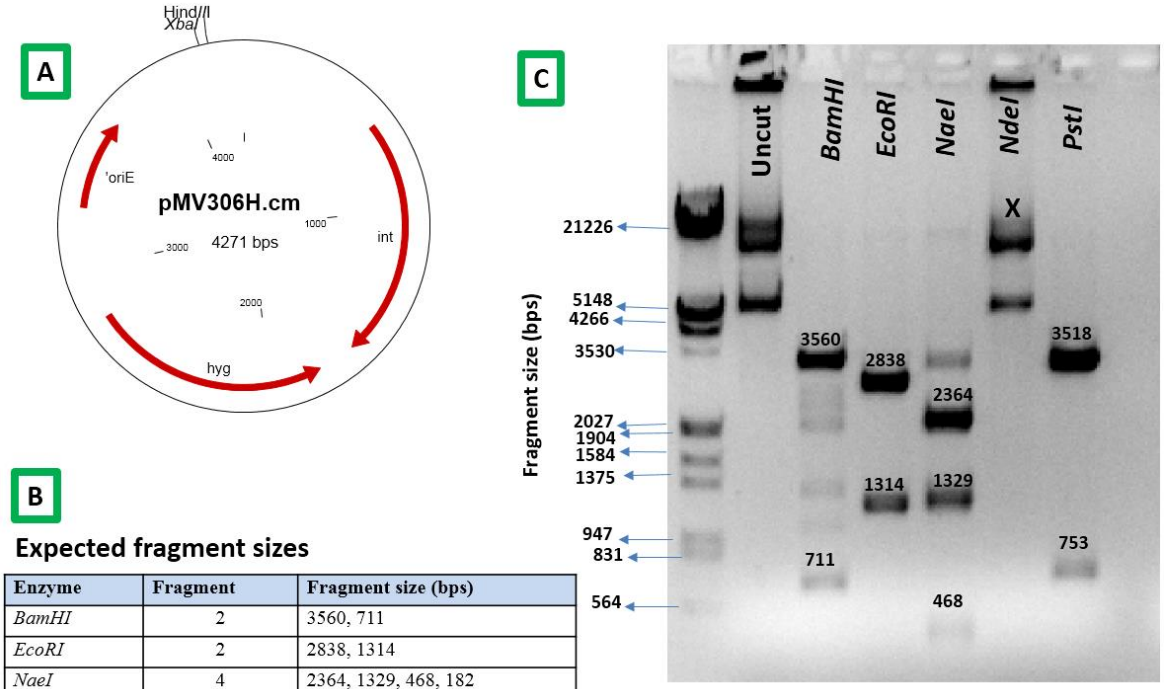


Figure F2: An illustration representing the sucrose sensitivity test to for suicide vector (p2NIL_2433_2432::pG19) used to create a DD- CPases double mutants (△2433△2432). In the presence of sucrose, represented by petri dish on the left, the single cross-over mutants (SCO) were sensitive when grown on LA agar containing antibiotics and sucrose. In the absence of sucrose, represented by petri dish on the right, the single cross-over mutants (SCO) were grown on LA agar containing only antibiotics with no sucrose and growth was observed. C5, C8 and C13 on the petri dishes represent random single cross-overs that were used for analysis and all of them were correct, but only C5 was taken for the mutant generation. The blue colour on the left petri dish represents the presence of the *lacZ* reporter gene. Serial dilutions of 10^1 to 10^6 were made for each sample. LA represents Luria-Bertani agar (solid media).

Appendix G: Integrating vectors and constructs used in this study

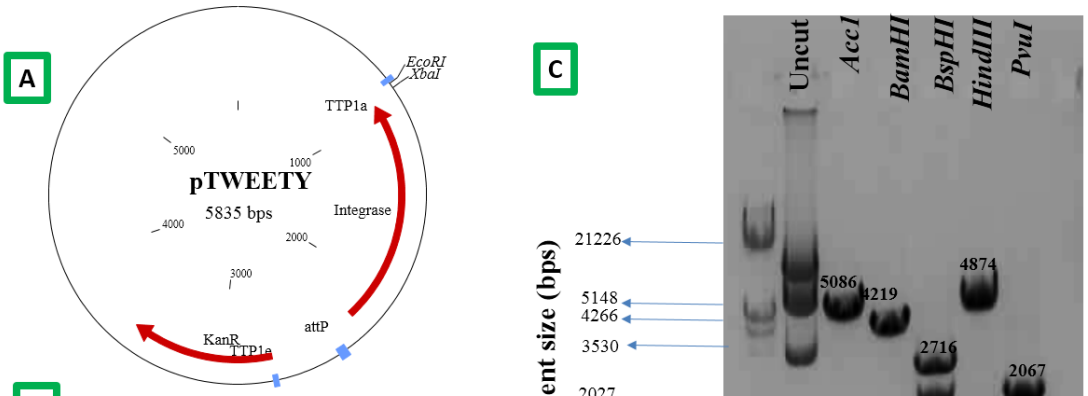


B

Expected fragment sizes

Enzyme	Fragment	Fragment size (bps)
BamHI	2	3560, 711
EcoRI	2	2838, 1314
NaeI	4	2364, 1329, 468, 182
NdeI	-	-
PstI	2	3518, 753

Figure G1.1: Restriction enzyme (profiling of the pMV306H integrating plasmid used to create reporter fusion proteins**(A)** Represents the map of pMV306 plasmid and the enzymes used for digesting this vector during cloning (*HindIII* and *XbaI*) which were selected from the multiple cloning sites of this vector. To confirm if the plasmid is correct, the expected fragment sizes **(B)** were compared to those observed **(C)** on the gel electrophoresis. The expected fragment sizes matched observed therefore plasmid was correct and was used for cloning purposes.



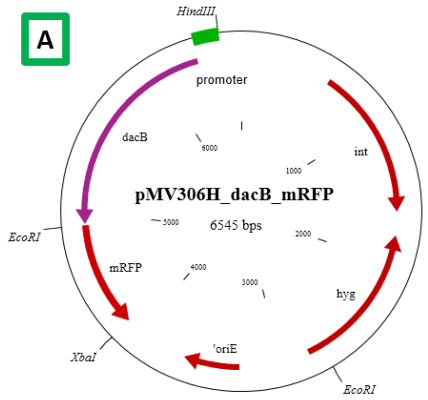
B

Expected fragment sizes

Enzyme	Fragment	Fragment size (bps)
AccI	3	5086, 575, 174
BamHI	3	4219, 1035, 581
BspHI	4	2716, 2006, 1008, 105
HindIII	2	4871, 961
Pvul	4	2067, 1962, 1368, 438

Figure G1.2: Restriction enzyme profiling of the pTweety integrating plasmid used to create reporter fusion proteins. **(A)** Represents the pTweety plasmid map showing the enzymes used for digesting this vector during cloning (*EcoRI* and *XbaI*) which were selected from the multiple cloning sites of this vector. To confirm if the plasmid is correct, the expected fragment sizes **(B)** were compared to those observed **(C)** on the gel electrophoresis. The expected fragment sizes matched observed therefore plasmid as correct and was used for cloning purposes.

G2: Reporter genes created in this study



B

Expected fragment sizes

Enzyme	Fragment	Fragment sizes (in bps)
BglII	2	3522, 3023
MscI	3	3174, 2027, 1344
NaeI	6	2198, 2186, 1293, 486, 254, 182
NotI	4	4656, 1002, 752, 135
PstI	2	3854, 2691
PvuI	4	4962, 921, 432, 230

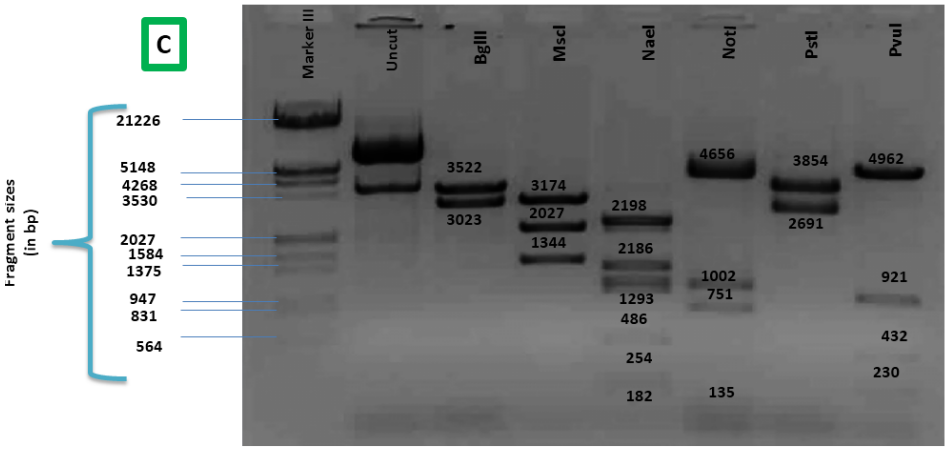
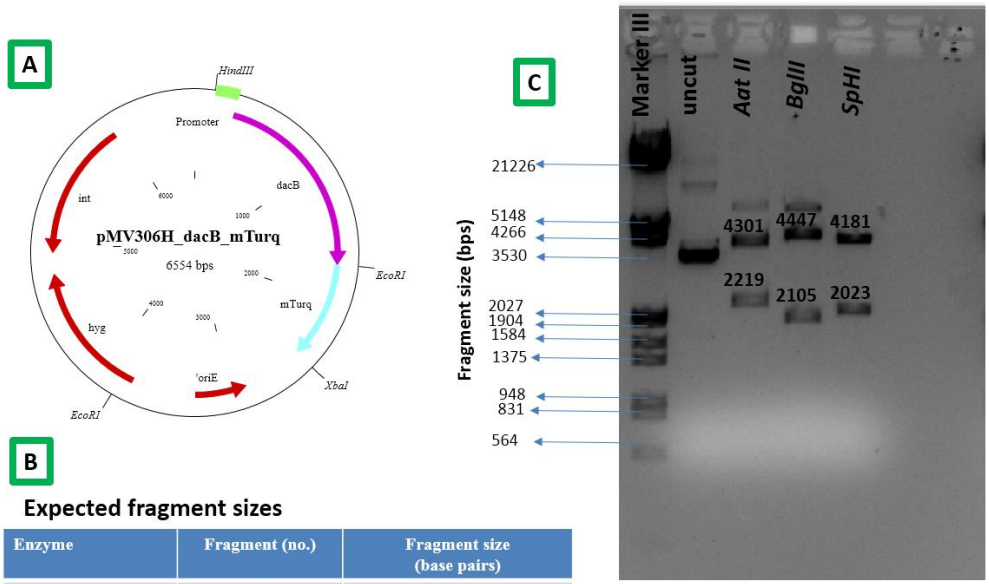


Figure G2.1: Restriction enzyme profiling of the pMV306H_dacB_mRFP construct **(A)** Represents the pMV306H_dacB_mRFP plasmid (Derivative of DacB carrying an in-frame C-terminal mRFP tag) and theenzymes used for creating the construct are; DacB (*HindIII* and *EcoRI*) mRFP (*EcoRI* and *XbaI)* and pMV306H (*HindIII* and *XbaI*). Restriction profiling was done and the expected fragment sizes **(B)** were compared to those observed **(C)** on the agarose gel. The expected sizes matched observed and this implied that construct created was correct.



B

Expected fragment sizes

Enzyme	Fragment (no.)	Fragment size (base pairs)
Aat II	2	4301, 2219
BglII	2	4447, 2105
SpHI	2	4181, 2031

Figure G2.2: The illustration above represents restriction enzyme (R.E) profiling of the pMV306H_dacB_mTurq construct **(A)** Represents the pMV306H_dacB_mTurq construct (Derivative of DacB carrying an in-frame C-terminal mTurq tag) and the R.E used for creating the construct are; DacB (*HindIII* and *EcoRI*) mTurq (*EcoRI* and *XbaI)* and pMV306H (*HindIII* and *XbaI*). To confirm this construct is correct, a R.E profiling was done and the expected fragment sizes **(B)** were compared to those observed **(C)** on the agarose gel. The expected fragment sizes matched observed and this implies that construct created is correct and this plasmid was be used for to track the localization pattern of DacB in *M. smegmatis* cells.

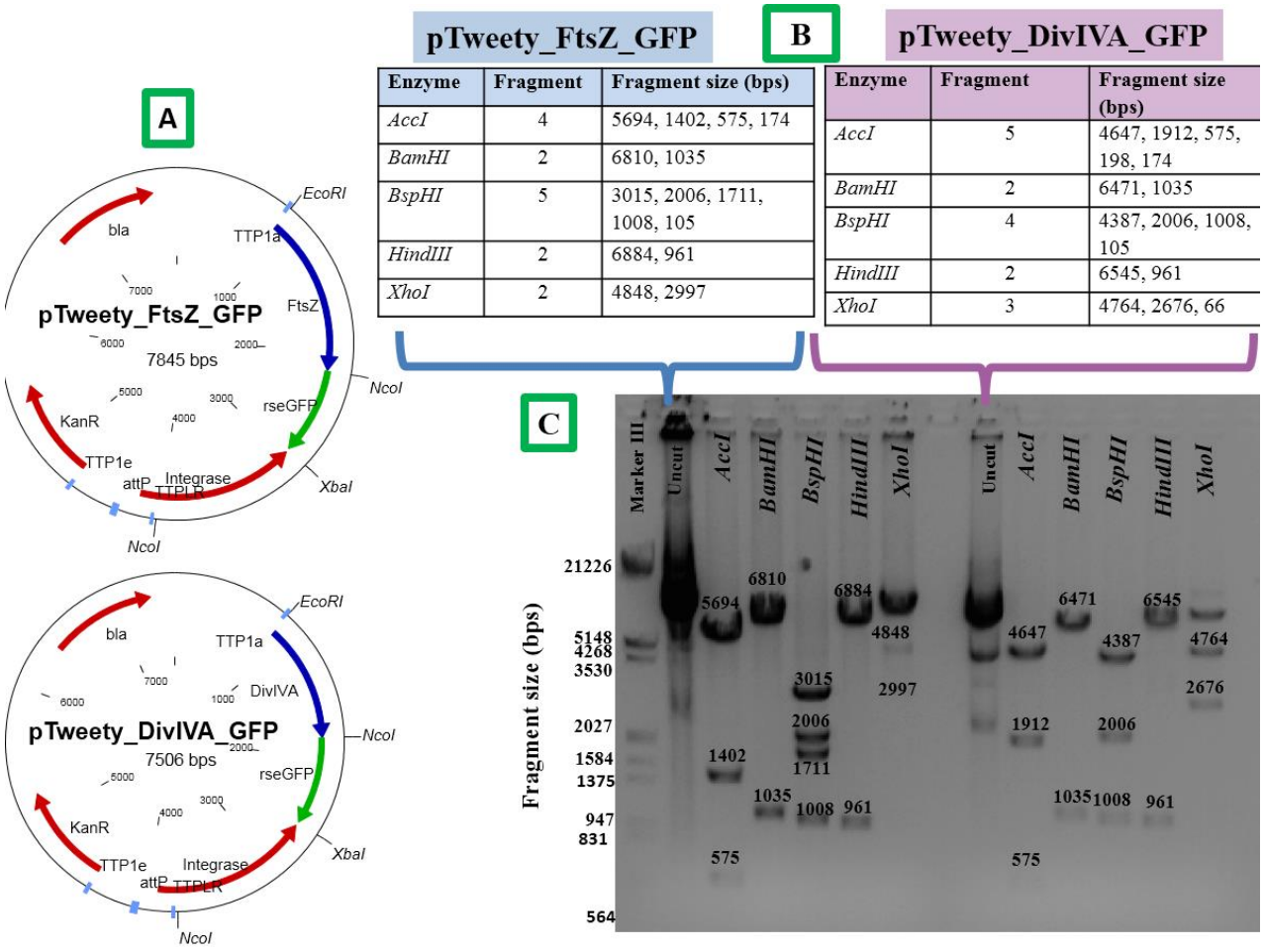
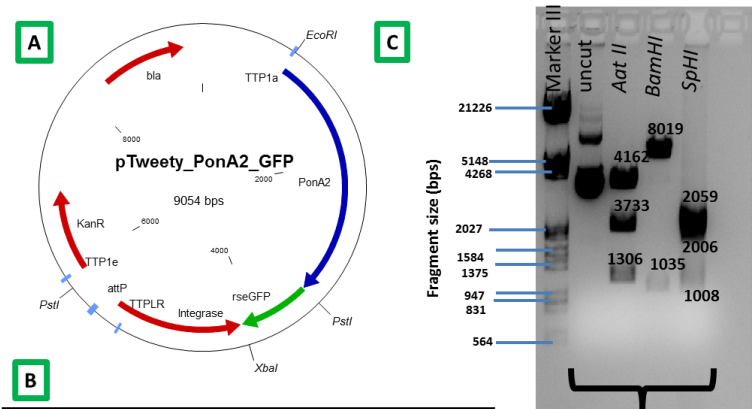


Figure G2.3: Restriction profiling of the pTweety_FtsZ_GFP and pTweety_DivIVA_GFP constructs **(A)** Represents the pTweety_FtsZ_GFP and pTweety_DivIVA_GFP maps (Derivative of FtsZ and DivIVA, respectively, carrying an in-frame C-terminal GFP tag). The enzyme used for creating the pTweety_FtsZ_GFP construct are; FtsZ (*EcoRI* and *NcoI*) GFP (*NcoI* and *XbaI)* and pMV306H (*EcoRI* and *XbaI*). The enzymes used for creating the pTweety_DivIVA_GFP construct are; DivIVA (*EcoRI* and *NcoI*) GFP (*NcoI* and *XbaI)* and pMV306H (*EcoRI* and *XbaI*). Restriction profiling was done and the expected fragment sizes **(B)** were compared to those observed **(C)** on the agarose gel. The expected sizes matched observed and implying that both these constructs were correct.

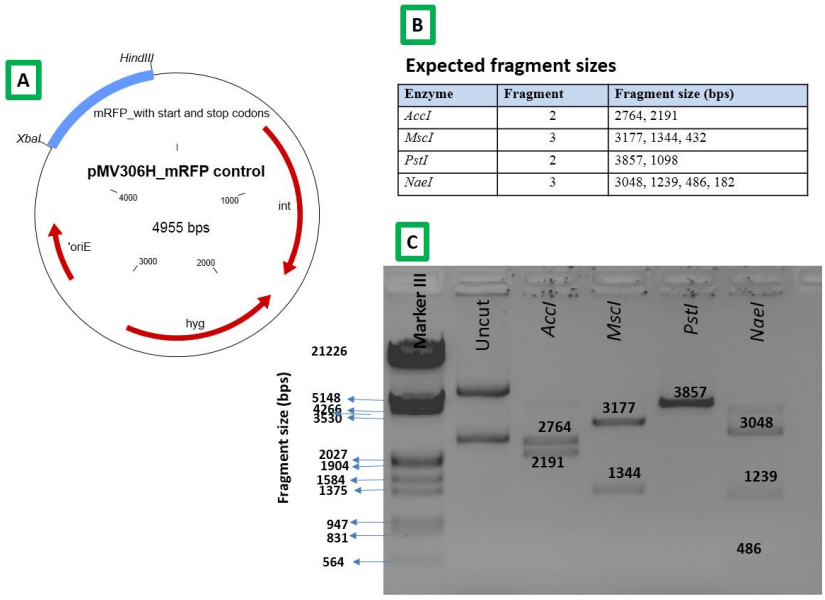


B

Enzyme	Fragment (no.)	Fragment size (base pairs)
AatII	3	4162, 3733,1159
BamHI	2	8019, 1035
BspHI	5	3876, 2059, 2006, 1008, 105

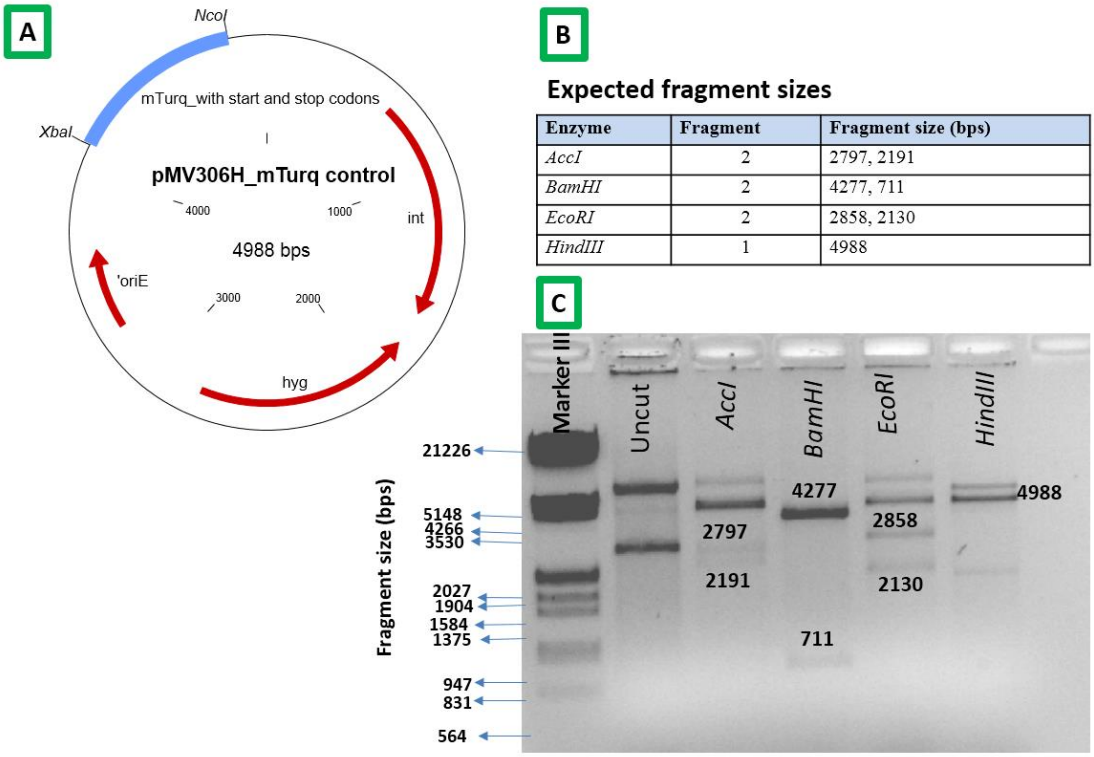
Figure G 2.4: Restriction enzyme profiling of the pTweety_PonA2_GFP construct **(A)** Represents pTweety_PonA2_GFP (Derivative of PonA2 carrying an in-frame C-terminal GFP tag). The enzymes used for creating the pTweety_PonA2_GFP construct are; GFP (*PstI* and *XbaI)*, PonA2 (*EcoRI* and *PstI*) and pTweety (*EcoRI* and *XbaI)*. Restriction profiling was done and the expected fragment sizes **(B)** were compared to those observed **(C)** on the agarose gel. The expected sizes matched observed and implying that the construct was correct.

G3: Controls for fluorescent tagging proteins



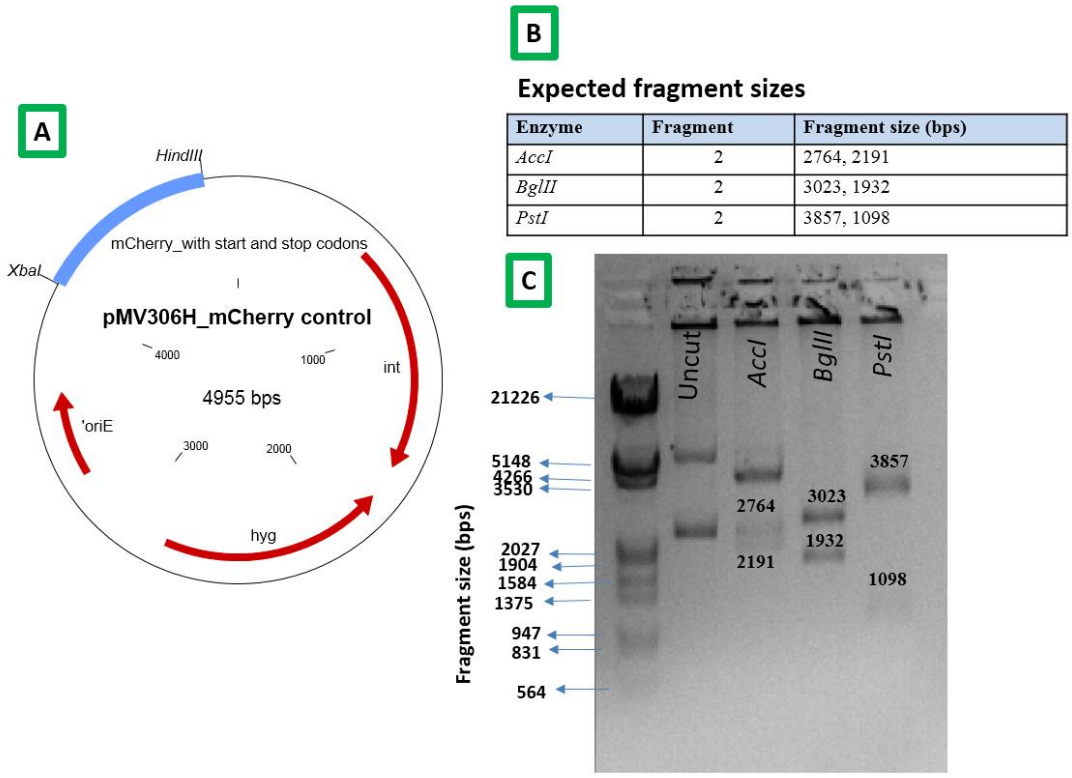
Enzyme	Fragment	Fragment size (bps)
AccI	2	2764, 2191
MscI	3	3177, 1344, 432
PstI	2	3857, 1098
NaeI	3	3048, 1239, 486, 182

Figure G3.1: Restriction enzyme profiling of the pMV306H_mRFP control construct **(A)** Represents the map of the pMV306H_mRFP (Derivative of mRFP retaining the native start and added stop codons). The enzymes used for creating the pMV306H_mRFP construct are; mRFP (*HindIII* and *XbaI)* and pMV306H (*HindIII* and *XbaI)*. Restriction profiling was done and the expected fragment sizes **(B)** were compared to those observed **(C)** on the agarose gel. The expected sizes matched observed and implying that the construct was correct.



Enzyme	Fragment	Fragment size (bps)
AccI	2	2797, 2191
BamHI	2	4277, 711
EcoRI	2	2858, 2130
HindIII	1	4988

Figure G3.2: Restriction enzyme profiling of the pMV306H_mTurq control construct **(A)** Represents the map of the pMV306H_mTurq (Derivative of mTurq retaining the native start and added stop codons). The enzymes used for creating the pMV306H_mTurq construct are; mTurq (*NcoI* and *XbaI)* and pMV306H (*NcoI* and *XbaI)*. Restriction profiling was done and the expected fragment sizes **(B)** were compared to those observed **(C)** on the agarose gel. The expected sizes matched observed and implying that the construct was correct.



Enzyme	Fragment	Fragment size (bps)
AccI	2	2764, 2191
BglII	2	3023, 1932
PstI	2	3857, 1098

Figure G3.3: Restriction enzyme profiling of the pMV306H_mCherry control construct **(A)** Represents the map for pMV306H_mCherry (Derivative of a mCherry retaining the native start and added stop codons). The enzymes used for creating the pMV306H_mCherry construct are; mCherry (*HindIII* and *XbaI)* and pMV306H (*HindIII* and *XbaI)*. Restriction profiling was done and the expected fragment sizes **(B)** were compared to those observed **(C)** on the agarose gel. The expected sizes matched observed and implying that the vector was correct. mCherry tag alone in *M. smegmatis* cells.

G4: Microscopic analysis of the fluorescent tags alone used in the study

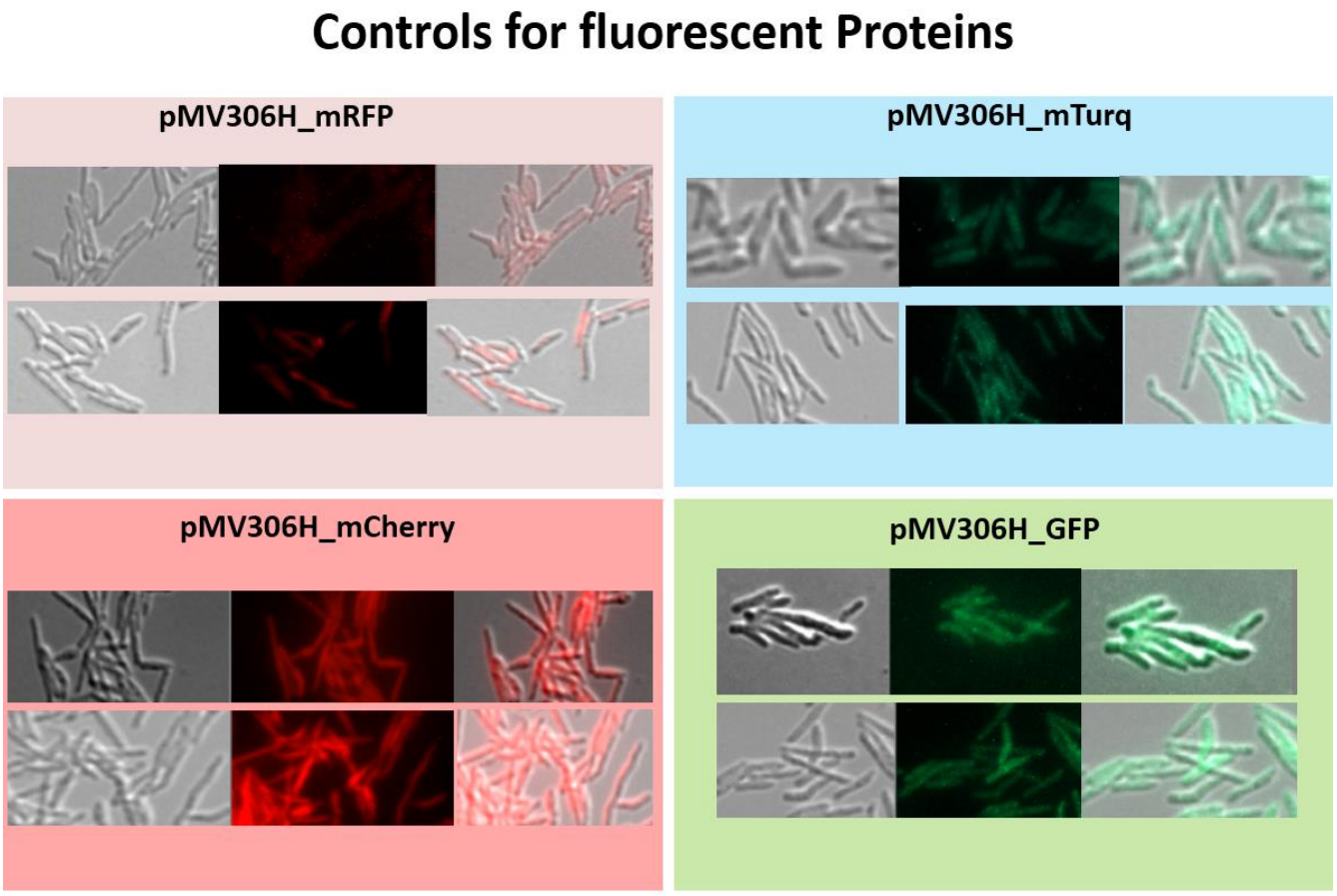


Figure G4: The illustration above representts the fluorescence intensity of the fluorescent tagging proteins that were used in this study in *M. smegmatis* cells. These tags were fused to the reporter gene investigated in this study and were used as references or controls to compare and determine precise localization pattern of various genes of interest. Different tags were also used to tag different genes for co-localization studies that have yet to be conducted. . The diffused staining pattern of these untagged control proteins confirmed that any localization observed with the tagged derivatives is due to the protein of interest and not the fluorescent tag.